Exciton Populations and Correlation Effects in Semiconductor Quantum Wires

Dissertation

zur Erlangung des Doktorgrades
der Naturwissenschaften
(Dr. rer. nat.)

dem Fachbereich Physik
der Philipps-Universität Marburg
vorgelegt von

Sven Siggelkow

aus

Hannover

Marburg/Lahn, Februar 2006

Vom Fachbereich Physik der Philipps-Universität Marburg als Dissertation angenommen am

Erstgutachter: Prof. Dr. Stephan W. Koch

Zweitgutachter: Prof. Dr. Reinhard Noack

Tag der mündlichen Prüfung:

Zusammenfassung

Halbleiter und ihre Eigenschaften werden schon seit $\Delta t \approx 1.7 \times 10^2$ Jahren wissenschaftlich untersucht [1]. In einer positiven Rückkopplung mit der Entwicklung immer neuer Anwendungen hat sich das wissenschaftliche Interesse an Halbleitern in dieser Zeitspanne potenziert. Zu den Meilensteinen dieser Entwicklung, die entsprechend gesteigertes Interesse an der Halbleiter-Physik nach sich zogen, gehören die Erfindung der ersten Solarzelle aus goldbeschichtetem Selen im Jahr 1887, der unaufhaltsame Siegeszug des 1947 entwickelten Transistors und die theoretische Beschreibung und experimentelle Realisierung des ersten Halbleiter-Lasers in den 60er Jahren des vergangenen Jahrhunderts. Entsprechend haben auch die Verfahren zur Herstellung von Halbleiter-Elementen im gleichen Zeitraum eine ähnlich rasante Entwicklung erfahren. Die durchschnittliche Größe der Strukturen auf Silizium-Chips liegt im Moment bei 65 Nanometern, eine weitere Reduktion auf 45 Nanometer steht bis 2008 in Aussicht. Durch die ständige Verbesserung der epitaktischen Verfahren zur Herstellung von Heterostrukturen kann heutzutage das Halbleiter-Wachstum auf der Ebene einzelner Atom-Schichten kontrolliert werden. Eine Vielfalt von Methoden ermöglicht eine weitergehende Strukturierung auf Nanometer-Skalen, zum Beispiel durch gezieltes Heizen einzelner Bereiche schon in der Wachstumsphase durch Laserstrahlen, oder gezieltes Abätzen einzelner Bereiche des fertigen Kristalls.

Durch die Möglichkeit, spezielle Strukturen mit größter Präzision herzustellen, lassen sich Halbleiter für gegebene experimentelle Zielsetzungen maßschneidern. So kann in Halbleitern zum Beispiel ein breites Spektrum an Ladungsträger-Dichten erzeugt werden, entweder bei der Herstellung durch Dotierung oder durch direkte optische oder elektrische Injektion während des Experiments. Durch die gezielte Verwendung von Materialien mit unterschiedlichen Bandlücken in Halbleiter-Heterostrukturen besteht weiterhin die Möglichkeit, die Bewegung der delokalisierten Bloch-Elektronen auf einer mesoskopischen Skala durch ein zusätzliches Potential zu beeinflussen. Wie aus den Grundlagen der Quantenmechanik bekannt, wird die Bewegung der Teilchen mit abnehmendem Abstand der Potentialwände zunehmend diskretisiert. Auf diese Weise können quasi-zweidimensionale Ladungsträger-Systeme in Quantenfilmen, eindimensionale Systeme in Quantendrähten und vollständig quantisierte Elektronen in Quantenpunkten untersucht werden. Eine weitere Möglichkeit, die Eigenschaften eines Halbleiter-Systems maßzuschneidern, auf die im weiteren Verlauf der vorliegenden Arbeit noch eingegangen wird, ist die Veränderung der Kopplungsstärke zwischen den Ladungsträgern in einer nieder-dimensionalen Quantenstruktur und dem quantisierten elektromagnetischen Feld. Dazu werden auf beiden Seiten des aktiven Materials Bragg-Spiegel aus alternierenden Materialschichten mit unterschiedlichen sta-

tischen Dielektrizitätszahlen aufgebaut. Je nachdem, ob die aktive Schicht in einem Bauch oder einem Knoten der elektromagnetischen Mode positioniert ist, ist eine stark erhöhte oder erniedrigte Kopplung zwischen Ladungsträgern und Feld zu beobachten [2, 3].

Eines der am häufigsten genutzten Instrumente zur Untersuchung von Halbleitern ist die Spektroskopie mit Licht im optischen oder im kurzwelligen Infrarot-Bereich. Auf makroskopischer Betrachtungsebene erzeugt das einfallende Licht, soweit die Energie der Photonen größer oder vergleichbar mit der Breite der Bandlücke ist, eine optische Polarisation des Mediums. In mikroskopischer Beschreibung induziert die Absorption eines Lichtquants den Übergang eines Valenz-Elektrons in eine kohärente Überlagerung eines Valenzband-Zustandes und eines Leitungsband-Zustandes. Die Phase der Oszillation wird dabei durch das einfallende Licht aufgeprägt.

Nachdem der anregende Lichtpuls das Material passiert hat, zerfällt die induzierte Polarisation mit einer Zerfallszeit von wenigen Pikosekunden. Zwei verschiedene Mechanismen tragen zu diesem Zerfall bei. Zum einen zerläuft die Phasen-Kohärenz dadurch, dass die Oszillatoren an unterschiedlichen Orten im Halbleiter leicht unterschiedliche Perioden besitzen, zum Beispiel durch eine räumliche Fluktuation des Durchmessers einer nieder-dimensionalen Struktur. Die Kohärenz eines Oszillators kann weiterhin durch die Streuung an einer Gitterschwingung oder an einem Ladungsträger zerstört werden.

In der Beschreibung eines angeregten Halbleiters ist es häufig von Vorteil, eine alternative Darstellung des Valenzbandes zu verwenden. In dieser Darstellung betrachtet man den Zustand, der unbesetzt zurückbleibt, nachdem ein Elektron ins Leitungsband angeregt wurde, als eigenständiges Teilchen. Der unbesetzte Zustand kann sich frei durch den Kristall "bewegen", indem Elektronen aus besetzten Zuständen in den freien Zustand wechseln, wobei sie dabei ihren vorherigen Zustand unbesetzt zurücklassen. Aus der Ladungs-Neutralität des gesamten Kristalls folgt, dass die Entfernung des negativ geladene Elektron ein positiv-geladenes "Loch" in der Abschirmung des Ionen-Potentials öffnet. Tatsächlich lässt sich die Bewegung aller $(N-1)$ Teilchen im Valenzband eindeutig durch die Bewegung eines positiv geladenen Loches beschreiben.

Mit dem Vorwissen der heutigen Sicht belastet, erscheint die Idee, dass sich das negative Ladungsträger-Elektron und das positive Valenzband-Loch zu einem dem Wasserstoff ähnlichen Teilchen verbinden, einem sogenannten Exziton, offensichtlich. Der erste Nachweis exzitonischer Resonanzen in Halbleitern wurde von Frenkel [4] erbracht und kurze Zeit später von Wannier [5] in der Bloch-Darstellung delokalisierter Elektronen wiederholt.

Es sei darauf hingewiesen, dass sich aus dem Auftreten wasserstoffähnlicher Spektrallinien in Absorptions- oder Lumineszenz-Messungen nicht auf die Existenz gebundener Exzitonen schließen lässt. Im Falle der Absorpti-

on wird, wie bereits erwähnt, nur eine Ein-Teilchen-Kohärenz aus Valenz- und Leitungsband-Zustand induziert, die keinen Aufschluss über einen Zwei-Teilchen-Zustand, wie es ein gebundenes Exziton darstellt, geben kann. In der Lumineszenz-Spektroskopie dagegen rekombinieren gebundene Elektron-Loch-Paare zwar unter Aussendung eines Photons mit der entsprechenden exzitonischen Energie; allerdings weist der strahlende Zerfall aus dem wechselwirkenden Elekron-Loch-Plasma die gleiche exzitonische Resonanzstruktur auf [6, 7]. In den vergangen Jahren sind deswegen neue experimentelle Methoden zur Detektion gebundener exzitonischer Besetzungen vorgeschlagen worden. So wurde zum Beispiel das gemessene Verhältnis von Lumineszenz und Absorptions-Spektrum mit den Vorhersagen der Kubo-Martin-Schwinger-Gleichung [8, 9] verglichen. Als Pass-Parameter wurde daraus die Zahl der Exzitonen emittelt [10]. In der letzten Zeit ist des Weiteren die THz-Spektroskopie in das Zentrum der Aufmerksamkeit gerückt. Durch das nieder-energetische Licht können Übergänge zwischen den exzitonischen Zuständen direkt angeregt werden, z.B. der 1s→2p Übergang. Eine hervorragende Übereinstimmung der experimentell gemessenen Spektren mit den theoretischen Vorhersagen wurde beobachtet [11–14].

Die theoretische Beschreibung von gebundenen Elektron-Loch-Paaren wird durch die Ununterscheidbarkeit der Teilchen kompliziert. Zwar ist eine Beschreibung eines gebunden Komplexes als Boson im Nieder-Dichte-Grenzfall möglich, so zum Beispiel in der Beschreibung verdünnter atomarer Gase. Für höhere Dichten treten aber signifikante Korrekturen durch die Fermionische Natur der Elektronen und Löcher auf. Eine konsistente Beschreibung gebundener Exzitonen wurde erst vor wenigen Jahren entwickelt [15].

Die vorliegende Arbeit untersucht die Eigenschaften inkohärenter Ladungsträger in zwei unterschiedlichen Situationen.

In Kapitel 2 wird die Stabilität gebundener Exzitonen gegenüber der Streuung mit Ladungsträgern und Gitterschwingungen untersucht. Zu diesem Zweck werden gekoppelte Bewegungsgleichungen für die relevanten Erwartungswerte hergeleitet. Die Vielteilchen-Hierarchie, die aus der Einbindung von Zwei-Teilchen-Wechselwirkungen in den Hamilton-Operator resultiert, wird durch die Cluster-Entwicklung [16–18] konsistent auf der Zwei-Teilchen-Ebene terminiert. Diese Entwicklung ermöglicht es, jeden N-Teilchen-Erwartungswert rigoros in echte N-Teilchen Korrelation und triviale Beiträge durch Korrelationen niedrigerer Ordnung aufzuspalten. Die Cluster-Entwicklung stellt damit sicher, dass bei dem Abbruch der Vielteilchen-Hierarchie auf der Zwei-Teilchen-Ebene die volle Dynamik der Singlet- und Doublet-Terme in den Bewegungsgleichung enthalten ist, und nur echte Drei-Teilchen-Korrelationen vernachlässigt werden. Die Extraktion einer physikalisch sinnvollen Exzitonen-Zahl aus den Elektron-Loch-Doublets wird durch

Gleichung (2.11) beschrieben.

Es sei darauf hingewiesen, dass die Ankopplung der Gitterschwingungen an die Ladungsträgerdichten aus numerischen Gründen nicht voll dynamisch berücksichtigt wird. Statt dessen nähern wir die Besetzung der Schwingungsmoden durch eine Bose-Einstein-Verteilung an. Korrelierte Phonon-Elektron-Erwartungswerte werden in Markov-Näherung beschrieben.

In Abschnitt 2.5 werden die Anfangsbedingungen für die numerische Integration der Bewegungsgleichungen diskutiert. Da insbesonderen physikalisch sinnvolle Anfangswerte für die Zwei-Teilchen-Korrelationen nicht bekannt sind, werden die Rechnungen für eine gegebene Dichte und Temperatur jeweils für mehrere unterschiedlichen Anfangsbedingungen wiederholt. Dieses Vorgehen wird im Nachhinein durch die Konvergenz der Rechnungen auf den selben Gleichgewichtszustand gerechtfertigt.

Da in den präsentierten Rechnungen die strahlende Rekombination von Elektronen und Löchern nicht beinhaltet ist, stellt auf obige Weise berechnete Anteil X_f der Elektronen und Löcher, die in gebundenen Paaren vorliegen, nur eine obere Grenze für den Wert dar, der in einer realen Halbleiterstruktur erwartet wird. Die Abhängigkeit des Exzitonen-Anteils X_f von den Ladungsträger-Dichten und den Gittertemperaturen wird in Abschnitt 2.6 dargestellt und diskutiert. Ein maximaler Anteil von $X_f \leq 0.4$ wird für die niedrigste Dichte bei niedrigster Temperatur vorhergesagt. Mit steigender Dichte oder Temperatur fällt X_f stark ab. Die dynamisch berechneten Werte von X_f werden mit den Vorhersagen eines einfachen Massenwirkungs-Gesetzes, wie es in den Lehrbüchern zu finden ist, verglichen.

Abschnitt 2.7 stellt eine Ergänzung zu den Ergebnissen dar, die in Ref. [15] veröffentlicht wurden. Während in dem zitierten Artikel die Bildungsraten von 1s Exzitonen untersucht wurden, werden in dieser Arbeit die Zerfallszeit von anfänglich erzeugten 2p- und 2s-Besetzungen untersucht. Zerfallszeiten in den Größenordnung der 1s-Bildungsraten werden errechnet.

In Kapitel 3 wird die Auswirkung inkohohärenter Ladungsdichten und Zwei-Teilchen-Korrelationen auf die Absorption untersucht. Insbesondere werden die experimentellen Funde zur anregungsinduzierten Dephasierung (excitation induced dephasing, EID) [19–22] sowie zum energetischen Schieben der Exziton-Resonanz [23–25] theoretisch untersucht. Das zur Berechnung der Spektren verwendete theoretische Modell und die Herleitung der Bewegungsgleichung sind in Abschnitt 3.2 zu finden. In 3.3 werden noch keine inkohärenten Zwei-Teilchen-Korrelationen berücksichtigt; statt dessen wird der Einfluss unkorrelierter Ein-Teilchen-Dichten mittels der verschiedenen Elemente der Bewegungsgleichungen verdeutlicht.

Bei Berücksichtigung der Zwei-Teilchen-Korrelation in Abschnitt 3.4 wird ein ausgeprägter Effekt durch gebundene Elektron-Loch-Paare beobachtet.

Nicht-diagonale Elektron-Loch-Korrelationen, sowie Elektron-Elektron- und Loch-Loch-Korrelationen haben dagegen nur einen vernachlässigbar kleinen Einfluss auf das Absorptionsspektrum. In der Analyse der Veränderung der Absorption durch gebunden Paare wird festgestellt, dass bezüglich der anregungsinduzierten Dephasierung und dem Abschirmen des Coulomb-Potentials die Bildung von Exzitonen den gleichen Effekt hat wie eine Verringerung der Dichte, während die Reduzierung der Oszillator-Stärke durch Phasen-Raum-Füllung nicht beeinflusst wird. Diese Beobachtung korrespondiert direkt mit den physikalischen Eigenschaften von Exzitonen. Es wird erwartet, dass sowohl die Streurate der Teilchen (durch die Bindung an den Partner) als auch die Abschirmung (durch die Neutralität der Gesamtladung im Exziton) im gebundenen Zustand reduziert wird. Dem entgegen besetzen auch die gebundenen Teilchen unverändert die Zustände im Phasenraum, so dass keine Reduzierung der Pauli-Abstoßung zu erwarten ist.

Die wichtigsten Ergebnisse der Arbeit sind in Kapitel 4 zusammengetragen. Zur Verbesserung der numerischen Stabilität der Gleichtgewichtsrechnungen wird eine höhere numerische Auflösung der Stützstellen in der Impulsdarstellung empfohlen. Des weiteren schlagen wir eine Erweiterung des Modells um die Beschreibung longitudinaler optischer (LO) Phononen vor, Dadurch lässt sich zum einen die schnelle Dynamik heißer Ladungsträgerverteilungen in GaAs beschreiben; zum anderen aber ist die Einbindung von LO-Phononen notwendig in der Beschreibung polarer Kristalle, so zum Beispiel Zink-Selenid (ZnSe), in denen die Wechselwirkung der Ladungsträger mit optischen Phononen stark erhöht ist im Vergleich zu nicht-polaren Halbleitern. Die Beschreibung der Exzitonen-Dynamik in ZnSe-basierten Strukturen ist unter anderem wegen der wesentlich größeren Bindungsenergie der Exzitonen in ZnSe interessant.

Bezüglich der Absorptionsrechnungen wird angeregt, zwei-dimensionale Systeme zu modellieren, um einen direkten Vergleich mit experimentell gemessenen Spektren zu ermöglichen. Die numerische Komplexität könnte dabei dadurch verringert werden, dass nur die Ein-Teilchen-Dichten und die diagonale Exziton-Korrelationen in den Rechnungen berücksichtigt werden, da Elekron-Elektron-, Loch-Loch- und nicht-diagonale Exziton-Korrelationen die Absorption nicht wesentlich beeinflussen.

In den Anhängen A und B werden die effektive ein-dimensionale Coulomb Wechselwirkung, sowie eine Verallgemeinerung der Wannier-Gleichung für endliche Ladungsträger-Dichten hergeleitet. Die numerische Stabilität der Gleichgewichtsrechnungen und die Wahl der Dephasierungskonstante für die dichteassistierten Polarisationen werden in den Anhängen C und D diskutiert. Anhang E gibt eine Übersicht über die Parameter, welche das modellierte Halbleiter-System charakterisieren.

Contents

Chapter 1

Introduction

From a scientific point of view, shedding light on semiconductors has a history of $\Delta t \approx 1.7 \times 10^2$ years [1]. During this time, locked in a feed-back loop with new applications, the scientific interest in semiconductors has continuously expanded. Hallmarks, which provided strong impulses for the development of the field, were the building of the first solar cell in 1887, the invention of the transistor in 1947, and the proposal and realization of semiconductor lasers in the 1960's [26]. In step with this development the manufacturing of semiconductor devices has seen constant refinement. Today, the average feature size on silicon chips is down to a mere 65 nanometers, with the perspective to reach 45 nm by 2008. Due to a comparable progress in epitaxy techniques, present-day semiconductor heterostructures are grown with unprecedented precision, offering the possibility to control the alloy composition of single atomic layers. Combined with nano-structuring techniques, such as selective etching or the self assembly of quantum dots, semiconductor structures can precisely be customized to a seemingly countless number of applications.

It is thus not surprising, that semiconductor heterostructures have been found to provide an ideal test bed for a wide range of experiments. With the ability to control the carrier density via doping, electric injection or optical excitation, the properties of both dilute and dense carrier plasmas can be studied. In semiconductor heterostructures, the carrier dynamics can be modified further, since the differences between the band gaps of the layers create mesoscopic potential landscapes for the carriers, thereby confining them. With decreasing width of the confinement regions, the motion of the carriers becomes quantized in the respective directions, reducing the carrier dynamics to two dimensions in so-called quantum wells, to one dimension in quantum wires, or even completely confining them to quantum dots. Another customizing option which is of importance for the work presented here is the possibility to change the coupling of the carriers to the quantized light field. For this, distributed Bragg mirrors are grown from alternating layers of materials with

different dielectric constants on both sides of the material. In this way, e.g. microcavities can be grown in which normal mode splitting between the cavity mode of the light field and the exciton resonance of the carrier plasma is observed [2]. Conversely, by placing the semiconductor in a field antinode of the cavity, the decreased light-matter coupling leads to a reduction of the radiative recombination rates [3].

Spectroscopy with lasers operating at optical or near-infrared frequencies has proven to be an invaluable tool for probing a wide range of properties of semiconductors. An incident beam with energy close to or exceeding the band gap of the material shifts the charge carriers from their equilibrium positions, thereby inducing a macroscopical polarization. Microscopically, this polarization corresponds to an excitation of electrons from the valence band into a coherent superposition of a valence-band state and a conduction-band state. The superposition oscillates in phase with the driving laser field.

After the laser pulse has traversed the sample, the macroscopic polarization of the sample decays on a picosecond timescale, governed by two distinct mechanisms. In the first, the phase coherence of the local oscillators spreads out due to spatial variations in the eigenfrequencies, e.g. caused by fluctuation in the width of the quantum well structure. In the second process, the phase is destroyed by scattering events with vibrations of the crystal lattice or with other charge-carriers.

For the following discussion, it is convenient to switch to a different picture for the description of the carriers within the valence band. In the ground state of an undoped semiconductor the positive charge of the ions is screened out by the surrounding electron cloud, ensuring the charge neutrality of the crystal. Thus, the excitation of a freely moving negative charge into the conduction band leaves behind a charge of the same size but with reversed sign at the vacated site in the valence band, where the positive charge of the ions is no longer screened by the electron. This empty site travels through the semiconductor as electrons from occupied sites move into the currently vacant state. In this picture, the dynamics of the $N-1$ electrons in the valence band are alternatively described as the movement of a single positively charged carrier, the so-called hole.

The picture of oppositely charged and freely moving electrons and holes raises the notion of the formation of bound electron-hole pairs, called excitons. Excitonic resonances in solid state bodies have first been described by Frenkel [4]. Wannier [5] reproduced Frenkels results in the basis of delocalized Bloch particles, showing the equivalence of the eigenequation of an interacting electron-hole pair with the Schrödinger equation of the hydrogen atom.

It it important to note, however, that the occurence of the 1s-resonance energy in absorption and photoluminescence does not imply the creation or decay of a bound electron-hole pair. As already mentioned, the absorption of a pho-

ton excites a *single* electron into a coherent superposition of a conduction- and valence-band state. Accordingly, the corresponding microscopic polarization is a one-particle quantity only and as such does not carry information about the existence of the two-particle complex of a bound pair. Similarly, it was pointed out a few years ago [6,7] that excitonic resonances observed in photoluminescence spectroscopy may equally be due to a resonance of the single-particle plasma or bound electron-hole pairs. Therefore, new experiments to probe the existence of bound electron-hole pairs have been suggested. In a recent experiment [10], the number of bound electron-hole pairs was obtained by comparing of the relation between experimental of luminescence and absorption spectroscopy with the predictions of the Kubo-Martin-Schwinger relation [8,9]. In a more direct approach, transitions between different excitonic states, e.g. the 1s→2p transition, are resonantly excited. Due to the small exciton binding energies THz fields are required to probe these transitions [11–14]. Excellent agreement between theoretical predictions and experimental spectra was reported.

As a further complication, the theoretical description of bound electron-hole pairs is not immediately clear, either. If the separation between the molecules is large compared to the Bohr radius, the composite particles can approximately be described as Bosons. With decreasing distance, however, corrections due to the Fermionic nature of the electrons and holes become increasingly important. In particular, these corrections prevent the rigorous definition of a number operator. A consistent theoretical description of bound excitons has only recently been introduced [15].

The presented work examines the properties of incoherent populations and two-particle correlations in two separate situations. In Chapter 2, the stability of bound electron-hole pairs against scattering with lattice vibrations and charge carriers is investigated. A best-case analysis is carried out to determine the equilibrium fraction X_f of bound electron-hole pairs in a coupled carrier-phonon system. The dependence of X_f on the density of the carriers and the lattice temperature of the sample is discussed. Additionally, the phonon-induced decay rates of higher excitonic states are investigated.

In Chapter 3 the effects of incoherent carrier densities and two-particle correlations on the coherent dynamics are explored, focussing on the reduction of the oscillator strength, broadening of the resonance by excitonic induced dephasing, and the energetic position of the lowest exciton resonance.

Chapter 2

Stability of Excitonic Populations

2.1 Model System

2.1.1 Quantum-Wire Structure

Two-dimensional heterostructures, so called quantum wells, provide an ideal test system for a wide range of measurements, due to the customizability of physical parameters they offer. The key to this customizability are the semiconductor growth techniques, notably metalorganic vapour phase epitaxy and molecular beam epitaxy, which provide precise control over the constituents of the grown crystal down to single atom layers. This allows the grower to place sheets of materials with different bandgaps next to each other, resulting in a variation of the potential landscape for the electrons. The movement of the electrons in the growth directions may thus become quantized to a series of subbands with an energetic structure which can be finely tuned via the thickness of the quantum-well layer. Furthermore, the strength of the light-matter coupling can be enhanced by growing distributed Bragg mirrors from alternating layers of materials with different background dielectric constants on both sides of the quantum well. Due to the constant improvement of the growth processes present day samples of quantum wells are of extraordinary high quality, with vanishing interface roughness.

In order to directly model experimentally accessible systems it would therefore be advantageous to use a two-dimensional model system for the theoretical analysis. However, as will be discussed in more detail in the next section, the description of bound electron-hole pairs in the density matrix approach necessarily involves the calculation of the two-particle correlations. These are functions of 3 independent vector variables $\mathbf{k}$, each of which has the dimensionality d of the heterostructure. With a further order of complexity arising from

the Coulomb interaction between the carriers, the number of instructions that have to be executed in each timestep of the numerical integration is of order $\mathcal{O}(N^{3d+1})$, where N is the amount of points in the numerical grid. Unfortunately, for the dynamical processes under investigation here, the computional power of today's computers is already reached for $d = 1$, thus forcing us to restrict our model to the description of an one-dimensional quantum wire.

In general, the material parameters of the modeled quantum-wire system were set to the values measured in bulk Gallium-Arsenide (GaAs), including the reduced mass, the static dielectric constant, the phonon coupling constants, and the gap energy. However, in order to reduce the extension of the hole distributions in wave-vector space, and hence the number of grid points required in the numerical evaluation, the ratio of the effective masses of electron and holes was changed from the GaAs value of $m_e/m_h \approx 0.15$ to $m_e/m_h = 1/3$. The effect of this change on the calculated equilibrium exciton fractions was numerically confirmed to be minor. The effective radius of the confinement potential was chosen such that the 1s binding energy was of the order of 10 meV for vanishing carrier densities, which is comparable to the one found in two-dimensional quantum wells. A complete list of the simulation parameters is found in Appendix E.

Although we restrict our calculations to a one-dimensional model, the following derivations are valid also for two- or three-dimensional systems. Vectors $\mathbf{r}$ are written in the notation $\mathbf{r} = (\mathbf{r}_{\|}, \mathbf{r}_{\perp})$, where $\mathbf{r}_{\|}$ indicates the components parallel to heterostructure and $\mathbf{r}_{\|}$ those perpendicular to it.

2.1.2 Photonic Environment

The carrier populations excited by an initial light pulse in the conduction and valence bands are not constant in time, but typically decay on a nanosecond timescale, thus reverting the semiconductor back to the unexcited ground state. Neglecting losses due to carriers escaping from the quantum well, this decay is governed by electron-hole recombination processes, most notably recombination at lattice defects, radiative decay due to the coupling to the electromagnetic field or direct and phonon-assisted Auger processes [27]. Obviously, the decay of the populations directly competes with the formation of excitons, which has been reported to take place on the same nanosecond timescale [15]. In order to investigate an equilibration of the exciton formation, we thus need to look for a semiconductor system in which the recombination rate is sufficiently slow.

A significant decay of electron-hole population is caused by the coupling of the charge carriers to the electro-magnetic field, which limits the lifetime of the excitons to the order of a few nanoseconds. [28] This is due to the possibility of radiative recombination of the carriers, where the electron spontaneously

merges with the hole in the conduction band under emission of a photon. The energy of the emitted photon is given by the energy difference between the electron and the hole, which, for GaAs-based semiconductors is of the order of 1.4 meV. Furthermore, the momentum parallel to the heterostructure is conserved, so that the center-of-mass momentum $\mathbf{q}_{||}$ of an exciton may not exceed the photon wave number. Since a photon energy of $h\nu = 1.4$ meV corresponds to a wave number $|\mathbf{p}| \approx 10^{-1} a_0^{-1}$ while the $\mathbf{q}_{||}$ distribution for the bound electron-hole pairs usually extends to $\sim 2a_0^{-1}$ for the temperature and density regime considered in this thesis, it follows that only excitons with very low center-of-mass momentum may recombine radiatively, leading to a strongly non-thermal distribution of excitons, as reported in Refs. [3, 15, 28] and preventing the system from equilibrating at a steady state. In our calculations, we have therefore set the coupling of the carriers with the light-field to zero. Experimentally, such a suppression of the radiative recombination may be realized by placing the heterostructure in a field node of a photonic environment [3, 29–31].

Obviously, with no decay mechanism present in the theoretical model, a best-case scenario of the correlated electron-hole populations is simulated and thus only an upper limit to the number of bound excitons for given densities and temperatures is obtained. The system does, however, provide an ideal testbed to study the interplay between the carrier distributions on the one hand and two-particle correlations on the other hand.

2.2 Theoretical Description

2.2.1 Cluster Expansion

In a two-component plasma which can form bound complexes, such as an electron-hole gas in a semiconductor system, a number operator the composite particles can not easily be defined [32]. By treating the bound electron-hole pairs in a first approximation as a separate species, the dynamics of the correlated plasma may be described by rate-equations for the conversion between the free electron and hole distributions, and exciton populations [33,34]. While this approach has phenomenologically been applied to dilute-plasma situations (such as hydrogen atoms, electrons and protons) over a wide range of densities and temperatures, it is expected to break down for increasingly dense plasmas, where the Fermionic nature of the composite particles becomes important.

In this work a microscopic description of the semiconductor is utilised, where only the carriers are treated as elementary species. Consequently, we start by setting up the equations of motion for the electron and hole densities. A physically meaningful exciton number is afterwards extracted from the state of the correlated carrier plasma.

The maximal obtainable information of a many-body system is given by the dynamics of the many-body density matrix $\hat{\rho}(t)$. With the knowledge of $\hat{\rho}(t)$ the expectation value of any many-body observable $\hat{A}$ can be calculated by the trace $\mathrm{tr}(\hat{\rho}(t)\hat{A})$ taken with any complete set of many-body eigenfunctions. Instead of calculating the time evolution of $\hat{\rho}(t)$ it is often advantageous to switch into the Heisenberg picture, where the density matrix $\hat{\rho}_{\mathrm{H}}(t) = \hat{\rho}(t_0)$ is described as being constant in time, while the dynamics of the system are incorporated into the time-evolution of the operators $\hat{A}_H(t)$. In this picture the equation of motion for an operator are obtained from the Heisenberg equation

$$i\hbar\frac{\partial}{\partial t}\hat{A}_{\mathrm{H}}(t) = [\hat{A}_{\mathrm{H}}, \hat{H}] \,, \tag{2.1}$$

where $\hat{H}$ is the Hamilton operator of the system. In the following, we use the Heisenberg picture for all operators and consequently drop the subscript H.

In order to obtain the expectation value $\langle\hat{A}(t)\rangle$ at a time t via Eq. (2.1) the knowledge of either $\hat{\rho}(t_0)$ or of an initial expectation value $\langle\hat{A}(0)\rangle = \mathrm{tr}(\rho(t_0)\hat{A}(t))$ is required. The quantities $\langle\hat{A}(t)\rangle$ at an arbitrary time t can then be obtained by taking the expectation value of Eq. (2.1) and numerically integrating the resulting equation from the initial value. It is clear, however, that the commutator between $\hat{A}$ and $\hat{H}$ on the right hand side of Eq. (2.1) may couple the dynamics of $\hat{A}(t)$ to those of other operators. In particular, any two-particle interaction, e.g. as the Coulomb Hamiltonian H_{Coul} or the electron-phonon interaction $H_{\mathrm{el-phon}}$, introduces a coupling of an M-particle operator to $M+1$-particle operators, leading to the so-called many-body hierarchy of equations of motion. Therefore, in order to calculate the full dynamics of a one-particle quantity one would have to extend the calculations first to the second-particle level, then to three-particles, up to and including the full N-particle level, where N is the number of carriers in the system. The $(N+1)$-particle expectation values vanish exactly.

Since the calculation of the full set of equations for a many-body system is not feasible numerically, a consistent scheme for the truncation of the hierarchy of equations has to be devised. In a first step we describe the system in the Hartree-Fock mean-field approximation by assuming that the N-particle wave function is given by a Slater determinant. It is easy to show that in this case an N-particle quantity $\langle\hat{a}_1^\dagger\cdots\hat{a}_N^\dagger\hat{a}_N\cdots\hat{a}_1\rangle$ containing N Fermionic creation and annihilation operators $\hat{a}_i^\dagger$ and $\hat{a}_i$, respectively, factorizes identically into products of single-particle expectation values according to

$$\langle\hat{a}_1^\dagger\cdots\hat{a}_N^\dagger\hat{a}_N\cdots\hat{a}_1\rangle = \sum_P(-1)^{\mathrm{sgn}(P)}\langle\hat{a}_1^\dagger\hat{a}_{P(N)}\rangle\langle\hat{a}_2^\dagger\hat{a}_{P(N-1)}\rangle\cdots\langle\hat{a}_N^\dagger\hat{a}_{P(1)}\rangle \,, \tag{2.2}$$

where the sum runs over all permutations P of the set $\{N, N-1, \ldots, 1\}$. The sign of the permutation $\mathrm{sgn}(P)$ as exponent to (-1) ensures antisymmetry of the Fermionic operators. In this approximation, since all higher order

correlations factorize, the physical information is completely contained in the single-particle quantities and the carriers behave like a system of N independent particles moving in the averaged field of the other particles.

In a next step, the two-particle correlations $\Delta\langle\hat{a}_1^\dagger\hat{a}_2^\dagger\hat{a}_3\hat{a}_4\rangle$ are introduced as the difference between the full four operator term and its Hartree-Fock part

$$\Delta\langle\hat{a}_1^\dagger\hat{a}_2^\dagger\hat{a}_3\hat{a}_4\rangle = \langle\hat{a}_1^\dagger\hat{a}_2^\dagger\hat{a}_3\hat{a}_4\rangle - \Big(\langle\hat{a}_1^\dagger\hat{a}_4\rangle\langle\hat{a}_2^\dagger\hat{a}_3\rangle - \langle\hat{a}_1^\dagger\hat{a}_3\rangle\langle\hat{a}_2^\dagger\hat{a}_4\rangle\Big) \ . \tag{2.3}$$

With this definition it is ensured that only the two-particle correlations beyond the trivial one-particle contribution are contained in $\Delta\langle\hat{a}_1^\dagger\hat{a}_2^\dagger\hat{a}_3\hat{a}_4\rangle$. In this sense, $\Delta\langle\hat{a}_1^\dagger\hat{a}_2^\dagger\hat{a}_3\hat{a}_4\rangle$ describe the "true" two-particle correlations.

In the generalization of this method to correlations between arbitrary numbers of particles, we abbreviate expectation values containing M creation and annihilation operators with $\langle M, M\rangle$ and subsequently define the true N-particle correlations recursively via

$$\Delta\langle N, N\rangle \equiv \langle N, N\rangle - \Big\{\Delta\langle N-1, N-1\rangle, \Delta\langle N-2, N-2\rangle, \ldots, \langle 1, 1\rangle\Big\} \ , \tag{2.4}$$

where the curled braces indicate the sum over all possible factorizations of $\langle N, N\rangle$ into products of correlations up to the $(N-1)$-particle level. This definition of the multiplets $\Delta\langle N, N\rangle$ allows the consistent truncation of the hierarchy of equations in a physically meaningful way: By setting $\Delta\langle M, M\rangle = 0$ for $M > N$, one disallows the formation of complexes containing more than N particles, while the dynamics up to the N-particle level is fully included. This so-called cluster-expansion has long been used in quantum-chemistry [16–18], but has already been successfully applied to a semiconductor system to describe the formation of excitons from incoherent carrier densities [15, 35].

Due to the limitations in available computational power, in this thesis we have restricted the numerical evaluation of the carrier-dynamics to the singlet/doublet level, i.e. only single-particle and two-particle expectation values are calculated dynamically, while all three-particle expectations values are set to zero. In the incoherent limit the only non-zero expectation values are the carrier distributions in band λ

$$f^\lambda_{\mathbf{k}_\parallel} = \langle\hat{a}^\dagger_{\lambda,\mathbf{k}_\parallel}\hat{a}_{\lambda,\mathbf{k}_\parallel}\rangle \ , \tag{2.5}$$

and the two-particle correlations

$$c_e(\mathbf{q}_\parallel, \mathbf{k}'_\parallel, \mathbf{k}_\parallel) = \Delta\langle\hat{a}^\dagger_{c,\mathbf{k}_\parallel}\hat{a}^\dagger_{c,\mathbf{k}'_\parallel}\hat{a}_{c,\mathbf{k}'_\parallel+\mathbf{q}_\parallel}\hat{a}_{c,\mathbf{k}'_\parallel-\mathbf{q}_\parallel}\rangle \ , \tag{2.6}$$

$$c_h(\mathbf{q}_\parallel, \mathbf{k}'_\parallel, \mathbf{k}_\parallel) = \Delta\langle\hat{a}^\dagger_{v,\mathbf{k}_\parallel}\hat{a}^\dagger_{v,\mathbf{k}'_\parallel}\hat{a}_{v,\mathbf{k}'_\parallel+\mathbf{q}_\parallel}\hat{a}_{v,\mathbf{k}'_\parallel-\mathbf{q}_\parallel}\rangle \ , \tag{2.7}$$

$$c_X(\mathbf{q}_\parallel, \mathbf{k}'_\parallel, \mathbf{k}_\parallel) = \Delta\langle\hat{a}^\dagger_{c,\mathbf{k}_\parallel}\hat{a}^\dagger_{v,\mathbf{k}'_\parallel}\hat{a}_{c,\mathbf{k}'_\parallel+\mathbf{q}_\parallel}\hat{a}_{v,\mathbf{k}'_\parallel-\mathbf{q}_\parallel}\rangle \ . \tag{2.8}$$

Here, $c_e(\mathbf{q}_\parallel, \mathbf{k}'_\parallel, \mathbf{k}_\parallel)$ and $c_h(\mathbf{q}_\parallel, \mathbf{k}'_\parallel, \mathbf{k}_\parallel)$ are the electron-electron and hole-hole correlations, respectively, while correlations between electrons and holes, and thus the information about bound particles, are contained in $c_X(\mathbf{q}_\parallel, \mathbf{k}'_\parallel, \mathbf{k}_\parallel)$.

2.2.2 Exciton Fraction

From Eq. (2.8) it is seen, that $c_X(\mathbf{q}_\parallel, \mathbf{k}'_\parallel, \mathbf{k}_\parallel)$ is defined in terms of the single-particle operators $\hat{a}^\dagger_{\lambda,\mathbf{k}_\parallel}$ and $\hat{a}_{\lambda,\mathbf{k}_\parallel}$, which describe the creation and annihilation of a single quasi particle with wave vector $\mathbf{k}_\parallel$ in the valence or conduction band, respectively. It is therefore not clear *a priori* how the information about bound excitons can be extracted from $c_X(\mathbf{q}_\parallel, \mathbf{k}'_\parallel, \mathbf{k}_\parallel)$. To this end we define excitonic operators

$$\hat{X}^\dagger_{\nu,\mathbf{q}_\parallel} = \sum_{\mathbf{k}_\parallel} \left[\Phi_{\nu,\mathbf{q}_\parallel}(\mathbf{k}_\parallel)\right]^* \hat{a}^\dagger_{c,\mathbf{k}_\parallel+\mathbf{q}^e_\parallel} \hat{a}_{v,\mathbf{k}_\parallel-\mathbf{q}^h_\parallel} \tag{2.9}$$

$$\hat{X}_{\nu,\mathbf{q}_\parallel} = \sum_{\mathbf{k}_\parallel} \Phi_{\nu,\mathbf{q}_\parallel}(\mathbf{k}_\parallel) \hat{a}^\dagger_{v,\mathbf{k}_\parallel-\mathbf{q}^h_\parallel} \hat{a}_{c,\mathbf{k}_\parallel+\mathbf{q}^e_\parallel} \ , \tag{2.10}$$

where $\Phi_{\nu,\mathbf{q}_\parallel}(\mathbf{k}_\parallel)$ are the eigenfunctions of the generalized Wannier equation introduced in Appendix B. Thus, $\hat{X}^\dagger_{\nu,\mathbf{q}_\parallel}$ and $\hat{X}_{\nu,\mathbf{q}_\parallel}$ create or annihilate interband coherences, whose momentum distributions correspond to those of a bound electron-hole pair with relative wave vector $\mathbf{k}_\parallel$ and center-of-mass momentum $\mathbf{q}_\parallel$. With Eqs (2.9) and (2.10) correlations $\Delta\langle \hat{X}^\dagger_{\nu,\mathbf{q}_\parallel} \hat{X}_{\nu',\mathbf{q}_\parallel}\rangle$ between two excitonic operators are written as

$$f_\nu(\mathbf{q}_\parallel) \equiv \Delta\langle \hat{X}^\dagger_{\nu,\mathbf{q}_\parallel} \hat{X}_{\nu',\mathbf{q}_\parallel}\rangle = \sum_{\mathbf{k}_\parallel,\mathbf{k}'_\parallel} [\Phi_{\nu',\mathbf{q}_\parallel}(\mathbf{k}'_\parallel)]^* \Phi_{\nu,\mathbf{q}_\parallel}(\mathbf{k}_\parallel) c_X(\mathbf{q}_\parallel, \mathbf{k}'_\parallel - \mathbf{q}^h_\parallel, \mathbf{k}_\parallel + \mathbf{q}^e_\parallel) \ . \tag{2.11}$$

It has been shown that the quantity

$$n_\nu = \sum_{\mathbf{q}_\parallel} f_\nu(\mathbf{q}_\parallel) \tag{2.12}$$

is a measure for the density of excitons in state ν [36]. Correspondingly, $f_\nu(\mathbf{q}_\parallel)$ gives the distribution of the center-of-mass momentum $\mathbf{q}_\parallel$ of the excitons. Since in thermal equilibrium the majority of the excitons can be expected to be in the 1s ground state, we define the quantity

$$X_f \equiv \frac{n_{1\mathrm{s}}}{n_e} = \frac{1}{n_e} \sum_{\mathbf{q}_\parallel} \Delta\langle \hat{X}^\dagger_{1\mathrm{s},\mathbf{q}_\parallel} \hat{X}_{1\mathrm{s},\mathbf{q}_\parallel}\rangle \tag{2.13}$$

as the fraction of the total electron density n_e which forms bound 1s excitons.

On a side note it may be pointed out that the full dynamics of the system cannot be described in terms of the exciton operators, since for example any carrier expectation value containing only either electron or hole operators

cannot be expressed in terms of $\hat{X}^\dagger_{\nu,\mathbf{q}_\parallel}$ and $\hat{X}_{\nu,\mathbf{q}_\parallel}$ [3, 15]. The dynamical calculations are therefore carried out in terms of single-particle operators $\hat{a}^\dagger_{\lambda,\mathbf{k}_\parallel}$ and $\hat{a}_{\lambda,\mathbf{k}_\parallel}$, while the exciton fraction X_f is extracted from $c_X(\mathbf{q}_\parallel, \mathbf{k}'_\parallel, \mathbf{k}_\parallel)$ afterwards via Eq. (2.11). It is, however, possible to express the electron-hole correlation $c_X(\mathbf{q}_\parallel, \mathbf{k}'_\parallel, \mathbf{k}_\parallel)$ via the excitonic operators by using the completeness of the exciton basis functions. Multiplying Eqs (2.9) with $\Phi_{\nu,\mathbf{q}_\parallel}(\mathbf{k}_\parallel)$ and (2.10) with $\left[\Phi_{\nu,\mathbf{q}_\parallel}(\mathbf{k}_\parallel)\right]^*$ yields, after summation over ν,

$$\hat{a}^\dagger_{c,\mathbf{k}_\parallel+\mathbf{q}^e_\parallel}\hat{a}_{v,\mathbf{k}_\parallel-\mathbf{q}^h_\parallel} = \sum_\nu \Phi_{\nu,\mathbf{q}_\parallel}(\mathbf{k}_\parallel)\hat{X}^\dagger_{\nu,\mathbf{q}_\parallel} \tag{2.14}$$

$$\hat{a}^\dagger_{v,\mathbf{k}_\parallel-\mathbf{q}^h_\parallel}\hat{a}_{c,\mathbf{k}_\parallel+\mathbf{q}^e_\parallel} = \sum_\nu \left[\Phi_{\nu,\mathbf{q}_\parallel}(\mathbf{k}_\parallel)\right]^* \hat{X}_{\nu,\mathbf{q}_\parallel} \ . \tag{2.15}$$

With this, the inverse transformation of Eq. (2.11) is obtained as

$$c_X(\mathbf{q}_\parallel, \mathbf{k}'_\parallel - \mathbf{q}^h_\parallel, \mathbf{k}_\parallel + \mathbf{q}^e_\parallel) = \sum_{\nu,\nu'} [\Phi_{\nu,\mathbf{q}_\parallel}(\mathbf{k}_\parallel)]^* \Phi_{\nu',\mathbf{q}_\parallel}(\mathbf{k}'_\parallel) \Delta\langle \hat{X}^\dagger_{\nu,\mathbf{q}_\parallel}\hat{X}_{\nu',\mathbf{q}_\parallel}\rangle \ , \tag{2.16}$$

which allows the calculation of $c_X(\mathbf{q}_\parallel, \mathbf{k}'_\parallel, \mathbf{k}_\parallel)$ corresponding to a given exciton distribution $f_\nu(\mathbf{q}_\parallel)$.

2.2.3 Phonons

While the doublet level of the cluster expansion contains the information about the *state* of the correlated pairs of carriers, including excitons, it does not fully describe the *dynamics* of the two-particle expectation values. Specifically, the formation of bound excitons out of two free particles requires the interaction of the electron-hole pair with a third particle, e.g. an electron or a phonon, which absorbs the excess energy ΔE and momentum $\Delta\mathbf{k}_\parallel$. Similarly, the scattering of an exciton from center-of-mass momentum $\mathbf{q}_\parallel$ towards $\mathbf{q}'_\parallel$ is governed by a three-particle process in which the wave vectors of both electron and hole are changed while ΔE and $\Delta\mathbf{k}_\parallel$ are transfered to the third scattering participant. Therefore, in order to describe the formation as well as the center-of-mass dynamics of excitons, triplet contributions need to be included into the calculations.

In the density and temperature regime considered in this work, both electrons and longitudinal acoustical (LA) phonons are effective in taking up the excess energy and momentum of such processes. However, in order to keep the numerical complexity at a manageable level, only scattering events involving two carriers and one phonon have been included in the theoretical model, while processes involving three charge carriers have been neglected. The reason to include the former process is that the excess energy of the exciton formation

process is directly transfered out of the carrier system into the phonon bath, while for the latter process ΔE and $\Delta\mathbf{k}_\parallel$ are conserved within the carrier-system so that the build-up of an exciton-population is accompanied by a significant heating of the electron-hole plasma.

In the following we briefly examine the inclusion of Bosonic operators into the framework of the cluster expansion. A principal difference between the Fermionic carrier operators and the Bosonic phonon operators is seen in the electron-phonon interaction Hamiltonian $H_{\mathrm{el-phon}}$ given in Eqs (2.45) and (2.46), where the carrier operators appear in pairs of one annihilation operator $\hat{a}_{\lambda,\mathbf{k}_\parallel}$ and one creation operator $\hat{a}^\dagger_{\lambda,\mathbf{k}'_\parallel}$, while the Boson operators $\hat{D}^\dagger_{\mathbf{p}_\parallel,\mathbf{p}_\perp}$ and $\hat{D}_{\mathbf{p}_\parallel,\mathbf{p}_\perp}$ appear singly. This reflects the nature of the scattering process described in $H_{\mathrm{el-phon}}$, where a single electron is scattered out of its initial state $\mathbf{k}_\parallel$ into the final state $\mathbf{k}'_\parallel$ under absorption or emission of one LA phonon. The coupling of the phonon system to the carrier dynamics via $H_{\mathrm{el-phon}}$ thus results in a formal equivalence of one phonon operator to a pair of carrier creation and annihilation operators. This equivalence provides a method to consistently include phonon operators into the cluster expansion, e.g. the doublet contribution to phonon-assisted densities $\langle\hat{D}\hat{a}^\dagger_{\lambda,\mathbf{k}_\parallel}\hat{a}_{\lambda,\mathbf{k}_\parallel}\rangle$ is given by

$$\Delta\langle\hat{D}\hat{a}^\dagger_{\lambda,\mathbf{k}_\parallel}\hat{a}_{\lambda,\mathbf{k}_\parallel}\rangle = \langle\hat{D}\hat{a}^\dagger_{\lambda,\mathbf{k}_\parallel}\hat{a}_{\lambda,\mathbf{k}_\parallel}\rangle - \langle\hat{D}\rangle\langle\hat{a}^\dagger_{\lambda,\mathbf{k}_\parallel}\hat{a}_{\lambda,\mathbf{k}_\parallel}\rangle\ . \tag{2.17}$$

In general, N particle clusters $\Delta\langle\hat{D}[N-1][N-1]\rangle$ containing one Bosonic operator $\hat{D}$ and $N-1$ Fermionic creation and annihilation operators, respectively, are defined according to

$$\begin{aligned}
&\Delta\langle\hat{D}[N-1][N-1]\rangle \\
=\ &\langle\hat{D}[N-1][N-1]\rangle \\
&-\Big\{\Delta\langle\hat{D}[N-1][N-1]\rangle, \Delta\langle\hat{D}[N-2][N-2]\rangle, \ldots, \Delta\langle\hat{D}[1][1]\rangle, \langle\hat{D}\rangle, \\
&\quad \Delta\langle[N-1][N-1]\rangle, \Delta\langle[N-2][N-2]\rangle, \ldots, \langle[1][1]\rangle, \Big\}\ .
\end{aligned} \tag{2.18}$$

Similar expressions for expectation values containing more than one phonon operator are easily derived by observing the formal equivalence of $\hat{D}$ with a pair of carrier creation and annihilation operators.

In first order, the electron-phonon interaction couples the equations of motion of the single-particle densities and the carrier pair correlations to phonon-assisted densities

$$\langle\hat{\mathcal{G}}_{\mathbf{p}_\parallel,\mathbf{p}_\perp}\hat{a}^\dagger_{\lambda,\mathbf{k}_\parallel}\hat{a}_{\lambda,\mathbf{k}_\parallel+\mathbf{p}_\parallel}\rangle \tag{2.19}$$

and phonon-assisted two-particle correlations

$$\langle\hat{\mathcal{G}}_{\mathbf{p}_\parallel,\mathbf{p}_\perp}\hat{a}^\dagger_{\lambda,\mathbf{k}_\parallel}\hat{a}^\dagger_{\lambda',\mathbf{k}'_\parallel}\hat{a}_{\lambda',\mathbf{k}'_\parallel+\mathbf{q}_\parallel}\hat{a}_{\lambda,\mathbf{k}_\parallel-\mathbf{q}_\parallel+\mathbf{p}_\parallel}\rangle\ , \tag{2.20}$$

where $\hat{\mathcal{G}}_{\mathbf{p}_\parallel,\mathbf{p}_\perp}$ contains the sum of one phonon creation and annihilation operator $\hat{D}^\dagger_{\mathbf{p}_\parallel,\mathbf{p}_\perp}$ and $\hat{D}_{\mathbf{p}_\parallel,\mathbf{p}_\perp}$, respectively. Since the internal mechanics of the phonon system are not of interest in the framework of this thesis, these quantities are not calculated on the same level of approximation as the carrier correlations. Instead, we assume thermal Bose-Einstein distributions for the diagonal phonon-populations

$$N^{\mathrm{PH}}_{\mathbf{p}} \equiv \Delta\langle \hat{D}^\dagger_{\mathbf{p}_\parallel,\mathbf{p}_\perp} \hat{D}_{\mathbf{p}_\parallel,\mathbf{p}_\perp}\rangle = \frac{1}{\exp(\frac{\hbar\Omega_{\mathbf{p}}}{k_B T_L} - 1)} \,, \tag{2.21}$$

while off-diagonal phonon-correlations are set to zero. Here, $\hbar\Omega_{\mathbf{p}}$ is the energy of a phonon with momentum $\mathbf{p} = (\mathbf{p}_\parallel, \mathbf{p}_\perp)$ and T_L is the lattice temperature. Additionally, in the equations of motion for the phonon-assisted two-particle correlations only doublet-level contributions are taken into account, similar to the well-known second Born approximation [37, 38], to reduce the numerical complexity. The resulting equations of motion are then solved in Markov approximation [39].

2.2.4 Spin

While we did not explicitly include an index $s = \{\uparrow, \downarrow\}$ for the spin of the electrons, it can easily be introduced into the equations of motion derived below by replacing $\mathbf{k}$ with $(\mathbf{k}, s)$, as no spin-dependent interactions are included in the Hamilton operator. Subsequently, the number of observation values that have to be calculated dynamically can again be reduced by symmetry arguments. In this way, the effect of the spin is subsumed in a factor $\sigma = 2$ in the absorption calculations presented in the second part of this thesis. Conversely, in the equilibrium calculations discussed in this first part, no such factor was included. In doing so, we effectively describe the dynamics of only one type of excitons, e.g. 'bright' excitons which couple to the light field, and disallow the formation of the other. It should be mentioned, however, that the full carrier density, which includes both spins, is taken into account in the calculation of the screened Coulomb potential. Consequently, the values for carrier densities stated in this thesis are always the full two-spin values.

On a side note we point out that the carrier densities are given as na_0, i.e. in units of the inverse 3d Bohr radius. Since the half width of the 1s exciton wave function in our one-dimensional calculations is also of the order of a_0, the quantity na_0 is a measure for the probability of finding a third charge carrier in the vicinity of a bound electron-hole pair, allowing an intuitive estimation of scattering rates and the screening of the Coulomb potential.

2.3 Hamilton Operator

Using the model outlined above we identify the contributions of the Hamilton operator which have to be included in the mathematical description. In its most general form the Hamilton operator H_{tot} of the semiconductor crystal is given by the sum of the Hamilton operators for the kinetic energies of the weakly bound valence electrons H_{el} and the ion cores in the crystal lattice H_{ion}, respectively, and the Hamilton operator for Coulomb interaction between the carriers and ions $H_{\text{el-ion}}$ [40], i.e.

$$H_{\text{tot}} = H_{\text{el}} + H_{\text{ion}} + H_{\text{el-ion}} \,, \tag{2.22}$$

$$H_{\text{el}} = -\sum_i \frac{\hbar^2}{2m_0}\nabla^2_{\mathbf{r}_i} + \frac{1}{2}\sum_{\substack{i,j \\ i\neq j}} V(|\mathbf{r}_i - \mathbf{r}_j|) \,, \tag{2.23}$$

$$H_{\text{ion}} = -\sum_i \frac{\hbar^2}{2M_i}\nabla^2_{\mathbf{R}_i} + \frac{1}{2}\sum_{\substack{i,j \\ i\neq j}} V^{ion}(|\mathbf{R}_i - \mathbf{R}_j|) \,, \tag{2.24}$$

$$H_{\text{el-ion}} = \sum_{i,j} V^{el-ion}(|\mathbf{r}_i - \mathbf{R}_j|) \,. \tag{2.25}$$

Here, $\mathbf{R}_i(\mathbf{r}_i)$ and $M_i(m_0)$ specify position and mass of the i^{th} ion (electron), respectively. Although the coupling introduced by the last term prevents a clean separation between electronic and ionic degrees of freedom, it was pointed out by Born and Oppenheimer [41] that due to the mass ratio $m_0/M_i \approx 3 \times 10^4$ the comparatively fast moving electrons will adapt almost instantaneously to any changes in the potential introduced by the much slower ionic motion. Conversely, the ion dynamics is not sensitive to the specific motion of single electrons but rather to the average electron configuration, which in turn is a function of the ionic coordinates $\mathbf{R}_j$. In this way the ions can be described to move under the influence of an effective potential $V(\mathbf{R}_1, \ldots, \mathbf{R}_N)$. The functional form of $V(\mathbf{R}_1, \ldots, \mathbf{R}_N)$ is not *a priori* clear, of course, but it is usually sufficient to assume a harmonic dependence for small deviations from the equilibrium position and experimentally determine the corresponding elastic coupling constants. In the simplified case of a mono-atomic linear chain, the potential for the ion cores is thus written as

$$V(R_1, \ldots, R_N) = \frac{1}{2}\sum_l g\,(R_{l+1} - R_l)^2 \,, \tag{2.26}$$

where g is the second derivative of the interatomic potential function. Transformation into the reciprocal space lattice leads to a series of uncoupled harmonic oscillators for each momentum p. Following textbook discussions of the quantum mechanics for harmonic oscillators this yields the Hamiltonian [42]

in second quantization

$$\hat{H}_{\text{phon}} = \sum_p \hbar\Omega_p(\hat{D}_p^\dagger \hat{D}_p + \frac{1}{2}) \,, \tag{2.27}$$

where the operators $\hat{D}_p^\dagger$ and $\hat{D}_p$ create and annihilate lattice vibration quanta, respectively, the phonons. The dependence of the phonon energy Ω_p on the momentum p is given by the frequency $\Omega_p = 2\sqrt{g/M}|\sin(pa/2)|$, with $a = R_{j+1}^0 - R_j^0$ being the lattice constant and M the mass of the atoms. For small wave vectors this can be approximated by a linear dispersion

$$|\Omega_p|^2 = v_{\text{LA}}|p| \,, \tag{2.28}$$

where v_{LA} is the velocity of sound within the chain. In the generalized case of a bulk crystal each atom has three dimensions to move in, giving rise to three different phonon modes, i.e. the longitudinal mode in which the oscillations of the ions are parallel to the propagation direction $\mathbf{p}$ of the wave and two transverse modes in which the displacement is perpendicular to $\mathbf{p}$. In compound semiconductors the number of modes is raised further to $3k$, since the k different atoms in the base can move in phase or out of phase with each other. In this work, however, only the longitudinal acoustic (LA) phonon mode is taken into consideration, which dominates the phonon-carrier dynamics at low temperatures where the average kinetic energies of the carriers is below the excitation energy of longitudinal optical (LO) phonons. In tune with the other parameters of the simulation, we have used the velocity of sound v_{LA} measured in GaAs in the numerical evaluation.

2.3.1 Band Structure

In order to describe the movement of the valence band carriers in the presence of the ionic cores it is convenient to use the ground state of the lattice as a reference point and treat the changes arising from the displacement of the ions by phonons as perturbations. We first consider the behavior of electrons in bulk semiconductor material and then introduce the modifications due to the heterostructure. At zero temperature the ions are located at their equilibrium sites, forming an translationally invariant potential landscape for the electrons to move in. Based on the physical equivalence of the different lattice sites we choose the Bloch wave functions [43]

$$\Psi_\lambda(\mathbf{k}, \mathbf{r}) = \frac{1}{\sqrt{L^3}} e^{i\mathbf{k}\cdot\mathbf{r}} u_\lambda(\mathbf{k}, \mathbf{r}) \tag{2.29}$$

as the basis for the electronic wave functions. The function $u_\lambda(\mathbf{k}, \mathbf{r})$ has the periodicity of the lattice and sensitively depends on the shape of the ion potential, while the plane-wave envelope-function $e^{i\mathbf{k}\cdot\mathbf{r}}$ describes the change of

the electron wave function across several unit cells. The indices λ and $\mathbf{k}$ give the energy eigenvalue and the crystal momentum, respectively.

The energy dispersion $E_\lambda(\mathbf{k})$ of the Bloch electrons in the semiconductor forms continuous bands, of which only the highest occupied band and the lowest unoccupied band are taken into account in the work presented here. For excitations close to the band edge, i.e for vanishing carrier momentum $\mathbf{k}$, $E_\lambda(\mathbf{k})$ is approximated by a harmonic dependence

$$E_\lambda(\mathbf{k}) \approx \frac{\mathbf{k}^2}{2m_\lambda} , \tag{2.30}$$

with m_λ determined by the curvature of the band. In this sense the carriers close to the band edge behave like free particles with effective masses m_λ. For GaAs semiconductor systems, a ratio of $m_h/m_e \approx 7$ between the valence and the conduction band is measured. However, since the extension of the carrier distributions in reciprocal space – and consequently the numerical workload – increases with the effective mass, a ratio of $m_h/m_e = 3$ has been used in the calculations presented here.

2.3.2 Mesoscopic Confinement

The behavior of a free electron in the presence of an external potential is known from elementary quantum mechanics. In particular, electrons may become trapped in local minima of the potential, with their movement restricted to a discrete set of energy levels $E_\mu(\mathbf{r})$ and corresponding wave functions $\xi_\mu(\mathbf{r})$. If the potential $V_{\text{ext}}(\mathbf{r}_\perp)$ is a function only of one or two spatial directions $\mathbf{r}_\perp$ a separation ansatz for the electron wave function $\Psi(\mathbf{r})$ can be carried out. This yields

$$\Psi_{\mu,\mathbf{k}_\parallel}(\mathbf{r}_\perp, \mathbf{r}_\parallel) = \xi_\mu(\mathbf{r}_\perp) e^{i\mathbf{k}_\parallel \cdot \mathbf{r}_\parallel} , \tag{2.31}$$

where $e^{i\mathbf{k}_\parallel \cdot \mathbf{r}_\parallel}$ is the plane wave contribution of the unrestricted motion parallel to the equi-potential lines. A comparable situation arises in semiconductor heterostructures, where variations in the width of the bandgap E_g between the different materials result in a confinement potential $V_{\text{conf}}(\mathbf{r})$ for the electrons. If the length scale, on which $V_{\text{conf}}(\mathbf{r})$ varies, is large compared to the lattice constant, the periodic functions $u_\lambda(\mathbf{k}, \mathbf{r})$ which describe the dependence of the electron wave function on the ionic potential within one unit cell are approximately the same as in bulk material and only the long-range envelope functions are changed. Thus, a modified Bloch ansatz may be made for the electron wave functions

$$\Psi_\lambda(\mathbf{k}, \mathbf{r}) = \frac{1}{\sqrt{L^3}} \xi_\nu(\mathbf{r}) u_\lambda(\mathbf{k}, \mathbf{r}) , \tag{2.32}$$

where the plane wave functions $\exp(i\mathbf{k}\cdot\mathbf{r})$ of Eq. (2.29) are replaced with the envelope functions $\xi_\nu(\mathbf{r})$. For a confinement potential $V(\mathbf{r}_\perp)$ the plane wave solution $\xi_{\mathbf{k}_\parallel}(\mathbf{r}_\parallel) = \exp(i\mathbf{k}_\parallel \cdot \mathbf{r}_\parallel)$ is retained for movement parallel to the heterostructure but is replaced in perpendicular directions by the eigenfunctions $\xi_\mu(\mathbf{r}_\perp)$ of the potential. Due to the break of translational invariance the quasi-continuous crystal momentum $\mathbf{k}$ is no longer a good quantum number for the electronic movement perpendicular to the chain. Instead, the three-dimensional energy bands $\epsilon_{\lambda,\mathbf{k}}$ of the bulk material are split into one-dimensional subbands $\epsilon_{\lambda,\mu,\mathbf{k}_\parallel}$, which are energetically offset against each other by the eigenenergies $E_{\mu'} - E_\mu$ of the confinement potential.

In principle, the confining potential and the resulting envelope wave functions have to be calculated microscopically. However, knowledge of the exact shape of the confinement functions is not crucial for the work presented here, since the envelope functions primarily influence the strength of the Coulomb potential and the scattering probability with phonons. Thus, with the restriction of the calculations to the energetically lowest conduction band and highest valence subband, deviations in $\Phi_\mu(\mathbf{r}_\perp)$ result only in small factors to the interaction matrix elements. We therefore approximate the confinement potential by a parabolic function

$$V(\mathbf{r}_\perp) = \frac{1}{2} m\omega^2 \mathbf{r}_\perp^2 \ . \tag{2.33}$$

The ground state wave function is obtained from elementary quantum mechanics as [44]

$$\begin{aligned} \xi_0(\mathbf{r}_\perp) &= \sqrt{\frac{m\omega}{\pi\hbar}} \exp\left(\frac{-m\omega\mathbf{r}_\perp^2}{2\hbar}\right) \\ &= \frac{1}{\sqrt{2\pi}} \frac{1}{R} \exp\left(-\frac{\mathbf{r}_\perp^2}{4R^2}\right) \ , \end{aligned} \tag{2.34}$$

where we have substituted $R^2 = \hbar/(2m\omega)$. The ground-state energy of the confinement potential given in Eq. (2.33) equals the ground state energy of an infinitely deep rectangular potential well with diameter Ra_0. Thus, viewing the infinite-well model as a somewhat more realistic description of a real quantum-wire structure, the quantity Ra_0 may serve as an indication for the width of the wire model calculated here. With $Ra_0 = 8.25$ nm being of the order of the calculated exciton radius $a_0^{1\mathrm{d}} \approx a_0^{3\mathrm{d}} = 12.53$ nm the subbands are sufficiently separated so that the restriction of the model to the lowest two subbands is justified [45, 46].

Defining the bandgap E_G in the heterostructure as the sum of the bulk bandgap E_g and the confinement energies of the highest valence subband and the lowest conduction subband, the single-particle Hamiltonian for the carriers

is, in the Bloch basis, given by

$$\hat{H}_{\text{kin}} = \sum_{\mathbf{k}_\parallel} \left(\frac{\hbar^2 \mathbf{k}_\parallel^2}{2m_e} + E_G \right) \hat{a}^\dagger_{c,\mathbf{k}_\parallel} \hat{a}_{c,\mathbf{k}_\parallel} + \frac{\hbar^2 \mathbf{k}_\parallel^2}{2m_h} \hat{a}^\dagger_{v,\mathbf{k}_\parallel} \hat{a}_{v,\mathbf{k}_\parallel} \ . \tag{2.35}$$

2.3.3 Electron-Phonon Interaction

The Bloch wave functions $\Psi_{k,\lambda}(\mathbf{r})$ given in Eq. (2.34) are eigenstates of an electron in the heterostructure at zero temperature, i.e. when the ion cores are fixed at their respective lattice sites $\mathbf{R}_j^0$. At finite temperatures, the ions begin to oscillate around their equilibrium positions, creating perturbations of the potential landscape the electrons move in. In the following we derive the Hamilton operator describing the interaction of carriers with LA-phonons via the deformation potential. Scattering rates due to piezoelectric coupling have been shown to be two orders of magnitude lower than the deformation-potential contributions in low temperature GaAs structures [47] and are therefore neglected in this work.

The displacement $\mathbf{u}_j$ of the ions from their lattice site $\mathbf{R}_j$ can be expressed in terms of phonon creation and annihilation operators as [42]

$$\mathbf{u}(\mathbf{R}_j) = (-i) \sum_{\mathbf{p}} \sqrt{\frac{\hbar}{2\rho_m v_{\text{LA}} |\mathbf{p}| V}} \frac{\mathbf{p}}{|\mathbf{p}|} e^{i\mathbf{p}\cdot\mathbf{R}_j} \left(D^\dagger_{\mathbf{p}} - D_{-\mathbf{p}} \right) \ , \tag{2.36}$$

where ρ_m is the density of the semiconductor. For acoustical phonons these displacements $\mathbf{u}(\mathbf{R}_j)$ result – in the long wavelength limit – in a deformation of the semiconductor crystal, described by the tensor

$$\epsilon_{\alpha\beta}(\mathbf{R}_j) = \frac{\partial u_\alpha(\mathbf{R}_j)}{\partial R_\beta} \ , \tag{2.37}$$

where $\alpha, \beta = \{x, y, z\}$. Since the antisymmetric part of $\epsilon_{\alpha\beta}$ describes a rotation of the crystal as a whole and thus does not affect the internal dynamics of the system, we only need to consider the symmetric contribution

$$\epsilon^S_{\alpha\beta} = \frac{1}{2} \left(\frac{\partial u_\alpha}{\partial R_\beta} + \frac{\partial u_\beta}{\partial R_\alpha} \right) \ , \tag{2.38}$$

the so-called strain tensor. Inserting Eq. (2.36) into Eq. (2.38) we get

$$\epsilon^S_{\alpha\beta}(\mathbf{R}_j^0) = \frac{1}{2} \sum_{\mathbf{p}} \sqrt{\frac{\hbar}{2\rho_m v_p |\mathbf{p}| V}} \left(\frac{p_\beta p_\alpha}{|\mathbf{p}|} + \frac{p_\alpha p_\beta}{|\mathbf{p}|} \right) e^{i\mathbf{p}\cdot\mathbf{R}_j^0} \left(D^\dagger_{\mathbf{p}} - D_{-\mathbf{p}} \right) \ , \tag{2.39}$$

as the deformation associated with a LA phonon with momentum $\mathbf{p}$. The strain tensor given in Eq. (2.39) can be shown to describe both an oscillatory

dilation $\Delta V/V$ of the volume and a shearing [40]. In this work, we neglect the contribution due to the shear and only consider $\Delta V/V$, which is given by the trace of the strain tensor

$$\Delta V(\mathbf{R}_j)/V = \sum_{\alpha} \epsilon^S_{\alpha\alpha}(\mathbf{R}_j) = (-i) \sum_{\mathbf{p}} \sqrt{\frac{\hbar|\mathbf{p}|}{2\rho_m v_p V}} e^{i\mathbf{p}\cdot\mathbf{R}_j} \left(D^\dagger_{\mathbf{p}} - D_{-\mathbf{p}} \right) . \quad (2.40)$$

The deformation potential theory [48] associates $\Delta V/V$ with a correction of the electronic energies via the Hamilton operator $H^{\text{Schr.}}_{\text{el}-\text{phon}} = \sum_{\mathbf{R}_j} a(\Gamma_1)(\mathbf{R}_j)\Delta V/V$, where the volume deformation potential $a(\Gamma_1)$ can be obtained experimentally. Neglecting phonon induced interband scattering the Hamilton operator in second quantization is obtained as

$$\begin{aligned} \hat{H}_{\text{el}-\text{phon}} &= \int_V \hat{\Psi}^\dagger_\lambda(\mathbf{k}', \mathbf{r}) H^{\text{Schr.}}_{\text{el}-\text{phon}} \hat{\Psi}_\lambda(\mathbf{k}, \mathbf{r}) d^3r \\ &= \sum_{\mathbf{k}_\parallel, \mathbf{k}'_\parallel, \lambda} \sum_{\mathbf{p}} M^{\mathbf{p}}_{\lambda, \mathbf{k}_\parallel, \mathbf{k}'_\parallel} \left(\hat{D}^\dagger_{\mathbf{p}} - \hat{D}_{-\mathbf{p}} \right) \hat{a}^\dagger_{\lambda, \mathbf{k}'_\parallel} \hat{a}_{\lambda, \mathbf{k}_\parallel} \end{aligned} \quad (2.41)$$

where the matrix elements $M^{\mathbf{p}}_{\lambda, \mathbf{k}'_\parallel, \mathbf{k}_\parallel}$ are given by

$$M^{\mathbf{p}}_{\lambda, \mathbf{k}'_\parallel, \mathbf{k}_\parallel} = \sum_{\mathbf{R}_j} \int_{\mathbf{r}_\parallel, \mathbf{r}_\perp} \sqrt{\frac{\hbar|\mathbf{p}|a(\Gamma_1)^2}{2\rho_m v_p V}} e^{i(\mathbf{k}_\parallel - \mathbf{k}'_\parallel)\cdot\mathbf{r}_\parallel} e^{i\mathbf{p}\cdot\mathbf{R}^0_j} |\omega_\lambda(\mathbf{r})|^2 |\xi_0(\mathbf{r}_\perp)|^2 \mathrm{d}\mathbf{r}_\parallel \mathrm{d}\mathbf{r}_\perp . \quad (2.42)$$

In order to evaluate the spatial integration in Eq. (2.42) we shift the coordinate $\mathbf{r} = (r, \mathbf{r}_\perp)$ for each j to the unit cell where the ion is actually being moved. It is convenient to split the summation over the ion positions $\mathbf{R}_j$ into summations over $\mathbf{R}_\parallel$ and $\mathbf{R}_\perp$, with $\mathbf{R}_\perp$ running over all lattice sites in a plane perpendicular to the heterostructure, and $\mathbf{R}_\parallel$ giving the position parallel to it. Since the envelope functions $\xi_0(\mathbf{r}_\perp)$ and $\exp(i\mathbf{k}_\parallel \cdot \mathbf{r}_\parallel)$ only change weakly within one unit cell we may approximate $\xi_0(\mathbf{r}_\perp + \mathbf{R}_\perp) \approx \xi_0(\mathbf{R}_\perp)$ and $\exp(i\mathbf{k}_\parallel \cdot (\mathbf{r}_\parallel + \mathbf{R}_\parallel)) \approx \exp(i\mathbf{k}_\parallel \cdot \mathbf{R}_\parallel)$. With a subsequent integration over the unit cell one thus obtains

$$M^{\mathbf{p}}_{\lambda, \mathbf{k}'_\parallel, \mathbf{k}_\parallel} = \sum_{\mathbf{R}_\parallel, \mathbf{R}_\perp} \frac{V}{N} \sqrt{\frac{\hbar|\mathbf{p}|a(\Gamma_1)^2}{2\rho_m v_{\mathbf{p}} V}} e^{i(\mathbf{k}_\parallel - \mathbf{k}'_\parallel + \mathbf{p}_\parallel)\cdot\mathbf{R}_\parallel} e^{i\mathbf{p}_\perp \cdot \mathbf{R}_\perp} |\xi_0(\mathbf{R}_\perp)|^2 . \quad (2.43)$$

The summation over $\mathbf{R}_\parallel$ gives just the Kronecker delta $\delta_{\mathbf{k}'_\parallel, \mathbf{k}_\parallel + \mathbf{p}_\parallel}$, which describes the conservation of momentum in the directions parallel to the heterostructure. In contrast, the sum over $\mathbf{R}_\perp$ contains the confinement functions

$|\xi_0(\mathbf{R}_\perp)|^2$ as a weight, and we find

$$\begin{aligned} F(\mathbf{p}_\perp) &\equiv \sum_{R_\perp} e^{i\mathbf{p}_\perp\cdot\mathbf{R}_\perp}|\xi_0(\mathbf{R}_\perp)|^2 \\ &= \frac{1}{\Delta R_\perp}\int_{\mathbf{R}_\perp} e^{i\mathbf{p}_\perp\cdot\mathbf{R}_\perp}|\xi_0(\mathbf{R}_\perp)|^2 \mathrm{d}\mathbf{R}_\perp \\ &= \left(\frac{L}{2\pi}\right)^2 e^{-|\mathbf{p}_\perp|^2 R_W^2/2} \ . \end{aligned} \tag{2.44}$$

Thus, the quasi-one-dimensional phonon interaction is obtained as the average over the cross section of the wire weighted with the local electron density [49]. With Eqs (2.41)–(2.44) the Hamilton operator is finally written as

$$\begin{aligned} \hat{H}_{\mathrm{el-phon}} &= \sum_{\mathbf{k}_\parallel,\lambda}\sum_{\mathbf{p}_\parallel,\mathbf{p}_\perp}\sqrt{\frac{\hbar|\mathbf{p}|a(\Gamma_1)^2}{2\rho_m v_{\mathbf{p}} V}}\left(\hat{D}^\dagger_{\mathbf{p}} - \hat{D}_{-\mathbf{p}}\right)\hat{a}^\dagger_{\lambda,\mathbf{k}_\parallel}\hat{a}_{\lambda,\mathbf{k}_\parallel+\mathbf{k}_\parallel} \\ &= \sum_{k,p,\lambda}\hat{\mathcal{G}}^\dagger_{\mathbf{p}}\hat{a}^\dagger_{\lambda,\mathbf{k}_\parallel}\hat{a}_{\lambda,\mathbf{k}_\parallel+\mathbf{p}_\parallel} \end{aligned} \tag{2.45}$$

where the integration over the perpendicular part of the phonon momentum $\mathbf{p}_\perp$ is contained in the effective one-dimensional phonon operator

$$\hat{\mathcal{G}}^\dagger_{\mathbf{p}} = \sum_{\mathbf{p}_\perp}\sqrt{\frac{\hbar|\mathbf{p}|a(\Gamma_1)^2}{2\rho_m v_{\mathbf{p}} V}}e^{-\frac{|\mathbf{p}_\perp|^2 R_W^2}{2}}\left(\hat{D}^\dagger_{\mathbf{p}} - \hat{D}_{-\mathbf{p}}\right) \ . \tag{2.46}$$

2.3.4 Coulomb Interaction

In the limit of vanishing carrier densites two electrons at positions $\mathbf{r}_1$ and $\mathbf{r}_2 = \mathbf{r}_1 + \mathbf{r}$ in a bulk semiconductor material interact via the unscreened Coulomb potential $V(\mathbf{r}) = e^2/(4\pi\epsilon_0\epsilon_b|\mathbf{r}|)$, where ϵ_b is the dielectric constant of the material. In principle, in heterostructures consisting of materials with different ϵ_b, the effect of induced charges at the material interfaces has to be taken into account. However, this effect is seen to be neglegible in GaAs/AlGaAs structures, where the dielectric constants $\epsilon_b|_{\mathrm{GaAs}} = 10.6$ and $\epsilon_b|_{\mathrm{AlAs}} = 8.2$ are of comparable size.

The quasi-one-dimensional Coulomb interaction is obtained by integrating over the directions perpendicular to the wire $\mathbf{r}_\perp$, weighted with the charge density at $|\mathbf{r}_\perp|$. The calculation for the parabolic confinement conditions given in Eq. (2.33) have been derived in Appendix A. The corresponding Hamilton operator is given by

$$H_{\mathrm{Coul}} = \frac{L^2}{2}\sum_{\substack{\mathbf{q}_\parallel\neq 0\\ \lambda,\lambda'}} V_{\mathbf{q}_\parallel}\rho_{\lambda,-\mathbf{q}_\parallel}\rho_{\lambda,\mathbf{q}_\parallel} \ , \tag{2.47}$$

where $\rho_{\lambda,\mathbf{q}_\parallel}$ is the carrier density in band λ. In second quantized form $\rho_{\lambda,\mathbf{q}_\parallel}$ is replaced with the operator $\hat{\rho}_{\lambda,\mathbf{q}_\parallel}$, which may be expressed in terms of creation and destruction operators as

$$\hat{\rho}_{\lambda,\mathbf{q}_\parallel} = \frac{1}{L}\sum_{\mathbf{k}_\parallel} \hat{a}^\dagger_{\lambda,\mathbf{k}_\parallel-\mathbf{q}_\parallel}\hat{a}_{\lambda,\mathbf{k}_\parallel} \ . \tag{2.48}$$

Inserting this into Eq. (2.47) and applying normal ordering yields

$$\begin{aligned}
\hat{H}_{\mathrm{Coul}} &= \frac{1}{2}\sum V_{\mathbf{q}_\parallel}\hat{a}^\dagger_{\lambda,\mathbf{k}_\parallel+\mathbf{q}_\parallel}\hat{a}_{\lambda,\mathbf{k}_\parallel}\hat{a}^\dagger_{\lambda',\mathbf{k}'_\parallel-\mathbf{q}_\parallel}\hat{a}_{\lambda',\mathbf{k}'_\parallel} \\
&= \frac{1}{2}\sum V_{\mathbf{q}_\parallel}\hat{a}^\dagger_{\lambda,\mathbf{k}_\parallel+\mathbf{q}_\parallel}\hat{a}^\dagger_{\lambda,\mathbf{k}'_\parallel-\mathbf{q}_\parallel}\hat{a}_{\lambda',\mathbf{k}'_\parallel}\hat{a}_{\lambda,\mathbf{k}_\parallel} \\
&\qquad +\frac{1}{2}\sum_{\mathbf{k}_\parallel,\lambda}\hat{a}^\dagger_{\lambda,\mathbf{k}_\parallel}\hat{a}_{\lambda,\mathbf{k}_\parallel}\sum_{\mathbf{q}_\parallel\neq 0}V_{\mathbf{q}_\parallel} \\
&= \frac{1}{2}\sum V_{\mathbf{q}_\parallel}\hat{a}^\dagger_{\lambda,\mathbf{k}_\parallel+\mathbf{q}_\parallel}\hat{a}^\dagger_{\lambda,\mathbf{k}'_\parallel-\mathbf{q}_\parallel}\hat{a}_{\lambda',\mathbf{k}'_\parallel}\hat{a}_{\lambda,\mathbf{k}_\parallel} + \hat{N}\frac{1}{2}\sum_{\mathbf{q}_\parallel\neq 0}V_{\mathbf{q}_\parallel} \ ,
\end{aligned} \tag{2.49}$$

where the first sum is (always) taken over $\mathbf{k}_\parallel, \mathbf{k}'_\parallel, \mathbf{q}_\parallel, \lambda$ and λ'. The second term is cancelled exactly by a contribution arising from the interaction with the positive background charge of the ions [43], so that the Hamilton operator for the carrier-carrier interaction is finally obtained as

$$\hat{H}_{\mathrm{Coul}} = \frac{1}{2}\sum_{\substack{\mathbf{k}_\parallel,\mathbf{k}'_\parallel \\ \mathbf{q}_\parallel\neq 0,\lambda,\lambda'}} V_{\mathbf{q}_\parallel}\hat{a}^\dagger_{\lambda,\mathbf{k}_\parallel+\mathbf{q}_\parallel}\hat{a}^\dagger_{\lambda,\mathbf{k}'_\parallel-\mathbf{q}_\parallel}\hat{a}_{\lambda',\mathbf{k}'_\parallel}\hat{a}_{\lambda,\mathbf{k}_\parallel} \ . \tag{2.50}$$

In summary, the general Hamilton operator of the semiconductor crystal introduced in Eq. (2.22) is in this work approximated by

$$\hat{H} = \hat{H}_{\mathrm{phon}} + \hat{H}_{\mathrm{kin}} + \hat{H}_{\mathrm{Coul}} + \hat{H}_{\mathrm{el-phon}} \ , \tag{2.51}$$

where the single particle Hamilton operators describing the phonons and the Bloch electrons are given in Eq. (2.27) and Eq. (2.35), respectively. The electron-phonon interaction contributions is described in Eq. (2.41) and the Hamilton operator due to the Coulomb interaction between two charge carriers is given in Eq. (2.50).

2.4 Equations of Motion

In the following, we derive equations of motion for the expectation values describing the incoherent carrier system. As introduced before, these are the

single-particle densities $f^{e,h}_{\mathbf{k}}$ on the singlet level and the electron-electron, hole-hole and electron-hole correlations $c_e(q,k',k)$, $c_h(q,k',k)$ and $c_X(q,k',k)$ on the doublet-level, respectively. The coupling of the carriers to lattice vibrations is included via phonon-assisted densities and correlations given in Eqs (2.19) and (2.20).

According to Eq. (2.1) the time derivative for an operator $\hat{A}$ is given by the commutator with the Hamilton operator of the system. The equations of motion are obtained by taking the expectation value of the operators on both sides of the resulting equation. We calculate the commutator of the relevant operators with each part of the Hamiltonian operator separately, starting with the single-particle contribution H_0.

For convenience, we drop the index $\|$ in the following and adopt the notation $\mathbf{q} = (q, \mathbf{q}_\perp)$ instead, where the scalar quantity q indicates component of $\mathbf{q}$ parallel to the heterostructure.

One immediately obtains

$$i\hbar \frac{\partial}{\partial t} f^{e,h}_k \Big|_{H_{\rm kin}} = 0 \tag{2.52}$$

and

$$i\hbar \frac{\partial}{\partial t} c_e(q,k',k) \Big|_{H_{\rm kin}} = (\epsilon^c_{k-q} + \epsilon^c_{k'+q} - \epsilon^c_{k'} - \epsilon^c_k) c_e(q,k',k) \;, \tag{2.53}$$

$$i\hbar \frac{\partial}{\partial t} c_h(q,k',k) \Big|_{H_{\rm kin}} = (\epsilon^v_{k-q} + \epsilon^v_{k'+q} - \epsilon^v_{k'} - \epsilon^v_k) c_h(q,k',k) \;, \tag{2.54}$$

$$i\hbar \frac{\partial}{\partial t} c_X(q,k',k) \Big|_{H_{\rm kin}} = (\epsilon^v_{k-q} + \epsilon^c_{k'+q} - \epsilon^v_{k'} - \epsilon^c_k) c_X(q,k',k) \;, \tag{2.55}$$

where $\epsilon^v_{k'}$ are the unrenormalized single-particle energies. The Coulomb Hamiltonian $H_{\rm Coul}$ couples the carrier densities to the two-particle expectation values via

$$\frac{\partial}{\partial t} f^e_k \Big|_{\rm Coul} = \frac{2}{\hbar} \sum_{k',q\neq 0} {\rm Im}\left[c_e(q,k',k) - c_X(q,k',k)\right] \;, \tag{2.56}$$

$$\frac{\partial}{\partial t} f^h_k \Big|_{\rm Coul} = -\frac{2}{\hbar} \sum_{k',q\neq 0} {\rm Im}\left[c_h(q,k',k) - c_X(q,k,k')\right] \;. \tag{2.57}$$

As discussed previously, a closed set of equations is obtained by neglecting the contributions of three-carrier complexes to the dynamics of the two-particle correlations. The three-particle expectation values in the equations of motion for c_e, c_h and c_X are thus separated into singlet, doublet and triplets terms,

and the latter are subsequently set to zero. A rather lengthy calculation yields

$$
\begin{aligned}
& i\hbar\frac{\partial}{\partial t}c_X(q,k',k)\Big|_{\text{Coul}} \\
&= \left(\sum_l V_l\left\{f^e_{k+l}+(1-f^h_{k'+l})-f^e_{k'+q+l}-(1-f^h_{k-q+l})\right\}\right)c_X(q,k',k) \\
&\quad + V_{k'+q-k}\Big\{(1-f^e_k)f^h_{k'}f^e_{k'+q}(1-f^h_{k-q})-f^e_k(1-f^h_{k'})(1-f^e_{k'+q})f^h_{k-q} \\
&\qquad\quad + (f^e_k-f^e_{k'+q})\left[c_X(l+q-k,k',l)+c_h(l+q-k,k',l)\right] \\
&\qquad\quad + (f^h_{k-q}-f^h_{k'})\left[c_X(k'+q-l,l,k)+c_e(k'+q-l,l,k)\right]\Big\} \\
&\quad + (1-f^e_k-f^h_{k-q})\sum_l V_{l-k}c_X(q,k',l) \\
&\quad - (1-f^h_{k'}-f^e_{k'+q})\sum_l V_{l-k'}c_X(q,l,k) \\
&\quad + (f^e_k-f^h_{k'})\sum_l V_{l-q}c_X(l,k'+q-l,k-q+l) \\
&\quad - (f^e_{k'+q}-f^h_{k-q})\sum_l V_{l-q}c_X(l,k',k) \\
&\quad - (f^e_k-f^e_{k'+q})\sum_l V_{l-k}c_X(l+q-k,k',l) \\
&\quad + (f^h_{k'}-f^h_{k-q})\sum_l V_{l-k'}c_X(k'+q-l,l,k)\ , \qquad (2.58)
\end{aligned}
$$

where the terms in the first line of this equation describe the renormalization of the single-particle energies. Similar equations have been derived for the electron-electron and hole-hole correlations and can be found in Ref. [35].

Lastly, the electron-phonon interaction introduces a coupling of the carrier dynamics to phonon-assisted densities and correlations. In the derivation of the dynamics for these quantities, some care has to be taken to account for the signs $\sigma^\lambda_{\text{PH}}$ of the phonon interaction in the valence and conduction band. Using a Markov approximation to express the momentary state of the phonon-assisted densities in terms of the carrier system expectation values one obtains

$$
\begin{aligned}
\text{PH}^c_{k,p} &\equiv \sigma^c_{\text{PH}}\Delta\langle\hat{\mathcal{G}}_p\hat{a}^\dagger_{c,k}\hat{a}_{c,k-p}\rangle \\
&= (N^{+,c}_{k,p}+N^{-,c}_{k,p})(f^e_k-f^e_{k-p}) \\
&\quad + M^{-,c}_{k,p}f^e_k(1-f^e_{k-p})-M^{+,c}_{k,p}f^e_{k-p}(1-f^e_k) \\
&\quad - \sum_l (M^{+,c}_{l+p,p}-M^{-,c}_{l+p,p})c_e^{p,l,k} \\
&\quad - \sum_l (M^{+,v}_{l+p,p}-M^{-,v}_{l+p,p})c_X(k-p-l,l,k) \qquad (2.59)
\end{aligned}
$$

and

$$\begin{aligned}
\mathrm{PH}^{v}_{k,p} &\equiv \sigma^{v}_{\mathrm{PH}}\Delta\langle\hat{\mathcal{G}}_p\hat{a}^{\dagger}_{v,k}\hat{a}_{v,k-p}\rangle \\
&= (N^{+,v}_{k,p}N^{-,v}_{k,p})(f^{h}_{k-p}-f^{h}_{k}) \\
&\quad +M^{-,v}_{k,p}f^{h}_{k-p}(1-f^{h}_{k})-M^{+,v}_{k,p}f^{h}_{k}(1-f^{h}_{k-p}) \\
&\quad -\sum_{l}(M^{+,v}_{l+p,p}-M^{-,v}_{l+p,p})c^{p,l,k}_{h} \\
&\quad -\sum_{l}(M^{+,c}_{l+p,p}-M^{-,c}_{l+p,p})c_X(l+p-k,k,l)\ , \qquad (2.60)
\end{aligned}$$

where we have used the abbreviations

$$M^{\pm,\lambda}_{k,p} \equiv \sum_{\mathbf{p}_\perp}\frac{|G_{p,\mathbf{p}_\perp}|^2}{\epsilon^{\lambda}_{k}-\epsilon^{\lambda}_{k-p}\pm\hbar\Omega_{p,\mathbf{p}_\perp}+i\gamma_{\mathrm{PH}}}\ , \qquad (2.61)$$

$$N^{\pm,\lambda}_{k,p} \equiv \sum_{\mathbf{p}_\perp}\frac{|G_{p,\mathbf{p}_\perp}|^2 N^{\mathrm{PH}}_{p,\mathbf{p}_\perp}}{\epsilon^{\lambda}_{k}-\epsilon^{\lambda}_{k-p}\pm\hbar\Omega_{p,\mathbf{p}_\perp}+i\gamma_{\mathrm{PH}}}\ . \qquad (2.62)$$

Analogously, the equations of motion for the phonon-assisted two-carrier correlations are solved in Markov approximation. As discussed previously only the doublet contributions to the dynamics have been taken into account. With the definitions

$$\begin{aligned}
\gamma^{c}_{k,p} &\equiv (N^{+,c}_{k,p}+N^{-,c}_{k,p})+(1-f^{e}_{k})M^{+,c}_{k,p}+f^{e}_{k}M^{-,c}\ , &(2.63)\\
\tilde{\gamma}^{c}_{k,p} &\equiv (N^{+,c}_{k,p}+N^{-,c}_{k,p})+(1-f^{e}_{k-p})M^{+,c}_{k,p}+f^{e}_{k-p}M^{-,c}\ , &(2.64)\\
\gamma^{v}_{k,p} &\equiv (N^{+,v}_{k,p}+N^{-,v}_{k,p})+f^{h}_{k}M^{+,v}_{k,p}+(1-f^{h}_{k})M^{-,v}\ , &(2.65)\\
\tilde{\gamma}^{v}_{k,p} &\equiv (N^{+,v}_{k,p}+N^{-,v}_{k,p})+f^{h}_{k-p}M^{+,v}_{k,p}+(1-f^{h}_{k-p})M^{-,v} &(2.66)
\end{aligned}$$

one obtains

$$\begin{aligned}
&\Delta\langle\hat{G}_{\mathbf{p}_\parallel,\mathbf{p}_\perp}\hat{a}^{\dagger}_{\{\lambda,k\}}\hat{a}^{\dagger}_{\{\lambda',k'\}}\hat{a}_{\{\tilde{\lambda}',k'+q\}}\hat{a}_{\{\tilde{\lambda},k-q-p\}}\rangle \\
&=\sigma^{\tilde{\lambda}_1}_{\mathrm{PH}}\tilde{\gamma}^{\tilde{\lambda}}_{k-q,p}\Delta\langle\hat{a}^{\dagger}_{\{\lambda,k\}}\hat{a}^{\dagger}_{\{\lambda',k'\}}\hat{a}_{\{\tilde{\lambda}',k'+q\}}\hat{a}_{\{\tilde{\lambda},k-q\}}\rangle \\
&\quad -\sigma^{\tilde{\lambda}_2}_{\mathrm{PH}}(\tilde{\gamma}^{\tilde{\lambda}'}_{k'+q,-p})^{*}\ \Delta\langle\hat{a}^{\dagger}_{\{\lambda,k\}}\hat{a}^{\dagger}_{\{\lambda',k'\}}\hat{a}_{\{\tilde{\lambda}',k'+q+p\}}\hat{a}_{\{\tilde{\lambda},k-q-p\}}\rangle \\
&\quad -\sigma^{\lambda_2}_{\mathrm{PH}}\tilde{\gamma}^{\lambda}_{k',-p}\Delta\langle\hat{a}^{\dagger}_{\{\lambda,k\}}\hat{a}^{\dagger}_{\{\lambda',k'-p\}}\hat{a}_{\{\tilde{\lambda}',k'+q\}}\hat{a}_{\{\tilde{\lambda},k-q-p\}}\rangle \\
&\quad -\sigma^{\lambda_1}_{\mathrm{PH}}\tilde{\gamma}^{\tilde{\lambda}}_{k,p}\Delta\langle\hat{a}^{\dagger}_{\{\lambda,k-p\}}\hat{a}^{\dagger}_{\{\lambda',k'\}}\hat{a}_{\{\tilde{\lambda}',k'+q\}}\hat{a}_{\{\tilde{\lambda},k-q-p\}}\rangle\ . \qquad (2.67)
\end{aligned}$$

Using Eqs (2.59)–(2.67) the contribution of the electron-phonon interaction to the dynamics of the carrier densities may be expressed as

$$\frac{\partial}{\partial t}f^{e}_{k} = \frac{2}{\hbar}\sum_{p}\mathrm{Im}(\mathrm{PH}^{c}_{k,p})\ , \qquad (2.68)$$

$$\frac{\partial}{\partial t}f^{h}_{k} = -\frac{2}{\hbar}\sum_{p}\mathrm{Im}(\mathrm{PH}^{v}_{k,p})\ . \qquad (2.69)$$

Similarly, the equations of motion for the two-particle correlations are obtained as

$$
\begin{aligned}
i\hbar\frac{\partial}{\partial t}c_X(q,k',k)\Big|_{\mathrm{el-ph}} &= \mathrm{PH}^{v}_{k',k'+q-k}\left(f^{e}_{k}-f^{e}_{k'+q}\right)-\mathrm{PH}^{c}_{k,k-q-k'}\left(f^{h}_{k'}-f^{h}_{k-q}\right)\\
&+\sum_{l}\left(-(\tilde{\gamma}^{c}_{k,l})^{*}-(\tilde{\gamma}^{v}_{k',l})^{*}+\tilde{\gamma}^{c}_{k'+q,l}+\tilde{\gamma}^{v}_{k-q,l}\right)c_X(q,k',k)\\
&+\sum_{l}\left((\tilde{\gamma}^{v}_{k-q,l-q})^{*}+(\tilde{\gamma}^{c}_{k'+q,q-l})^{*}\right)c_X(l,k',k)\\
&-\sum_{l}\left(\tilde{\gamma}^{c}_{k,q-l}+\tilde{\gamma}^{v}_{k',l-q}\right)(c_X(l,k-q,k'+q))*\\
&+\sum_{l}\left(\tilde{\gamma}^{c}_{k,k-l}+(\tilde{\gamma}^{v}_{k-q,k-l})^{*}\right)c_X(q,k',l)\\
&+\sum_{l}\left(\tilde{\gamma}^{v}_{k',k'-l}+(\tilde{\gamma}^{c}_{k'+q,k'-l})^{*}\right)c_X(q,l,k)\\
&-\sum_{l}\left(\tilde{\gamma}^{v}_{k',l-q}+(\tilde{\gamma}^{v}_{k-q,l-q})^{*}\right)c_X(l,k'+q-l,k)\\
&-\sum_{l}\left(\tilde{\gamma}^{c}_{k,q-l}+(\tilde{\gamma}^{c}_{k'+q,q-l})^{*}\right)c_X(l,k',k-q+l) \qquad (2.70)
\end{aligned}
$$

and

$$
\begin{aligned}
i\hbar\frac{\partial}{\partial t}c_e(q,k',k)\Big|_{\mathrm{el-ph}} &= \mathrm{PH}^{c}_{k',-q}\left(f^{e}_{k}-f^{e}_{k-q}\right)+\mathrm{PH}^{c}_{k,q}\left(f^{e}_{k'}-f^{e}_{k'+q}\right)\\
&-\mathrm{PH}^{c}_{k,k-q-k'}\left(f^{e}_{k'}-f^{e}_{k-q}\right)-\mathrm{PH}^{c}_{k',k'+q-k}\left(f^{e}_{k}-f^{e}_{k'+q}\right)\\
&+\sum_{l}\left(-(\tilde{\gamma}^{c}_{k,l})^{*}-(\tilde{\gamma}^{c}_{k',l})^{*}+\tilde{\gamma}^{c}_{k'+q,l}+\tilde{\gamma}^{c}_{k-q,l}\right)c_e(q,k',k)\\
&+\sum_{l}\left((\tilde{\gamma}^{c}_{k-q,l-q})^{*}+(\tilde{\gamma}^{c}_{k'+q,q-l})^{*}\right)c_e(l,k',k)\\
&-\sum_{l}\left(\tilde{\gamma}^{c}_{k,q-l}+\tilde{\gamma}^{c}_{k',l-q}\right)(c_e(l,k-q,k'+q))^{*}\\
&+\sum_{l}\left(\tilde{\gamma}^{c}_{k,k-l}+(\tilde{\gamma}^{c}_{k-q,k-l})^{*}\right)c_e(q,k',l)\\
&+\sum_{l}\left(\tilde{\gamma}^{c}_{k',k'-l}+(\tilde{\gamma}^{c}_{k'+q,k'-l})^{*}\right)c_e(q,l,k)\\
&-\sum_{l}\left(\tilde{\gamma}^{c}_{k',l-q}+(\tilde{\gamma}^{c}_{k-q,l-q})^{*}\right)c_e(l,k'+q-l,k)\\
&-\sum_{l}\left(\tilde{\gamma}^{c}_{k,q-l}+(\tilde{\gamma}^{c}_{k'+q,q-l})^{*}\right)c_e(l,k',k-q+l)\,. \qquad (2.71)
\end{aligned}
$$

The equation of motion for the hole-hole correlations is obtained from Eq. (2.71) by replacing the indices e and c with h and v, respectively, and reverting the signs in the first two lines.

2.5 Initial Conditions

In general, the time evolution of a set of expectation values $\{\langle\hat{A}_1\rangle, \ldots, \langle\hat{A}_N\rangle\}$ is determined by a closed set of equations of motion and the knowledge of the state of the system at some time t_0, i.e by the specification of a set of initial conditions $\{\langle\hat{A}_1\rangle(t_0), \ldots, \langle\hat{A}_N\rangle(t_0)\}$. Whereas any set of values within the domain of the differential equation may be used as a starting point, these will, in most cases, not relate to a situation which can be experimentally prepared. In order to simulate the dynamics of a physical system, the initial conditions have to match the state of the experiment at t_0. For an undoped semiconductor system one possibility to achieve this is to use the unexcited system, where all densities and correlations vanish, as the initial state of the theoretical description. In that case, however, the excitation process necessarily has to be included in theoretical model, which greatly increases the complexity of the numerical evaluation. Calculations of exciton formation process including the excitations process have only recently been performed [50].

Alternatively, t_0 can be chosen to refer to a time when densities are already present within the system. For optical excitation processes, the theoretical description is further simplified if t_0 is sufficiently large, so that all coherences have decayed and the system dynamics is determined entirely by incoherent quantities. Nevertheless, in general the initial properties of such a system are not easily determined, either. The Coulomb interaction of the carrier densities introduces non-vanishing higher-order correlations into the system, which, in turn, lead to deviations of the one-particle distributions from ideal Fermi-Dirac distributions.

However, since the focus of the work presented here is to calculate the equilibrium positions of a system, the exact knowledge of the initial conditions may not be required. Instead, one can repeat the numerical integration for a wide range of values encompassing the estimated physical states for given excitation processes. The choice of initial conditions is justified, if the calculations evolve toward the same quasi-equilibrium state.

In the following we discuss the initial states that have been used in the calculations presented in this work. It should be stressed once more, that in our model the system dynamics is entirely determined by the density operators $f_k^{e,h}(t)$ and the carrier-carrier correlations $c_e(q,k',k,t)$, $c_h(q,k',k,t)$, and $c_X(q,k',k,t)$. Conversely, the phonon populations are given by a static Bose-Einstein distributions, while the phonon-carrier correlations are solved in

Markov approximation and, as such, do not carry a memory of the previous states of the system. Instead they are momentarily calculated from the dynamical variables specified above. Therefore, initial conditions only have to be assigned to the carrier densities and the electronic two-particle correlations.

For the carrier densities, two different initial distributions are used. For the first case the system is assumed to be optically excited in resonance with the 1s exciton energy. In the coherent limit, the carrier distributions can then be expressed as [43]

$$f_k^{e,h} = |P_k^{cv}|^2 + \mathcal{O}(E^4) \propto |\Psi_{1s}(k)|^2 + \mathcal{O}(E^4) \,, \tag{2.72}$$

where the $\mathcal{O}(E^4)$ indicates corrections which are of at least fourth order in the exciting electrical field. Subsequent scattering converts the interband coherences into incoherent bound states where the carrier distribution are to a good degree still described by Eq. (2.72). If on the other hand the carriers have already relaxed within their bands, then in a first approximation the Fermi-Dirac functions, which describe the equilibrium state of an ideal non-interacting Fermi gas, can be used as initial distributions for the calculations.

As shown in the previous section, information about bound electron-hole pairs is encoded in the electron-hole correlation operator $c_X(q,k',k)$ and can be extracted by the basis transformation described in Eq. (2.11). Conversely, utilizing Eq. (2.16) in the form

$$c_X(q,k',k)|_{t_0} = \left[\Phi_{1s}(k' + \frac{m_h}{M}q)\right]^* \left[\Phi_{1s}(k - \frac{m_h}{M}q)\right] \Delta\langle \hat{X}^\dagger_{1s,q}\, \hat{X}_{1s,q}\rangle\Big|_{t_0} \tag{2.73}$$

provides a means to calculate the electron-hole correlations $c_X(q,k',k)|_{t=0}$ corresponding to a given distribution $f_{1s}(q,\ t\ =\ 0)$ of excitons.

For the calculations presented here two limiting cases for $f_{1s}(q,t=0)$ were chosen. Using the absolute square of the 1s wave function $f_{1s}(q) \propto |\Psi_{1s}(q)|^2$ results in a narrow distribution of excitons with prevailingly small center-of-mass momenta. In another set of runs the excitons were assumed to be described by a comparatively wide thermalised Bose-Einstein distribution

$$f_{1s}(q) \propto \frac{1}{\exp\left((\frac{\hbar q^2}{2M} - \mu)\beta\right) - 1} \,, \tag{2.74}$$

where $\hbar q^2/(2M)$ is the kinetic energy of the center-of-mass motion.

While, in principle, equation (2.73) can be extended to describe also the transformation between off-diagonal exciton correlations $\Delta\langle \hat{X}^\dagger_{\nu,q}\hat{X}_{\nu',q}\rangle(t=0)$ and the electron-hole correlations $c_X(q,k',k)$, the initial values for $\Delta\langle \hat{X}^\dagger_{\nu,q}\hat{X}_{\nu',q}\rangle(t=0)$ cannot easily be determined. Previous calculations have shown [15], however, that the off-diagonal exciton correlations are rapidly restored within a few picoseconds by the Coulomb interaction after being reset

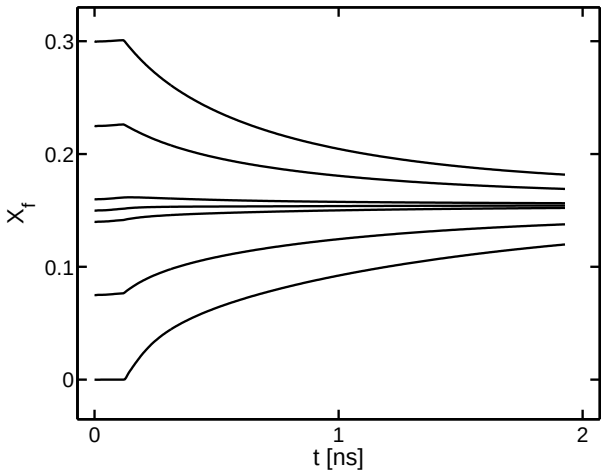

Figure 2.1: a) Fraction X_f of carriers bound as excitons as a function of time t. Initial fractions $X_f(t=0)$ are 0, 0.075, 0.14, 0.15, 0.16, 0.225 and 0.3 (from bottom to top). All calculations were performed for carrier density of $na_0 = 0.05$ at $T = 20$ K

to zero during the numerical integration. Likewise, the electron-electron and hole-hole correlations are generated on a fast picosecond timescale.

For the calculations presented in this work, only the single-particle densities and the diagonal exciton populations were seeded with non-vanishing initial values. In some of the calculations the electron-hole correlations $c_X(q, k', k)$ were then artificially kept constant for the first few picoseconds to allow the other two-particle correlations to build up. This was seen to dampen out initial oscillations of the exciton numbers, the runs converged to the same final states, however.

Figure (2.1) shows the results from a set of calculations where the initial exciton fractions were varied from $X_f(t=0) = 0$ to $X_f(t=0) = 0.3$. In all cases, carrier densities of $na_0 = 0.05$ were inserted in Fermi-Dirac distributions at the lattice temperature $T_L = 20$ K. The runs are seen to converge to a well-defined equilibrium fraction of $X_f = 0.154$. The center-of-mass distributions $f_{1s}(q)$ of the the excitons at time $t = 0.6$ ns are shown in Fig. (2.2). Results of calculations where the initial exciton fraction was less (greater) than the equilibrium fraction $X_f = 0.15$ are plotted as dashed (dash-dotted) lines, respectively, while the run with $X_f(t=0) = 0.15$ is represented by the solid line. In all calculations, initial distributions of center-of-mass momenta was proportional to the 1s wave function, but have been broadened into much wider distribution at time $t = 0.6$ ns. Although the exciton fractions have not fully converged after 0.6 ns, the *shape* of $f_{1s}(q)$ is seen to be the comparable for the runs started with $X_f(t=0)$ close to 0.15. In comparison, the

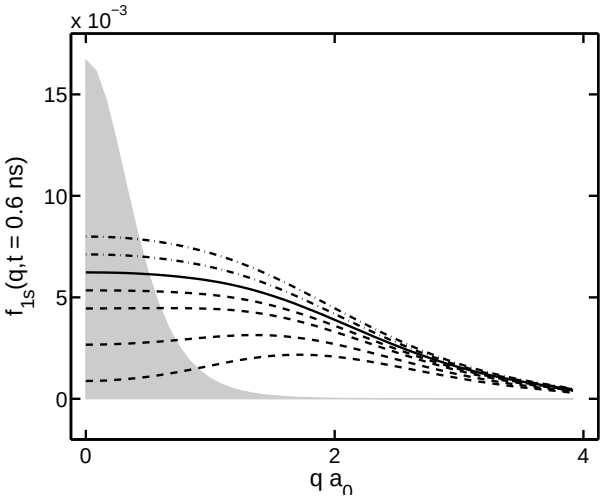

Figure 2.2: Shown are the distributions of the center-of-mass momenta at time $t = 0.6$ ns for various initial fractions $X_f(t = 0)$. The dashed (dash-dotted) lines give $f_{1s}(q)$ for calculations where $X_f(t = 0)$ was lower (greater) than the equilibrium fraction $X_f = 0.15$, respectively, while the solid line shows the result where $X_f(t = 0) = 0.15$. Initially, the $f_{1s}(q)$ were proportional to the 1s wave function, given by the shaded area. The runs were carried out for $na_0 = 0.05$ and $T = 20$ K.

center-of-mass distribution is shifted towards higher q in the runs with initially low exciton fractions. This shift results directly from the q-dependence of the exciton-formation process via LA-phonon scattering.

In further calculations we have established that the final state of the system is independent of the initial shape of both the carrier distributions and the distribution of the exciton center-of-mass momenta. While falling short of mathematical proof, these results suggest that the equilibrium position of the system is sufficiently stable against variations of the initial conditions, justifying the decision not to include the excitation of the system into the theoretical model. Indeed, the independence of the final state on the initial exciton population provides a convenient tool to determine the equilibrium exciton fractions. Instead of starting the calculation with vanishing exciton correlations and dynamically calculating the slow build-up of excitonic correlations by phonon scattering, a set of short calculations with varying exciton fractions is carried out. From these an approximate equilibrium fraction can be estimated. Providing subsequent calculations with this value as a starting point leads to fast convergence towards a steady state. The majority of the equilibrium exciton fractions presented in the next section have been calculated this way. The notable exceptions are the calculations at very low temperatures

and densities. For these, numerical instabilities introduced by the unphysically large grid of lattice points disturb the equilibration of the system to a steady state. A more detailed discussion of these effects is given in Appendix C.

On a side note it should also be pointed out that slight variations in $X_f(t)$ are observed in Fig. (2.1) during the initial 120 ps, even though $c_X(q, k', k)$ is kept constant. This behavior can be explained by the time dependence of the exciton wave function entering in Eq. (2.11). As discussed previously, non-vanishing carrier densities $f_k^{e,h}$ introduce a phase-space filling factor $(1-f_k^e-f_k^h)$ into the generalized Wannier equation. Through this factor dynamical changes of the carrier distributions influence the shape of the excitonic wave functions. This effect is most pronounced during the start of the calculation when the system is far from it's equilibrium state, and fast changes of $f_k^{e,h}$ in lead to the observed fluctuations in the exciton fractions calculated from $c_x(q, k', q)$

2.6 Equilibrium Exciton Fractions

By repeating the numerical integration detailed above for different combinations of carrier-densities and lattice temperatures one arrives at the phase diagram for the equilibrium exciton fraction shown in Fig. (2.3). It is seen that fractions $X_f > 0.3$ are only stable for a narrow parameter range where $na_0 \leq 0.05$ and $T_L \leq 15$K while X_f decreases monotonously for either increasing temperatures and densities. Qualitatively, the dependence of X_f on the temperature is readily explained by thermodynamical arguments, since changes in the kinetic energy of the carrier plasmas directly influence the probability of thermally ionizing a bound electron-hole pair. In order to explain the effect of the carrier density on the equilibrium exciton fractions three main contributions are identified: (i) The screening of the Coulomb potential is strongly density dependent. Increasing the carrier density weakens the attractive interaction between electrons and holes, leading to a reduced exciton binding energy and thus an increased ionization of the weakly bound pairs. (ii) At low densities the excitons may be described as being approximatively Bosonic with a well-defined number operator. The Fermionic substructure becomes increasingly important when the mean distance between the electrons within a band is decreased. (iii) Non-linear carrier-carrier scattering is strongly enhanced for elevated carrier densities.

It should be pointed out that the equilibrium exciton fractions X_f plotted in Fig. (2.3) differ from those reported in Ref. [51] at low carrier densities. The deviations stem from a different treatment of the signs $\sigma_{\mathrm{PH}}^{e,h}$ in the carrier-phonon interaction matrix elements in the valence or conduction band. Whereas in Ref. [51] the same sign $\sigma_{\mathrm{PH}}^e = \sigma_{\mathrm{PH}}^h$ was used, in the calculations presented here an opposite sign $\sigma_{\mathrm{PH}}^e = -\sigma_{\mathrm{PH}}^h$ was assumed.

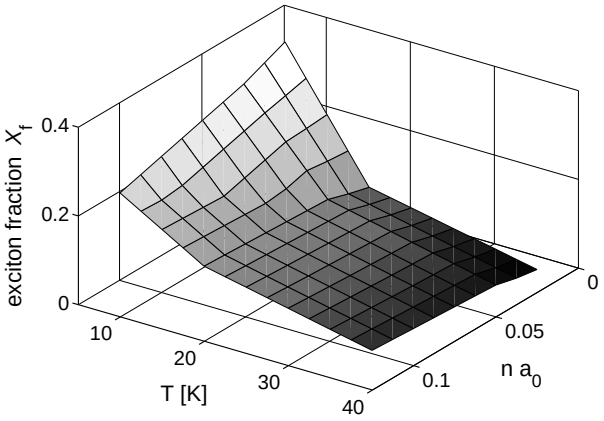

Figure 2.3: Quasi-equilibrium exciton fractions as function of density and temperature.

It is interesting to compare the dynamical calculations of X_f with theoretical predictions based on equilibrium thermodynamics. In these calculations the carrier densities $n^{e,h}$ are written as the sum of an unbound contribution $n_0^{e,h}$ and the correlated density $n_{\rm corr}^{e,h}$

$$n^{e,h} = n_0^{e,h} + n_{\rm corr}^{e,h} \; . \tag{2.75}$$

The degree of ionization is defined as

$$\alpha = \frac{n_0^e}{n^e} = \frac{n_0^e}{n_0^e + n_{\rm corr}^e} \tag{2.76}$$

Various schemes to to calculate n_0^e have been propoesed in the last fifty years [52–54]. In this work, however, we use the basic textbook version [52] of the so-called mass-action law, which is still frequently found in literature.

The underlying idea of the mass-action law is to identify the uncorrelated densities $n_0^{e,h}$ with populations of free electrons and holes, respectively, while the correlated part $f_{1\rm s} \equiv n_{\rm corr}^{e,h}$ is assumed to describe an independent population of bound excitons. The transformation of carriers into bound pairs is governed by the ionization reaction

$$\text{exciton} \rightleftharpoons h^+ + e^- \; . \tag{2.77}$$

In this picture, Eq. (2.75) is written as $n^{e,h} = n_0^{e,h} + n_X$, which ensures the conservation of carriers under the chemical reaction described by Eq. (2.77). In the thermodynamic equilibrium the free energy necessarily is minimal with respect to the particle numbers, i.e.

$$\frac{\partial F}{\partial n_0^e}\delta n_0^e + \frac{\partial F}{\partial n_0^h}\delta n_0^h + \frac{\partial F}{\partial n_{1\rm s}}\delta n_{1\rm s} = 0 \; . \tag{2.78}$$

Using the definition of the chemical potential

$$\mu_i = \left(\frac{\partial F}{\partial n_i}\right)_{T,V} \tag{2.79}$$

and Eq. (2.75) the condition for the equilibrium,

$$\mu_e + \mu_h = \mu_{1\mathrm{s}} \tag{2.80}$$

can be derived. Describing in a first approximation the particles as ideal particles in Boltzmann distributions, one obtains the so-called Saha equation, which for a one-dimensional system is given by

$$\frac{n_{1\mathrm{s}}}{(n_0 - n_{1\mathrm{s}})^2} = \frac{\hbar\sqrt{2\pi}}{\sqrt{m_{\mathrm{red}} k_B T}} e^{E_{1\mathrm{s}}/(k_B T)} \equiv f(T, n_0) \; . \tag{2.81}$$

The right hand side of Eq. (2.81) is a function $f(T, n_0)$ of the temperature and density, due to the appearance of the carrier distributions in the generalized Wannier equation (B.4) which determines the exciton binding energy $E_{1\mathrm{s}}$. Solving Eq. (2.81) for $n_{1\mathrm{s}}$ leads to

$$n_{1\mathrm{s}}(T, n_0) = n_0 + \frac{1}{2f(T, n_0))} \pm \sqrt{\frac{n_0}{f(T, n_0)} + \frac{1}{(2f(T, n_0))^2}} \; , \tag{2.82}$$

where the branch of solutions with the plus in front of the square root can be neglected, since in that case $n_{1\mathrm{s}} > n_0$. From Eq. (2.82) the equilibrium exciton fraction is obtained as a function of density and temperature according to $X_f(T, n_0) = \frac{n_{1\mathrm{s}}(T, n_0)}{n_0}$ for $n_0 > 0$. In order to calculate X_f with the mass action law, exciton binding energies $E_{1\mathrm{s}}$ have to be inserted into Eq. (2.82). The basic approximation of a density independent $E_{1\mathrm{s}}$ yields a monotonous rise of X_f for increasing n_0, with $X_f \to 0$ for $n_0 \to 0$ and $X_f \to 1$ for $n_0 \to \infty$. This non-physical behavior is alleviated, when the density dependence of the binding energies is taken into account, e.g. by the introduction of a screened Coulomb potential. In our calculations the binding energies are obtained from the numerical evalution of the generalized Wannier equation (B.4) as the difference between the lowest energy eigenvalue and the eigenvalue of the lowest degenerate band state. In this way, as explained above, the densities have a two-fold effect on the exciton binding energies, namely via the Lindhardt screening of the Coulomb potential and the Fermionic Pauli-blocking factor $(1 - f_k^e - f_k^h)$. Additionally, since Eq. (B.4) is also used for the calculation of X_f from the electron-hole correlations via (2.11) the density dependence predicted from the mass-action law and the dynamical calculations can be compared directly. In Fig. (2.4) the resulting exciton fractions X_f are

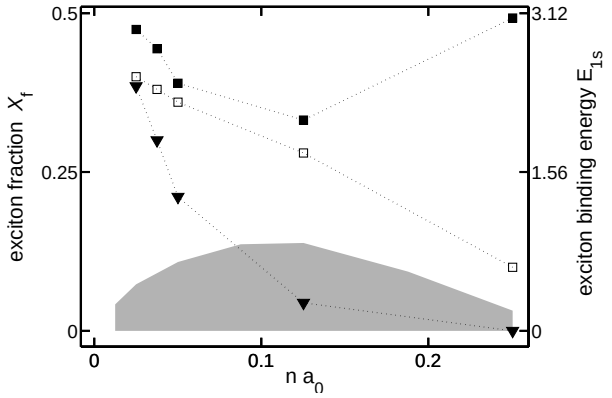

Figure 2.4: The equilibrium exciton fractions X_f obtained with the microscopical model (open squares) are compared to the result of a mass action law calculation (solid squares). The formation rate is indicated by shaded area in units of 1/ns. The solid triangles the exciton binding energies as function of density, the corresponding energy scale is plotted at the right hand side ordinate. The connecting lines are guides to the eye.

plotted as functions of the carrier density for a constant lattice temperature of $T = 10$ K. While the mass-action law (solid squares) is seen to approximatively reproduce the dynamical calculations (open squares) at low densities, it clearly fails for medium and high densities. In order to analyze the mass-action-law results, the density dependence of the exciton binding energy is plotted in Fig. (2.4) as a triangles; the energy scale is given on the axis on the right-hand side. It can be seen that the negative gradient at low densities in the mass-action-law calculations coincides with a drop in the binding energies. Going to higher densities, however, in spite of the further decline of E_{1s} the simple mass-action law predicts X_f to rise again. In Ref. [54] a modified mass-action law was used to calculate the degree of ionization α of a two-dimensional electron-hole plasma. The rise of the correlated carrier densities with increasing n_0 as predicted by the simple-mass action law is reported to result from the restriction of the calculations to the 1s exciton state. Inclusion of scattering states is shown to result in a significantly increased degree of ionization, yielding better agreement with the results presented here.

2.7 Stability of 2p Excitons

Analoguous to the atomic spectroscopy transitions of the carriers between the exciton states can be excited optically, however, since the transition energies are typically of the order of 1 meV, the frequency of the absorbed photons is

in the Terahertz (THz) regime [11,13,14].

At this point, a short side remark is required regarding the labels of the exciton states. In bulk semiconductors, the state of the excitons is described by three quantum numbers (neglecting spin), namely the principal quantum number ν arising from the radial Schrödinger equation and the orbital quantum numbers l and m. With the quantization of the motion perpendicular to the quantum wire the charge carriers are restricted to a one-dimensional motion and an exciton between an electron in the energetically lowest conductions and a hole in the highest valence band is fully described by the quantum number ν labeling the eigenstates of the generalized Wannnier equation (B.4). It is nevertheless convenient to label the three lowest states in analogy to the hydrogen atom as $\nu = 1\mathrm{s}$, $\nu = 2\mathrm{p}$ and $\nu = 2\mathrm{s}$, respectively, as indication of their symmetry. Since the possibility of an optical transition between two states is determined by the matrix element of the dipole operator $\langle er \rangle$, only transitions between two states with opposite symmetry are allowed. With the labeling $\nu \in \{1\mathrm{s}, 2\mathrm{p}, 2\mathrm{s}\}$ the well known optical selection rules of the hydrogen atom are regained for the transitions between the one-dimensional excitons considered in this thesis.

In a recent publication [50] the conversion of a coherent polarization into incoherent exciton populations has been investigated. It was found that for resonant pumping at the 2s exciton energy the created polarization is converted mainly into 2s and 2p populations while only vanishing fractions 1s excitons are created, leading to an inversion between the excited states and the ground state, respectively. While the selection rules forbid an optical transition from 2s to 1s, probing of the 2p-1s resonance is calculated to yield a pronounced THz response.

In the cited reference, the conversion ratio of polarization into incoherent 2p excitons was found to be density dependent, peaking at roughly 40% of 2s excitons converted into 2p populations for densities around $na_0 = 0.025$. To our knowledge, the stability of these populations against non-radiative decay into the 1s ground state has not yet been investigated. The decay due to carrier-phonon scattering can directly be simulated with the model introduced earlier in this chapter.

Since the eigenfunctions of a single electron hole pair in a quantum-wire system are determined by the Wannier equation (B.3), which is formally equivalent to the radial wave equation of an isolated hydrogen atom, the zero density exciton spectrum is known to consists of an infinite series of both bound and ionized states. For non-vanishing carrier densities, however, many particle effects such as phase-space filling and screening of the Coulomb potential become increasingly important. Consequently, the binding energies calculated by the generalized Wannier equation (B.4) are reduced with respect to the zero-density case and the weakly bound states merge into the free-particle

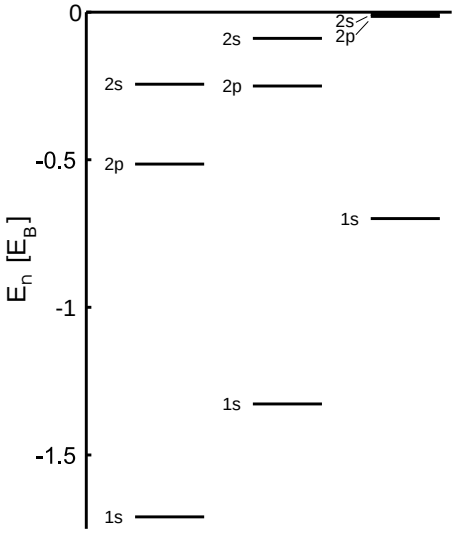

Figure 2.5: The binding energies for the 1s, 2p and 2s exciton state are shown for three different parameter sets. The energies on the left were calculated for $na_0 = 0.025$ at $T = 30$ K, the middle ones for $na_0 = 0.025$ and $T = 10$ K and the energies on the right for $na_0 = 0.05$ at $T = 10$ K.

continuum. At a temperature of $T = 10$ K an increase of the density from $na_0 = 0.025$ to $na_0 = 0.1$ decreases the number of bound states from seven to merely one. The last bound state vanishes at $na_0 \approx 0.5$, i.e. when the density is so high that the probability to find another charge carrier within one exciton diameter $2a_0$ approaches unity, in close agreement with Motts gedankenexperiment [55]. In Fig. (2.5) the energy spectrum of the exciton eigenstates for three different combinations of temperature and carrier density is plotted.

The calculations in the presented work were limited to a comparatively narrow range of densities. The upper boundary is marked by the merging of the 2p state with the carrier plasma for $na_0 > 0.1$. At low densities, the numerical calculations were found to become increasingly unstable, limiting the investigated densities to $na_0 \geq 0.025$. In the calculations of the 2p stability, the radius parameter R was by a factor of 1.25, compared to the equilibrium calculations, resulting in an increase in the matrix elements of the electron-phonon and the Coulomb interaction, according to Eqs (2.44) and (A.9).

2.7.1 Initial Distributions

In the equilibrium-level calculations we had chosen to start the simulation with Fermi-Dirac distributed carriers and electron-hole correlations corresponding to an initial distribution $f_{1s}(q)$ of 1s excitons. All other correlations were

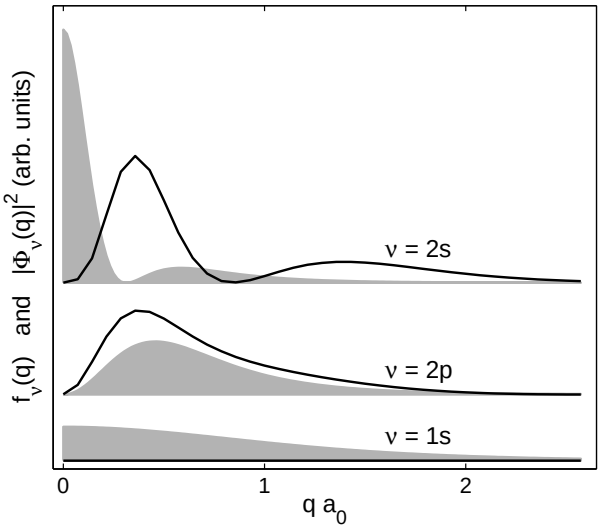

Figure 2.6: Shown are the square of the wave functions (shaded areas) and the initial distributions of center-of-mass momenta (lines) for the excitonic states $\nu = 1\mathrm{s}, 2\mathrm{p}$ and 2s.

initially set to zero, but were allowed to build up for an initial 4 ps, while the diagonal exciton correlations were artificially kept constant.

In this chapter we again start the calculations at t_0 after the initial excitation when the coherences have already decayed. The carriers are assumed to have relaxed towards a thermalized distribution at temperatures $T_{\mathrm{e,h}}$ close to the lattice temperature. The initial distributions $f_{2s}(q)$ and $f_{2p}(q)$ were added after a few picoseconds into the numerical calculations, to allow the off-diagonal exciton correlation, as well as $c_e(q,k',k)$ and $c_h(q,k',k)$ to build up.

The diagonal populations of 2s and 2p excitons were set to be proportional to the absolut square of the scattering matrix elements $M_{\nu,q}$ given in Ref. [50],

$$M_{\nu,q} = \sum_k (\Phi_\nu(k))^* [P^{cv}_{k+q_e} - P^{cv}_{k-q_h}] \,, \tag{2.83}$$

where P^{cv}_k is the excited interband polarization. For weak pumping of the 2s resonance one may approximate $P_k \propto \Phi_{2s}(k)$ and thus obtains

$$f_{2p}(q) \propto \left| \sum_k (\Phi_{2p}(k))^* [\Phi_{2s}(k+q_e) + \Phi_{2s}(k+q_h)] \right|^2 \tag{2.84}$$

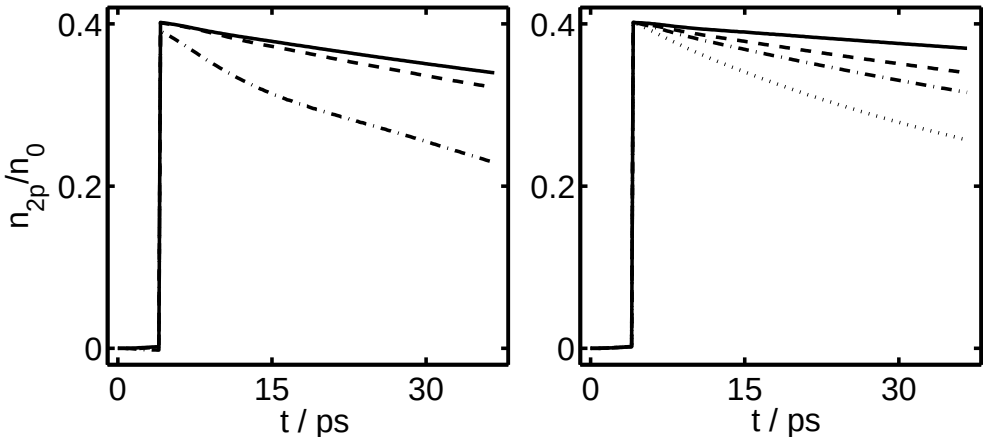

Figure 2.7: The time evolution of a population of 2p excitons is plotted for different temperatures and densities. The left-hand figure shows simulations carried out at $T = 10$ K with densities $na_0 = 0.025$ (solid line), $na_0 = 0.05$ (dashed line) and $na_0 = 0.1$ (dash-dotted line). In all calculations plotted in the right-hand figure the density was kept at $na_0 = 0.025$, while the temperature was set to $T = 4$ K (solid line), $T = 10$ K (dashed line), $T = 15$ K (dash-dotted line) and $T = 30$ K (dotted line).

and

$$f_{2s,q} \propto \left| \sum_k (\Phi_{2p}(k))^* [\Phi_{2s}(k + q_e) - \Phi_{2s}(k - q_h)] \right|^2 . \tag{2.86}$$

The resulting center-of-mass distributions are plotted together with the exciton wave functions of the three lowest states in Fig. (2.6).

In Fig. (2.7) the decay of the 2p populations in the absence of 2s excitons is plotted. The plots show the expected strong dependence of the decay times on carrier density and temperature. The extracted decay rates γ_{2p} of the 2p populations are given in Table 2.1. For the lowest temperatures and densities the phonon induced decay rate is $\gamma_{2p} \approx 3$/ns, which is of order of the exciton formation rates reported in Ref. [15]. The density dependence of the 2p stability is explained by the reduction of the 2p-binding energy with increasing carrier densities.

From comparison with Fig. (2.5) it is seen that the decay rate $\gamma_{2p} = 15$/ns at $na_0 = 0.1$ represents an extremal value for the phonon-assisted 2p annihilation process, since at that density the 2p excitons are so weakly bound that they almost merge with the ionization continuum. The 2p excitons are found

na_0	T [K]	$n_{2s}(t=0)$	γ_{2p} [ns^{-1}]
0.025			5
0.05	10	0	6.8
0.1			15
	4		2.4
0.025	15	0	7.2
	30		12.8
		0.2	4.2
0.025	10	0.4	3.5
		0.6	2.8

Table 2.1: The decay rates γ_{2p} of the 2p excitons are listed for different densities and temperatures. The results shown in the last section of the table were obtained when an additional population n_{2s} was inserted at $t = 0$.

to primarily decay into the ionized electron-hole pairs, as only insignificant phonon-induced conversion of 2p populations into 1s excitons is observed (not plotted).

In order to probe the conversion of X_ν to $X_{\nu'}$ for $\nu \neq \nu'$ a set of low-temperature and low-density calculations were performed, where varying initial fractions X_{2s} of 2s excitons were inserted at the same time as the 2p populations. The corresponding decay rates are found on the last three lines of table (2.1), exhibiting a decrease of the 2p decay rates for increasing fraction X_{2s} as the 2p population is 'refilled' by scattering from 2s states.

Chapter 3

Signatures of Incoherent Populations in Absorption

3.1 Linear Absorption

In first approximation, the polarization $P(t)$ induced in a semiconductor crystal by a weak incident light pulse scales linearly with the amplitude $E(t)$ of the electric field, with non-linear contributions becoming increasingly important for elevated $E(t)$. In a pump-probe experiment the carriers are excited by a pump pulse which precedes the probe beam by the time τ. The linear response of the system is measured if τ is long compared to the decay time T_2, so that the coherent polarization induced by the first pulse has completely decayed before the system is probed. Conversely, e.g. the four-wave mixing (FWM) signal is generated in third order of the incident fields. The polarization (first order) of the probe beam interferes with the residual polarization (second order) induced by the pump pulse to create density grating, of which the probe field (third order) is then diffracted [56]. Consequently, the FWM signal vanishes for $\tau \gg T_2$.

While FWM experiments have extensively been studied in the past, yielding detailed insight into the coherent dynamics of semiconductors, the influence of incoherent populations on pump-probe experiments has, to the best of our knowledge, not yet been fully investigated [57, 58]. In particular, the effects of incoherent populations of bound electron-hole pairs on linear absorption has not been described by a microscopical theory.

We start this chapter with a short review on experimentally observed features in pump-probe spectroscopy. In order to describe the system theoretically, a closed set of equations of motions for the linear optical response of a semiconductor is derived which consistently includes the effect of incoherent carrier-populations. In the subsequent numerical evaluation of the equations, the terms containing incoherent expectation values are switched on consecu-

tively, in order to determine the effects of each contribution separately. Thus, as a first step, only uncorrelated densities $f_k^{e,h}$ are taken into account. Afterwards, diagonal exciton populations and, lastly, electron-electron, hole-hole and off-diagonal electron-hole correlations are included in the calculations.

3.1.1 Definition of Terms

The optical response of a semiconductor of non-interacting electrons and holes is equivalent to that of a system of non-interacting two-level absorbers and is, in the weak coupling regime, described by the optical Bloch equations. In this limit the absorption spectrum is proportional to the density of states and thus does not exhibit any features energetically below the bottom of the conduction band. Inclusion of the Coulomb interaction leads, in first order, to the appearance of a series of excitonic resonances energetically below the bandgap and also introduces an enhancement factor to the continuum transitions. The linear susceptibility of the system may be then described by the Elliott formula [59]

$$\chi(\omega) = \sum_{\nu} \frac{f_\nu}{\hbar\omega - E_\nu + i\hbar\gamma_\nu} \,, \tag{3.1}$$

where the index ν runs over all states, i.e. both discrete bound and continuous unbound states, and E_ν and $\hbar\gamma_\nu$ are the energy and the broadening of each transition ν, respectively. The spectral weight of the transition is given by the so-called oscillator strength f_ν, which in the zero-density limit is proportional to the absolute square of the interband dipole matrix element times the probability of finding electron and hole in the same unit cell, i.e.

$$f_\nu \propto |d^{vc}|^2 |\Phi_\nu(r=0)|^2 \,. \tag{3.2}$$

In this chapter, the changes in the absorption of the lowest excitonic resonance introduced by incoherent carrier densities and bound excitons are investigated. Adopting the conventions found in the literature we use the following names for the observed effects. A change in the absolute energy E_{1s} of the peak position is called *absorption line shift*. A *reduction in the oscillator strength (ROS)* occurs when the integrated area of the absorption line is diminished with respect to the reference value. A direct cause for ROS is the phase-space filling factor in the polarization equation (3.16), where occupation of states by finite densitiesy inhibits the further polarization of the semiconductor. The increased scattering of the interband polarization at non-vanishing carrier distributions leads to a reduction of the life time of the polarization, which is reflected by a *broadening* of the excitonic absorption line. This so-called *excitation induced dephasing (EID)* is accompanied by a reduction in the overall peak height, but does not change the integrated spectral weight of the transition. Finally, the term

bleaching encountered in the literature signifies an increased transmission at the center of the exciton line, i.e. any effect that causes the peak absorption to become smaller is said to bleach the exciton. Thus, bleaching of the exciton resonance may be caused by both excitation induced dephasing or a reduction of the oscillator strength.

3.1.2 Experimental Findings

The bleaching of the 1s exciton resonance by optically generated carriers has been observed in a number of experiments in both bulk GaAs [60, 61] and quantum-well structures [19, 20]. While, at first, the underlying mechanisms were somewhat uncertain [21], differential transmission spectra allowed for direct measurement of both ROS and broadening. In this way, the bleaching by a carrier density of $n \times \frac{4\pi}{3} a_0^3 = 0.07$ in a wide well was shown to originate from excitation induced dephasing [22]. Similarly, in thin 10 nm wells a prevalence of EID was reported for densities $n \times \pi a_0^2 = 0.07$, while for higher carrier densities up to $n \times \pi a_0^2 = 0.74$ strong contributions due to ROS were observed [62].

In another line of experiments, the energetic position of the exciton resonance E_{1s} as a function of carrier density was investigated. While E_{1s} was found to be independent of the carrier density in bulk GaAs [61], a strong blue-shift of the peak position with increasing density was reported in 1982 for a multiple-quantum-well structure [23]. Further experiments [24,25] confirmed this dependence of the energy shift on the thickness d of the samples, yielding a strong density dependence of the resonance energy in narrow ($d < 100$ nm) wells, while weak shifts were reported for $d = 200$ nm [63,64]. The blue-shift is attributed to bound excitons, since the charge neutrality of the system should lead to reduced screening and hence enhanced binding energies. However, previous theoretical calculations of the blueshift were limited to the singlet level semiconductor Bloch equations [38, 65] and thus did not include the effect of bound electron-hole pairs.

3.2 Theoretical Model

3.2.1 Microscopic Calculation of Absorption Spectra

If a light field $\mathcal{E}(t)$ incident on a semiconductor sample has the proper energy, it can excite electrons from their equilibrium positions, resulting in a macroscopic polarization $P(t)$ of the sample. The relation between $\mathcal{E}(t)$ and $\mathcal{P}(t)$ is given by the optical susceptibility $\chi(\omega)$ which is defined as the complex coefficient between the Fourier transformations $\mathcal{E}(\omega)$ and $\mathcal{P}(\omega)$ in the frequency domain,

$$\chi(\omega) = \frac{\mathcal{P}(\omega)}{\mathcal{E}(\omega)} \,. \tag{3.3}$$

Following textbook discussions it is easy to show that the imaginary part of the susceptibility is connected to the absorption coefficient $\alpha(\omega)$ via

$$\alpha(\omega) = \frac{4\pi\omega}{n_b c}\mathrm{Im}(\chi)(\omega) \,, \tag{3.4}$$

where n_b denotes the background refractive index. In the following, equations of motion are derived which allow a direct calculation of the polarization induced by a probe field E(t). The resulting equations are then solved numerically.

In the quantum-mechanical description of the system the macroscopic polarization is given by

$$\mathcal{P}(t) = \mathrm{tr}(\rho(t)d) \,, \tag{3.5}$$

where $\rho(t)$ is the one-particle density matrix and $d = er$ is the projection of the dipole operator in direction of the electric field. Evaluation of the trace

$$\mathrm{tr}(\rho(t)d) = \sum_n \langle n|\rho(t)d|n\rangle \tag{3.6}$$

in the Bloch basis yields

$$\mathcal{P}(t) = \sum_{\mathbf{k},\lambda} \langle \mathbf{k},\lambda|\rho(t) \left(\sum_{\mathbf{k}',\lambda'} |\mathbf{k}',\lambda'\rangle\langle \mathbf{k}',\lambda'| \right) d|\mathbf{k},\lambda\rangle \,, \tag{3.7}$$

where we have used the completeness of the Bloch states to insert the unity operator $\hat{\mathbf{1}}$ in the round brackets. Following textbook derivations [43], the interband dipole matrix element $\langle \mathbf{k}',\lambda'|d|\mathbf{k},\lambda\rangle$ is obtained as

$$\langle \mathbf{k}',\lambda'|d|\mathbf{k},\lambda\rangle(1-\delta_{\lambda,\lambda'}) \simeq \delta_{\mathbf{k},\mathbf{k}'}(1-\delta_{\lambda,\lambda'})d_{\lambda,\lambda'}(\mathbf{k}=0) \,, \tag{3.8}$$

where the constant $d_{\lambda,\lambda'}(\mathbf{k}=0)$ is obtained by integrating the momentum operator $\mathbf{p}$ with the lattice-periodic Bloch functions

$$d_{\lambda,\lambda'}(\mathbf{k}=0) = \frac{ie}{m_0 E_G}\frac{1}{V_{\mathrm{u.c.}}}\int_{\mathrm{u.c.}} dV u^*_{\lambda'}(\mathbf{k}=0,\mathbf{r})\mathbf{p}u_\lambda(\mathbf{k}=0,\mathbf{r}) \tag{3.9}$$

over one unit cell (u.c.). Using Eqs (3.7) and (3.9) the macroscopic interband polarization is thus given by

$$\mathcal{P}(t) = \sum_{\mathbf{k}} P^{cv}(\mathbf{k},t)d^{vc}(\mathbf{t}) + c.c. \,, \tag{3.10}$$

where

$$P^{cv}(\mathbf{k},t) = \langle \mathbf{k},c|\rho(t)|\mathbf{k},v\rangle \tag{3.11}$$

is the off-diagonal matrix element of the one-particle density matrix. In the following sections equations of motion for $P^{cv}(\mathbf{k},t)$ are derived and subsequently solved numerically. The linear response of the system to the incident light field $\mathcal{E}(t)$ is then calculated via Eqs (3.3), (3.4) and (3.10).

3.2.2 Model System and Hamiltonian

As mentioned, the experimental conditions analyzed in this part of the thesis correspond to a time-resolved pump-probe setup, where a pump beam incident at time $t = -\tau$ excites the carrier system, which is then probed with a weak pulse at $t = 0$. The delay τ between the two pulses is chosen to fulfill $\tau \gg T_2$, so that the coherent information of the pump pulse has decayed before the absorption spectrum is measured. By tuning the spectral position of the pump pulse either to the 1s exciton resonance or into the continuum of states above the bandgap, the probed system thus contains either a large population of bound electron-hole pairs [50] or an electron-hole plasma.

If the sample is kept at low temperatures, a hot electron-hole plasma created by non-resonant excitation is rapidly scattered towards the center of the Brillouin zone by emission of LO-phonons [66, 67]. The equilibration of the carriers towards Fermi-Dirac distributions is governed by Coulomb-scattering which takes place on a femtosecond timescale [68]. We thus assume that under non-resonant excitation conditions the carrier are thermalized at or close to the lattice temperature by the time the system is probed.

The dynamics of the probe-induced polarization are assumed to be described by the Hamilton operator

$$H = H_{\text{kin}} + H_{\text{Coul}} + H_l \ , \tag{3.12}$$

where the contributions containing the single-particle energies H_{kin} and the Coulomb interaction H_{Coul} are given in Eqs (2.35) and (2.50), respectively.

Following the derivation in Ref. [43], the light-matter interaction Hamiltonian in the dipole approximation is obtained as

$$H_l = -e\mathbf{d} \cdot \mathcal{E} \ , \tag{3.13}$$

where $\mathbf{d}$ is the dipole operator. The second quantized form of the Hamilton operator again is obtained by expansion of the field operators in the Bloch basis

$$\begin{aligned} H_l &= -\int d^3r \hat{\Psi}^\dagger(r) e\mathbf{d} \cdot \mathcal{E} \hat{\Psi}(r) & (3.14) \\ &= \sum_k \left(\hat{a}^\dagger_{c,k} \hat{a}_{v,k} \mathbf{d} \cdot \mathcal{E}(t) + h.c. \right) \ . & (3.15) \end{aligned}$$

3.2.3 Hierarchy of Equations of Motion

As discussed in the previous chapter the inclusion of any two-particle interaction leads to the coupling of N-particle dynamics to $(N+1)$-particle expectation values. The hierarchy of equations resulting from the Coulomb interaction

again are cut at the doublet level of the cluster expansion. However, in comparison with the previous chapter, where only the incoherent carrier system was calculated dynamically (with the phonons being treated in a Markov approximation), the number of expectation values doubles with the inclusion of coherent expectation values. In addition to the single particle densities $f_k^{e,h}$ and the incoherent two-particle correlations $c_X(q,k',k)$, $c_{ee}(q,k',k)$ and $c_{hh}(q,k',k)$ now also the interband polarization P_k^{eh}, biexciton amplitudes $c_{BIX}(q,k',k)$ and density-assisted polarizations $c_{(\mathrm{e,h})\mathrm{p}}(q,k',k)$ have to be calculated. The numerical complexity of such a full simulation is at the limit of modern computer systems both in terms of available memory and raw calculation speed. We therefore restrict our calculations to the description of experiments with very weak probe pulse, which allows us to view the light-matter interaction as a small perturbation of the semiconductor system. According to the dynamics controlled truncation (DCT) scheme, the expectation values can then be classified according to the order of the electrical field in which they are excited [69–71]. The zeroth order term of the DCT contains all terms which are non-zero at $t = 0$ before the onset of the incident pulse. For incoherent initial conditions this amounts – on the singlet-doublet level – to the carrier densities and two-particle carrier correlations, i.e. electron-electron, hole-hole, and excitonic correlations. In first order the light field will only influence interband polarizations and density assisted polarizations, while changes in the incoherent occupations as well as biexciton amplitudes are induced in second order. For the description of linear absorption properties therefore constant values are assigned to $f^e(k)$, $f^h(k)$, $c_X(q,k',k)$, $c_{ee}(q,k',k)$, and $c_{hh}(q,k',k)$, while P^{cv}, as well as $c_{ep}(q,k',k)$ and $c_{hp}(q,k',k)$ are calculated dynamically.

3.2.4 Equations of Motion

Using the Heisenberg equation of motion given in Eq. (2.1) the equations of motion for the microscopic interband polarizations are given by

$$\begin{aligned} i\hbar\frac{\partial}{\partial t}P_k^{v,c} = (\tilde{\epsilon}_k^c - \tilde{\epsilon}_k^v - i\gamma_P)P_k^{v,c} - (1 - f_k^c - f_k^h)\Omega_k^{v,c} \\ + \sum_{k',q} V_q \Big\{ c_{\mathrm{pe}}(q,k',k) + c_{\mathrm{ph}}(q,k',k) \\ - c_{\mathrm{ep}}^*(q,k',k) - c_{\mathrm{hp}}^*(q,k',k) \Big\} , \end{aligned} \tag{3.16}$$

where

$$\tilde{\epsilon}_k^\lambda = \frac{\hbar^2 k^2}{2m_\lambda} + \sum_{k'} V_{k-k'} f_{k'}^\lambda \tag{3.17}$$

and

$$\Omega_k^{v,c} = \mathbf{d}^{v,c} \cdot \mathcal{E} + \sum_{k'} V_{k-k'} P_{k'}^{v,c} \tag{3.18}$$

are the renormalized single particle and Rabi energies, respectively. A constant background dephasing of the interband polarization is included phenomenologically via the decay constant $\gamma_P = 0.05$ meV$/\hbar$ [72]. In the second line abbreviations for the density-assisted polarizations

$$\begin{aligned} c_{\mathrm{pe}}(q,k',k) &= \Delta\langle v\dagger_k c\dagger_{k'} c_{k'+q} c_{k-q}\rangle \ , \\ c_{\mathrm{ph}}(q,k',k) &= \Delta\langle v\dagger_k v\dagger_{k'} v_{k'+q} c_{k-q}\rangle \ . \end{aligned} \tag{3.19}$$

and their complex conjugates

$$\begin{aligned} c_{\mathrm{ep}}(q,k',k) &= \langle c\dagger_k c\dagger_{k'} c_{k'+q} v_{k-q}\rangle = c^*_{\mathrm{pe}}(-q,k'+q,k-q) \\ c_{\mathrm{hp}}(q,k',k) &= \langle c\dagger_k v\dagger_{k'} v_{k'+q} v_{k-q}\rangle = c^*_{\mathrm{ph}}(-q,k'+q,k-q) \end{aligned} \tag{3.20}$$

have been defined.

The first term on the right hand side of Eq. (3.16) describes a rotation of the polarization with the renormalized one-particle energies $\tilde{\epsilon}_k^\lambda$. The light-matter interaction introduces the second term which, being non-zero for unexcited semiconductors, provides a source for the polarization dynamics. The Fermionic nature of the electrons modifies this source term by the Pauli blocking factor $(1 - f_k^c - f_k^h)$, preventing the excitation of carriers into states already occupied by the same species. The third term of Eq. (3.16) describes the scattering of the coherent polarizations with the incoherent carrier densities via the Coulomb interaction, thus coupling the interband polarization to the electron and hole-assisted polarizations $c_{\mathrm{pe}}(q,k',k)$ and $c_{\mathrm{ph}}(q,k',k)$, respectively.

To start the derivation of the equations of motion for $c_{\mathrm{pe}}(q,k',k)$ we calculate the commutator with the single particle and light field contributions to the Hamilton operator, respectively. This immediately yields

$$i\hbar\frac{\partial}{\partial t} c_{\mathrm{ep}}(q,k',k)|_{H_0} = (\tilde{\epsilon}^c_{k-q} + \tilde{\epsilon}^c_{k'+q} - \tilde{\epsilon}^c_{k'} - \tilde{\epsilon}^v_k - i\gamma_{\langle \mathrm{np}\rangle}) c_{\mathrm{ep}}(q,k',k) \tag{3.21}$$

and

$$\tag{3.22}$$

$$\begin{aligned} i\hbar\frac{\partial}{\partial t} c_{\mathrm{ep}}(q,k',k)|_{H_l} &= (\Omega_k^{c,v})^* c_{\mathrm{e}}(q,k',k) - (\Omega_{k'+q}^{c,v})^* c_{\mathrm{X}}(-q,k,k') \\ &\quad - (\Omega_{k-q}^{c,v})^* c_{\mathrm{X}}(k2+q-k1,k,k') \ . \end{aligned} \tag{3.23}$$

In Eq. (3.21) a dephasing constant $\gamma_{\langle \mathrm{np}\rangle}$ for the density-assisted polarizations is introduced. Due to the truncation of the hierarchy of equations of motion

on the doublet level, the broadening of the two-particle expectation values via triplet-level scattering terms is not included dynamically in our calculations, and a phenomenological density dependence of $\gamma_{\langle \mathrm{np} \rangle}$ was used instead. A more detailed discussion is given in Appendix E.

Using the cluster expansion to write the two-particle expectation values as the sum of the singlet and doublet contributions, the dynamics of the correlated density-assisted polarizations stemming from H_{Coul} are obtained as

$$\begin{aligned}
&i\hbar\frac{\partial}{\partial t}\Delta\langle v_k^\dagger c_{k'}^\dagger c_{k'+q} c_{k-q}\rangle|_{\mathrm{Coul}} \\
&\quad = i\hbar\frac{\partial}{\partial t}\,\langle v_k^\dagger c_{k'}^\dagger c_{k'+q} c_{k-q}\rangle\Big|_{\mathrm{Coul}} - i\hbar\frac{\partial}{\partial t}\,\{\langle v_k^\dagger c_{k'}^\dagger c_{k'+q} c_{k-q}\rangle\}_{\mathrm{s}}\Big|_{\mathrm{Coul}} \\
&\quad = \sum_{l,p} V_p\Big[- \langle v_{k-p}^\dagger c_{k'}^\dagger c_l^\dagger c_{l-p} c_{k'+q} c_{k-q}\rangle - \langle v_{k-p}^\dagger c_{k'}^\dagger v_l^\dagger v_{l-p} c_{k'+q} c_{k-q}\rangle \\
&\qquad\qquad - \langle v_k^\dagger c_{k'-p}^\dagger c_l^\dagger c_{l-p} c_{k'+q} c_{k-q}\rangle - \langle v_k^\dagger c_{k'-p}^\dagger v_l^\dagger v_{l-p} c_{k'+q} c_{k-q}\rangle \\
&\qquad\qquad + \langle v_k^\dagger c_{k'}^\dagger c_l^\dagger c_{l-p} c_{k'+q+p} c_{k-q}\rangle + \langle v_k^\dagger c_{k'}^\dagger v_l^\dagger v_{l-p} c_{k'+q+p} c_{k-q}\rangle \\
&\qquad\qquad + \langle v_k^\dagger c_{k'}^\dagger c_l^\dagger c_{l-p} c_{k'+q} c_{k-q+p}\rangle + \langle v_k^\dagger c_{k'}^\dagger v_l^\dagger v_{l-p} c_{k'+q} c_{k-q+p}\rangle\Big] \\
&\quad + \sum_p V_p\,\Big[\langle v_k^\dagger c_{k'}^\dagger c_{k'+q+p} c_{k-q-p}\rangle - \langle v_{k-p}^\dagger c_{k'+p}^\dagger c_{k'+q} c_{k-q+p}\rangle\Big] \\
&\quad - i\hbar\frac{\partial}{\partial t}\,\{\langle v_k^\dagger c_{k'}^\dagger c_{k'+q} c_{k-q}\rangle\}_{\mathrm{s}}\Big|_{\mathrm{Coul}} \,. \qquad (3.24)
\end{aligned}$$

Splitting the six-operator expectation values (3.24) into triplets, doublets and singlets and neglecting the true three-particle correlations yields, after an error prone calculation,

$$i\hbar\frac{\partial}{\partial t} c_{\mathrm{ep}}(q,k',k)|_{\mathrm{coul}} = \mathrm{HF}[c_{\mathrm{ep}}] + s[c_{\mathrm{ep}}] + S[c_{\mathrm{ep}}] \,. \qquad (3.25)$$

Here, the Hartree-Fock level contributions have been collected into

$$\begin{aligned}
&\mathrm{HF}[c_{\mathrm{ep}}] = \\
&+V_{k'+q-k}\Big\{ P_{k'+q}^{v,c}\,\big[f_{k-q}^c(1-f_k^v)(1-f_{k'}^c) + (1-f_{k-q}^c) f_k^v f_{k'}^c\big] \\
&\qquad - P_k^{v,c}\,\big[f_{k'}^c(1-f_{k'+q}^c)(1-f_{k-q}^c) + (1-f_{k'}^c) f_{k'+q}^c f_{k-q}^c\big] \\
&\qquad + P_{k-q}^{v,c}(P_{k'}^{v,c})^*(P_k^{v,c} - P_{k'+q}^{v,c})\Big\} \\
&+V_q\sigma\Big\{ P_k^{v,c}\,\big[f_{k'}^c(1-f_{k-q}^c)(1-f_{k'+q}^c) + (1-f_{k'}^c) f_{k-q}^c f_{k'+q}^c\big] \\
&\quad - P_{k-q}^{v,c}\,\big[f_{k'+q}^c(1-f_k^v)(1-f_{k'}^c) + (1-f_{k'+q}^c) f_k^v f_{k'}^c\big] \\
&\quad + P_{k'+q}^{v,c}(P_{k'}^{v,c})^*(P_{k-q}^{v,c} - P_k^{v,c})\Big\} \,, \qquad (3.26)
\end{aligned}$$

where the factor $\sigma = 2$ subsumes the effect of the two spin directions, while the terms containing doublet contributions are given by

$$
\begin{aligned}
& s[c_{\mathrm{ep}}] = \\
& -V_q\sigma \left[P^{v,c}_{k-q} - P^{v,c}_{k}\right] \sum_l \left(c_{\mathrm{e}}(q,k',l) + c_{eh}(-q,l,k')\right) \\
& +V_q\sigma \left[f^{c}_{k'} - f^{c}_{k'+q}\right] \sum_l \left(c_{\mathrm{pe}}(q,l,k) + c_{\mathrm{ph}}(q,l,k)\right) \\
& -V_{k'+q-k} \left[f^{c}_{k'} - f^{c}_{k-q}\right] \sum_l \left(c_{\mathrm{pe}}(k-q-k',l,k) + c_{\mathrm{ph}}(k-q-k',l,k)\right) \\
& +V_{k'+q-k} \left[P^{v,c}_{k'+q} - P^{v,c}_{k}\right] \sum_l \left(c_{\mathrm{e}}(k'+q-k,l,k') + c_{eh}(k'+q-k,l,k')\right)
\end{aligned}
\tag{3.27}
$$

and

$$
\begin{aligned}
& S[c_{\mathrm{ep}}] = \\
& -\left(f^{c}_{k-q} + f^{c}_{k'+q} - 1\right) \sum_l V^{s}_{l-q} c_{\mathrm{eh}}(l,k',k) \\
& +\left(f^{v}_{k} + f^{c}_{k'} - 1\right) \sum_l V^{s}_{l+q} c^{*}_{1}(l,k'+q,k-q) \\
& -\sum_l \left\{V^{s}_{l-k}\left[\left(f^{v}_{k} - f^{c}_{k-q}\right) c_{\mathrm{eh}}(q,k',l)\right] - V^{s}_{l-k'}\left[\left(f^{c}_{k'} - f^{c}_{k-q}\right) c_{\mathrm{eh}}(k-q-k',l,k)\right]\right\} \\
& -\sum_l \left\{V^{s}_{l-k'}\left[\left(f^{c}_{k'} - f^{c}_{k'+q}\right) c_{\mathrm{eh}}(q,l,k)\right] - V^{s}_{l-k}\left[\left(f^{v}_{k} - f^{c}_{k'+q}\right) c_{\mathrm{eh}}(k-q-k',k',l)\right]\right\} \\
& -P^{v,c}_{k-q} \sum_l \Big[+ V^{s}_{l+q} c_{eh}(l,k,k') + V^{s}_{l-k'} c_{\mathrm{X}}(k'+q-k,k,l) \\
& \qquad\qquad - V^{s}_{l-k} c_{eh}(-q,l,k')\Big] \\
& -P^{v,c}_{k'+q} \sum_l \Big[V^{s}_{l+q} c_{\mathrm{X}}(l,k,k') + V^{s}_{l-k} c_{eh}(k'+q-k,l,k') \\
& \qquad\qquad - V^{s}_{l-k'} c_{\mathrm{X}}(-q,k,l)\Big] \\
& +P^{v,c}_{k} \sum_l \Big[V^{s}_{l+q} c_{e}(l,k'+q,k-q)^{*} + V^{s}_{l-k} c_{e}(k-q-k',k',l) \\
& \qquad\qquad - V^{s}_{l-k} c_{e}(q,k',l)\Big] \,.
\end{aligned}
\tag{3.28}
$$

In the last term biexcitonic contributions – being excited in second order the exciting light field – have already been neglected.

In order to keep the computationally demanding evaluation of the Coulomb sums contained in $S[c_{\rm eh}]$ to a minimum we introduce new quantities

$$\Sigma_{y-1}^{q,k',k} = \sum_l V_{l-k}^s c_y(q,k',l) \;, \tag{3.29}$$

$$\Sigma_{y-2}^{q,k',k} = \sum_l V_{l-k'}^s c_y(q,l,k) \;, \tag{3.30}$$

$$\Sigma_{y-3}^{q,k',k} = \sum_l V_{l-q}^s c_y(l,k',k) \;, \tag{3.31}$$

where the sums over the incoherent carrier correlations, i.e. $y \in \{\mathrm{X},\mathrm{h},\mathrm{e}\}$, are constant in the weak excitation regime and therefore are evaluated only once at the start of the calculations, while the sums over the dynamic variables $y = \{\mathrm{pe},\mathrm{ph}\}$ have to be evaluated once in each time step. With these definitions Eq. (3.28) is condensed to

$$\begin{aligned} S[c_{\rm eh}] = & -\left(f_{k-q}^c + f_{k'+q}^c - 1\right)\Sigma_{8-3}^{q,k',k} \\ & +\left(f_k^v + f_{k'}^c - 1\right)\left(\Sigma_{1-3}^{-q,k'+q,k-q}\right)^* \\ & -\left(f_k^v - f_{k-q}^c\right)\Sigma_{8-1}^{q,k',k} + \left(f_{k'}^c - f_{k-q}^c\right)\Sigma_{8-2}^{k-q-k',k',k} \\ & -\left(f_{k'}^c - f_{k'+q}^c\right)\Sigma_{8-2}^{q,k',k} + \left(f_k^c - f_{k'+q}^v\right)\Sigma_{8-1}^{k-q-k',k',k} \\ & -P_{k-q}^{v,c}\left[\Sigma_{eh-3}^{-q,k,k'} + \Sigma_{X-1}^{k'+q-k,k,k'} - \Sigma_{eh-2}^{-q,k,k'}\right] \\ & -P_{k'+q}^{v,c}\left[\Sigma_{X-3}^{-q,k,k'} + \Sigma_{eh-2}^{k'+q-k,k,k'} - \Sigma_{X-1}^{-q,k,k'}\right] \\ & +P_k^{v,c}\left[\left(\Sigma_{e-3}^{-q,k'+q,k-q}\right)^* + \Sigma_{e-1}^{k-q-k',k',k} - \Sigma_{e-1}^{q,k',k}\right] . \end{aligned} \tag{3.32}$$

The equations of motion for c_{hp}

$$\begin{aligned} i\hbar\frac{\partial}{\partial t}c_{\rm hp}(q,k',k) = & \left(\tilde{\epsilon}_{k-q}^c + \tilde{\epsilon}_{k'+q}^v - \tilde{\epsilon}_{k'}^v - \tilde{\epsilon}_k^v - i\gamma_{\langle \rm np\rangle}\right)c_{\rm hp}(q,k',k) \\ & +\Omega^{q,k',k}[c_{\rm hp}] + \mathrm{HF}[c_{\rm hp}] + s[c_{\rm hp}] + S[c_{\rm hp}] \end{aligned} \tag{3.33}$$

has been derived in a similar way. Here, $\Omega^{q,k',k}[c_{\rm hp}]$ is defined as

$$\begin{aligned} \Omega^{q,k',k}[c_{\rm hp}] = & +\Omega_k^{v,c}c_{eh}(q,k',k) \\ & +\Omega_{k'}^{v,c}c_X(-q,k,k') \\ & -\Omega_{k-q}^{v,c}c_{\rm h}(q,k',k) \;. \end{aligned} \tag{3.34}$$

The Hartree-Fock expectation values again are contained in

$$\begin{aligned}
\mathrm{HF}[c_{\mathrm{hp}}] &= +V_{k'+q-k}\Big\{P^{v,c}_{k-q}\left[f^{v}_{k'+q}(1-f^{v}_{k'})(1-f^{v}_{k})+(1-f^{v}_{k'+q})f^{v}_{k'}f^{v}_{k}\right] \\
&\quad -P^{v,c}_{k'}\left[f^{v}_{k}(1-f^{c}_{k-q})(1-f^{v}_{k'+q})+(1-f^{v}_{k})f^{c}_{k-q}f^{v}_{k'+q}\right] \\
&\quad +P^{v,c}_{k}(P^{v,c}_{k'+q})^{*}(P^{v,c}_{k'}-P^{v,c}_{k-q})\Big\} \\
&\quad +V_{q}\sigma\Big\{P^{v,c}_{k}\left[f^{v}_{k'}(1-f^{c}_{k-q})(1-f^{v}_{k'+q})+(1-f^{v}_{k'})f^{c}_{k-q}f^{v}_{k'+q}\right] \\
&\quad -P^{v,c}_{k-q}\left[f^{v}_{k'+q}(1-f^{v}_{k})(1-f^{v}_{k'})+(1-f^{v}_{k'+q})f^{v}_{k}f^{v}_{k'}\right] \\
&\quad +P^{v,c}_{k'}(P^{v,c}_{k'+q})^{*}(P^{v,c}_{k-q}-P^{v,c}_{k})\Big\}\,, \qquad (3.35)
\end{aligned}$$

while

$$\begin{aligned}
s[c_{\mathrm{hp}}] &= -V_{q}\sigma\left[P^{v,c}_{k-q}-P^{v,c}_{k}\right]\sum_{l}\left(c_{\mathrm{h}}(q,k',l)+c_{eh}(q,k',l)\right) \qquad (3.36)\\
&\quad +V_{q}\sigma\left[f^{v}_{k'}-f^{v}_{k'+q}\right]\sum_{l}\left(c_{\mathrm{hp}}(q,l,k)+c_{8}(q,l,k)\right) \\
&\quad +V_{k'+q-k}\left[f^{v}_{k'+q}-f^{v}_{k}\right]\sum_{l}\left(c_{\mathrm{hp}}(k'+q-k,l,k')+c_{8}(k'+q-k,l,k')\right) \\
&\quad -V_{k'+q-k}\left[P^{v,c}_{k'}-P^{v,c}_{k-q}\right]\sum_{l}\left(c_{\mathrm{h}}(k-q-k',l,k)+c_{eh}(k'-k+q,k,l)\right)\,,
\end{aligned}$$

and

$$\begin{aligned}
S[c_{\mathrm{hp}}] &= +\left(f^{v}_{k}+f^{v}_{k'}-1\right)\left(\Sigma^{-q,k'+q,k-q}_{7-3}\right)^{*} \\
&\quad -\left(f^{c}_{k-q}+f^{v}_{k'+q}-1\right)\Sigma^{q,k',k}_{14-3} \\
&\quad +\left(f^{c}_{k-q}-f^{v}_{k}\right)\Sigma^{q,k',k}_{14-1}-\left(f^{v}_{k'+q}-f^{v}_{k}\right)\Sigma^{k'+q-k,k,k'}_{14-2} \\
&\quad +\left(f^{v}_{k'+q}-f^{v}_{k'}\right)\Sigma^{q,k',k}_{14-2}-\left(f^{v}_{k-q}-f^{c}_{k'}\right)\Sigma^{k'+q-k,k,k'}_{14-1} \\
&\quad +P^{v,c}_{k}\left[\left(\Sigma^{-q,k'+q,k-q}_{eh-3}\right)^{*}+\Sigma^{k-q-k',k',k}_{X-1}-\Sigma^{q,k',k}_{eh-1}\right] \\
&\quad +P^{v,c}_{k'}\left[\left(\Sigma^{-q,k'+q,k-q}_{X-3}\right)^{*}+\Sigma^{k'-k+q,k,k'}_{eh-1}-\Sigma^{-q,k,k'}_{X-1}\right] \\
&\quad -P^{v,c}_{k-q}\left[\Sigma^{q,k',k}_{h-3}+\Sigma^{k'+q-k,k,k'}_{h-1}-\Sigma^{q,k',k}_{h-1}\right] \qquad (3.37)
\end{aligned}$$

give the doublet contributions.

3.3 Excitation Induced Dephasing

The following analysis of the influence of the incoherent carrier system on the absorption is split into four steps. We start by discussing the density

dependence of the spectra by using the full equations of motion but with incoherent two-particle correlations set to zero. This density-dependence is analysed in the next step, where we compare the result of this calculation with results from commonly used further approximations. In this way, by switching on the terms in the equations of motion one by one, the effect of each contribution is made apparent. Following that the the influence diagonal exciton correlations, i.e. a population of bound electron-hole pairs is analysed. Finally, in order to gauge the importance of electron-electron, hole-hole and off-diagonal exciton correlations, expectation values $c_{e,h,X}(q,k',k)$ extracted from dynamical equilibrium calculations, as desribed in the previous chapter, were included in the calculations.

The absorption spectra of a quantum wire containing different densities of an uncorrelated electron-hole plasma are plotted in Fig. (3.1). The sum $f(k) = f^e(k) + f^h(k)$ of the electron and hole distributions at $T = 20$ K for densities ranging from $na_0 = 0.0125$ to $na_0 = 0.25$ is given in the inset. The spectrum for $na_0 = 0.0125$ represents the zero-density limit, as $\alpha(\omega)$ is unaffected by further reductions of n. The excitonic resonance is seen to be well resolved, lying $2.48E_B$ below the unrenormalized bandgap E_G. The spectral width of the pulse is given by the phenomenological background dephasing $\gamma_P = 0.05$ meV.

With increasing density, the exciton resonance is found to broaden by a factor of up to 1.8. The renormalization of the bandgap shifts the band continuum towards the resonance energy, merging with it at density $na_0 = 0.25$. A small redshift of the resonance is observed, with $\Delta E_{1s} = 0.038E_B$ between the peak positions for $na_0 = 0.0125$ and $na_0 = 0.125$. Comparison of the integrated peak areas also reveals a reduction of the oscillator strength, as discussed later in this chapter.

All spectra in the following comparisons were calculated at the moderately high density $na_0 = 0.125$, were pronounced effects of the incoherent carrier densities are visible and the excitonic resonance is still well resolved against the continuum absorption above the bandgap.

3.3.1 Hartree Fock and Screened Hartree Fock

The linear absorption limit of the semiconductor Bloch equations is the most basic approximation we consider. On this level, the equations of motion reduce to the first line of (3.16). The incoherent carrier densities enter the dynamics only via the Pauli blocking factor and the renormalization of the single particle energies. In Fig. (3.2) the Hartree-Fock absorption spectra are compared to calculations which included the thermalized carrier densities $f_k^{e,h}$ and the density-assisted polarizations $c_{\rm pe}$ and $c_{\rm ph}$ but where the incoherent correlations $c_X(q,k',k)$, $c_e(q,k',k)$ and $c_h(q,k',k)$ were set to zero (for convenience

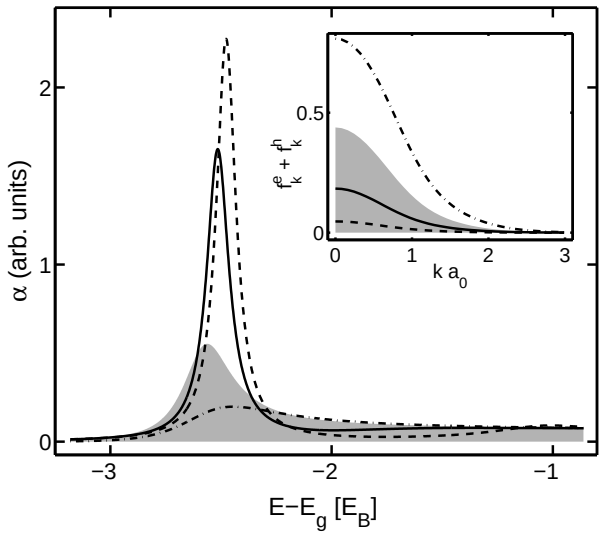

Figure 3.1: Calculated absorption spectra for the carrier densities $na_0 = 0.0125$ (dashed line), $na_0 = 0.06$ (solid line), $na_0 = 0.125$ (shaded area), and $na_0 = 0.25$ (dash-dotted line). The energy scale is given as the difference between the photon energy $\hbar\omega$ and the un-renormalized bandgap E_g in units of the 3d exciton binding energy E_B. All calculations were performed at $T = 20$ K.

termed 'doublet level calculations with uncorrelated carrier densities' in the following). Most notably, the energetic position of both the 1s exciton resonance and the continuum band edge are not very well approximated by the singlet level result. Furthermore, contrary to experiments, in the Hartree-Fock spectra the excitonic resonances are clearly discernible even for exciton quantum numbers $n > 1$. This may be attributed to an overestimated attractive interaction between the particles, since the screening of the one-particle expectation values, which is governed by higher-order correlations, is not included microscopically in the singlet-level calculations. Instead, as a first improvement of the Hartree-Fock result, the unscreened Coulomb potential may be replaced by the statically screened Lindhard potential. This affects the renormalizations of both the single particle energies and the Rabi frequency given by Eqs (3.17) and (3.18), respectively. Plotted in Fig. (3.2) as dashed line, the screened Hartree-Fock approximation indeed shows greatly reduced excitonic binding energies, where the resonances for $n > 1$ have already merged with the single-particle excitation spectrum. However, from the comparison with the doublet-level calculation it is seen that the correction in the resonance energies is overestimated by the static screening. Furthermore, no broadening of the 1s absorption line is observed in the Hartree Fock limit. This is readily understood in the context of the cluster expansion, since carrier-carrier scattering is

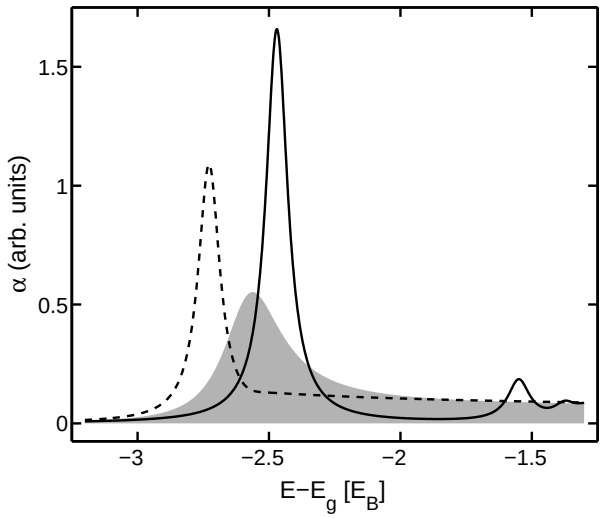

Figure 3.2: Absorption spectra calculated in Hartree-Fock (solid line) and statically screened Hartree-Fock (dashed line) approximation are compared to doublet level calculations for uncorrelated carrier densities (shaded area). All spectra were calculated for $na_0 = 0.25$ at $T = 20$ K.

a higher-order process and not included in the HF approximation.

3.3.2 Second Born Approximation

Within the context of linear absorption spectroscopy the next step to improve theoretical predictions is to include the density-assisted polarizations into the second Born approximation [37, 38]. In this limit, the many-body interaction contribution to the dynamics of $c_{\rm pe}$ and $c_{\rm ph}$ are assumed to be completely determined by the singlet-level contributions HF$[c_{\rm pe}, c_{\rm ph}]$ given in Eqs (3.26) and (3.35).

It should be pointed out, that since the screening of the interband polarizations is described microscopically by the inclusion of the two-particle terms, in the following calculations the unscreened Coulomb interaction is used in Eq. (3.16). On the other hand, in the second Born approximation of the doublet expectation values, the screening of the density-assisted polarizations $\langle {\rm np} \rangle$ is *not* included microscopically and a Lindhard screened Coulomb potential is used instead.

A commonly applied method to solve the second Born level equations of motion is to treat the density-assisted polarizations in Markov approximation, which already has been introduced in the previous chapter for the treatment of phonon-assisted three-particle correlations. The application to the $\langle {\rm np} \rangle$ terms

is straightforward and for the state of $c_{\rm pe}(q,k',k,t)$ at time t yields

$$
\begin{aligned}
&c_{\rm pe}(q,k',k,t)\\
&\quad= V_{k'-k+q}\Big\{\frac{P^{vc}_{k'+q}(t)\left(f^c_{k-q}(1-f^v_k)(1-f^c_{k'})-(1-f^c_{k-q})f^v_k f^c_{k'}\right)}{\tilde{E}(c_{\rm pe})-\tilde{\epsilon}^{cv}_{k'+q}}\\
&\qquad\quad-\frac{P^{vc}_{k}(t)\left(f^c_{k'}(1-f^c_{k'+q})(1-f^c_{k-q})-(1-f^c_{k'})f^c_{k'+q}f^c_{k-q}\right)}{\tilde{E}(c_{\rm pe})-\tilde{\epsilon}^{cv}_{k}+}\\
&\qquad\quad+\frac{P^{vc}_{k-q}(t)(P^{vc}_{k'}(t))^*P^{vc}_{k}(t)}{\tilde{E}(c_{\rm pe})-\tilde{\epsilon}^{cv}_{k-q}+\tilde{\epsilon}^{cv}_{k'}-\tilde{\epsilon}^{cv}_{k}}-\frac{P^{vc}_{k-q}(t)(P^{vc}_{k'}(t))^*P^{vc}_{k'+q}(t)}{\tilde{E}(c_{\rm pe})-\tilde{\epsilon}^{cv}_{k-q}+\tilde{\epsilon}^{cv}_{k'}-\tilde{\epsilon}^{cv}_{k'+q}}\Big\}\\
&\quad+V_q\Big\{\frac{P^{vc}_{k}(t)\left(f^c_{k-q}(1-f^c_{k-q})(1-f^c_{k'+q})-(1-f^c_{k'})f^c_{k-q}f^c_{k'+q}\right)}{\tilde{E}(c_{\rm pe})-\tilde{\epsilon}^{cv}_{k}}\\
&\qquad\quad-\frac{P^{vc}_{k-q}(t)\left(f^c_{k'+q}(1-f^v_k)(1-f^c_{k'})-(1-f^c_{k'+q})f^v_k f^c_{k'}\right)}{\tilde{E}(c_{\rm pe})-\tilde{\epsilon}^{cv}_{k-q}}\\
&\qquad\quad+\frac{P^{vc}_{k'+q}(t)(P^{vc}_{k'}(t))^*P^{vc}_{k-q}(t)}{\tilde{E}(c_{\rm pe})-\tilde{\epsilon}^{cv}_{k-q}+\tilde{\epsilon}^{cv}_{k'}-\tilde{\epsilon}^{cv}_{k}}-\frac{P^{vc}_{k'+q}(t)(P^{vc}_{k'}(t))^*P^{vc}_{k}(t)}{\tilde{E}(c_{\rm pe})-\tilde{\epsilon}^{cv}_{k-q}+\tilde{\epsilon}^{cv}_{k'}-\tilde{\epsilon}^{cv}_{k}}\Big\}
\end{aligned}
\tag{3.38}
$$

where we define

$$
\tilde{E}(c_{\rm pe})=(\tilde{\epsilon}^c_{k-q}+\tilde{\epsilon}^c_{k'+q}-\tilde{\epsilon}^c_{k'}-\tilde{\epsilon}^v_k-i\gamma_{\langle {\rm np}\rangle}) \tag{3.39}
$$

and

$$
\tilde{\epsilon}^{cv}_k=(\tilde{\epsilon}^c_k-\tilde{\epsilon}^v_k)\,. \tag{3.40}
$$

A corresponding equation is easily derived for the hole-assisted polarizations $c_{\rm ph}(q,k',k,t)$ and the resulting expressions are inserted in the last terms of Eq. (3.16).

The results of the numerical evaluation of Eqs. (3.16) and (3.38) are plotted in Fig. (3.3) showing that the inclusion of the density-assisted polarization in the calculations causes pronounced bleaching of the exciton resonances. Since in Fig. (3.5) the oscillator strengths predicted by the Hartree-Fock approximation and the statically screened second Born calculations are seen to be of comparable size, the observed bleaching can be attributed to excitation induced dephasing. This result directly corresponds to the physical interpretation of the cluster expansion given earlier, as the scattering of the one-particle polarization described by the interaction to the two-particle $\langle pn\rangle$ terms.

Comparing in Fig. (3.3) the results obtained in second Born calculations with and without using the Markov approximation, the excitation induced dephasing is seen to be of comparable size. However, while the 1s resonance in the Markov approximation is centered at approximately the same energy as in the HF calculations, a red-shift is observed in the dynamical calculations,

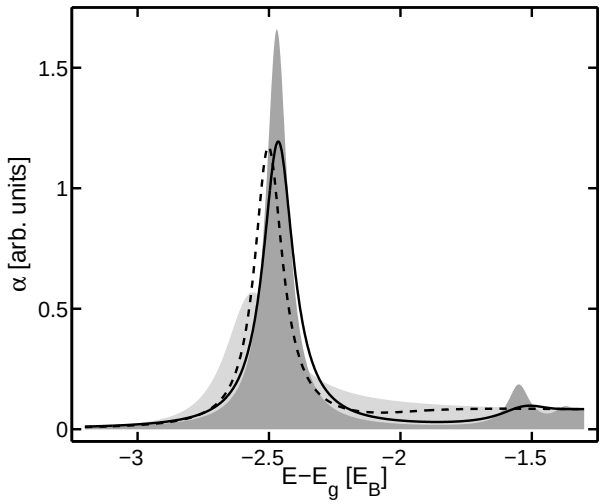

Figure 3.3: Absorption spectra in statically screened second Born approximation with (dashed line) and without (solid line) memory effects are compared to Hartree-Fock approximation (dark shaded area). The result of the doublet level calculations for uncorrelated carrier densities is indicated by the light shaded area. All spectra were calculated for $na_0 = 0.25$ at $T = T20$ K.

indicating that memory-effects of the $\langle pn \rangle$ terms play a role in the screening of the one-particle polarization.

Finally, with the inclusion of the terms labeled $s[c_{\rm pe}]$ and $s[c_{\rm ph}]$ given in Eqs (3.25) and (3.33), respectively, screening of the density-assisted polarizations is described microscopically in the calculations, causing a further red shift of the resonance energy as well as another broadening of the absorption line. In Fig. (3.4) the normalized difference $\frac{1}{C}(\alpha_{\rm Full} - \alpha_{\rm 2ndB})$ between the dynamically screened spectrum $\alpha_{\rm 2ndB}$ and the result obtained from the doublet level calculations for an uncorrelated electron-hole plasma $\alpha_{\rm Full}$ is plotted. The scattering contributions subsumed as $S[c_{\rm pe}]$ and $S[c_{\rm ph}]$ in Eqs (3.28) and (3.37) are seen to have only have a minor impact on the spectrum, resulting in a negligible blue shift and a slight narrowing of the 1s resonance.

3.3.3 Oscillator Strength

In Fig. (3.5) the density dependence of the oscillator strength $f_{\rm 1s}$ is plotted for the different approximations. The oscillator strength in the low-density limit of the unscreened Hartree-Fock approximation was used to normalize the plots. From the comparison with the Pauli-blocking factor $1 - f^e_{k=0} - f^h_{k=0}$ given by the solid circles it is seen that the density-dependent reduction of oscillator strength is mainly governed by phase-space filling. The Hartree-Fock,

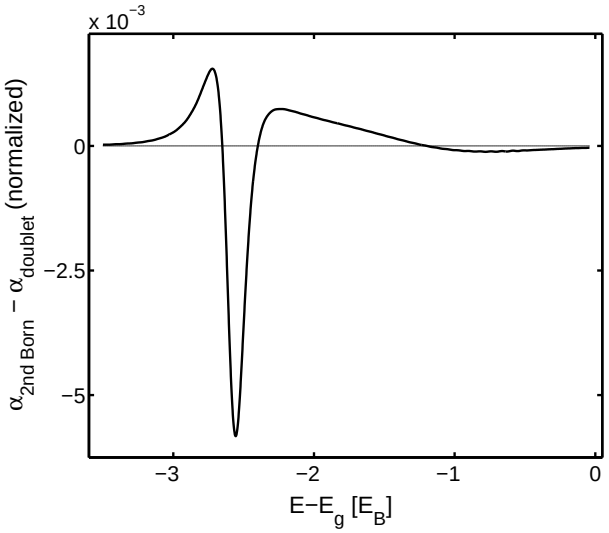

Figure 3.4: Differential spectrum showing the normalized difference between the absorption calculated with the dynamically screened second Born approximation and the doublet level calculations for incoherent carrier plasma. The spectra were calculated for $na_0 = 0.25$ and $T = 20$ K.

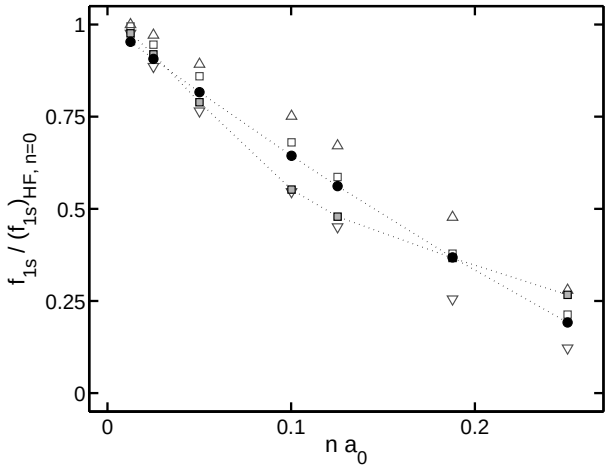

Figure 3.5: The predicted density dependence of the oscillator strength of the 1s resonance is plotted for the Hartree-Fock(triangles), screened Hartree Fock (reversed triangles), statically screened second Born (squares) approximation and the doublet level calculations for uncorrelated densities (solid squares). The solid circles give the phase-space filling $1-f^e_{k=0}-f^h_{k=0}$. The lines are guides to the eye. All spectra were calculated with carrier temperature $T = 10$ K.

screened Hartree-Fock and statically screened Hartree-Fock approximations (all but solid squares) show a characteristic deviation from the phase-space filling contributions, which does not vary strongly with carrier-densities. Conversely, the oscillator strength for the full doublet level calculations for uncorrelated carrier-densities display a distinctly different behavior. Reduction of oscillator strength beyond the phase-space filling contribution is observed at intermediate densities, while in the high-density regime the oscillator strength is restored in comparison to the Pauli-blocking factor. Since the inclusion of the terms $S[c_{\rm ep}, c_{\rm hp}]$ given in Eqs. (3.28) and (3.37) does not significantly affect the calculated absorption spectra we can attribute the deviations to the terms $s[c_{\rm ep}, c_{\rm hp}]$ given in Eqs. (3.27) and (3.36) which govern the dynamical screening of the density-assisted polarizations.

3.4 Exciton Population Effects

In the calculations so far presented, the incoherent carrier densities were assumed to be uncorrelated, i.e. only Fermi-Dirac distributed populations f_k^e and f_k^h were inserted, with $c_e(q,k',k)$, $c_h(q,k',k)$ and $c_X(q,k',k)$ being identically zero. In the following the effect of many-body correlations, especially the presence of bound electron-hole pairs, on the linear absorption measurement is investigated. The discussion is split into two steps, in the first, the dynamical interactions by which the carrier densities and the two-particle correlations are coupled are ignored. Instead, carrier distributions $f_k^{e,h}$ and diagonal exciton populations, calculated via Eq. (2.16), are treated as separate quantities. This enables us to independently control the exciton fraction X_f, the shape of the carrier distributions and the center-of-mass momentum distribution $f_{\rm 1s}(q)$ of the bound pairs and to compare their respective effects on the absorption spectrum. In a second step, the dynamically equilibrated final state of the steady-state calculations is imported into the absorption calculation. By switching on different terms separately, the importance of electron-electron, hole-hole and off-diagonal exciton correlations can thus be judged.

3.4.1 Bound Electron-Hole Pairs

In order to analyze the effect of diagonal exciton correlations on the absorption, in Fig. (3.6) spectra calculated for $X_f = 0, 0.25, 0.5$ and 0.75 are plotted. In all cases, a carrier density of $na_0 = 0.125$ was inserted in a $T = 20$ K thermal distribution, and the center-of-masses of the excitons were assumed to follow a Bose-Einstein distribution at the same temperature. The spectral position of the absorption peak, the width of the resonance and the calculated oscillator strength are plotted in the inset of Fig. (3.6) and in Fig. (3.7), re-

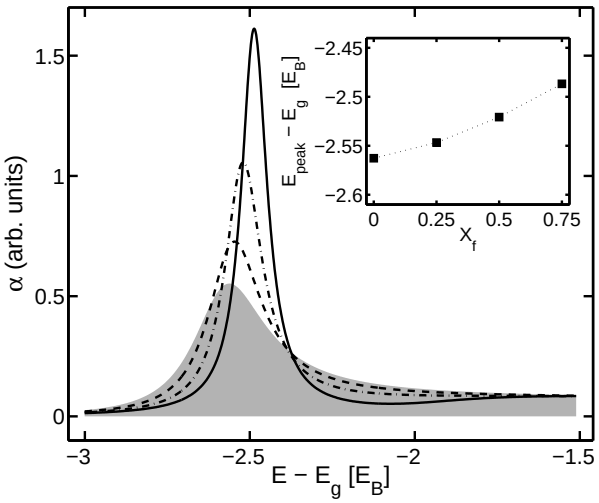

Figure 3.6: Absorption spectra, where the fraction of excitons X_f is varied from $X_f = 0$ (shaded area) over $X_f = 0.25$ (dashed line) and $X_f = 0.5$ (dash-dotted line) to $X_f = 0.75$ (solid line). The inset shows the energetic position of the 1s resonance peak as a function of X_f.

spectively. Increases in the exciton fraction are seen to result in a blue shift of the 1s resonance energy and a narrowing of the linewidth. From a comparison with the carrier-density dependent calculation – the spectrum for $X_f = 0$ in Fig. (3.6) is identical to the one for $na_0 = 0.125$ in Fig. (3.1) – it is seen that the effect of increasing the exciton fraction on the absorption is similar to that of a reduced screening of the Coulomb potential. This can be understood by the charge neutrality of excitons. Due to the vanishing monopole moment the screening efficiency of excitons is greatly reduced compared to unbound carriers. Conversely, the reduction of the oscillator strength with increasing densities is expected not to be significantly changed by the presence of bound pairs since the phase-space filling of the carriers is a consequence of their Fermionic nature and is not affected by the formation of excitons.

It should be pointed out, that in the results presented above, only the direct contribution of excitonic populations via the electron-hole correlations $c_X(q, k', k)$ has been taken into account. However, if significant percentages of the carriers form bound excitons, the carrier distributions are expected to significantly differ from a thermal distribution. The possible effects of such changes are discussed below.

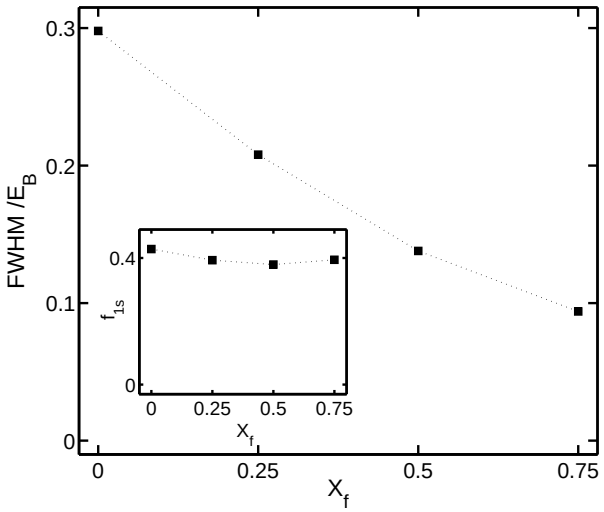

Figure 3.7: The calculated width of the exciton resonance is plotted as a function of the exciton fraction X_f. The inset show the corresponding changes in the oscillator strength.

3.4.2 Variation of Distributions

The shape of the carrier populations in a semiconductor will, initially, strongly depend on the excitation method. Subsequent scattering among the carriers and with the phonons eventually, in first order, thermalizes the carrier densities towards the lattice temperature. As has been discussed in the previous chapter, the carrier distributions are further modified by many-particle correlations, most notably bound electron-hole pairs. Since the initial fraction of excitons in the system depends on the excitation process, too, the carrier distribution at a time t after the excitation is not easily specified, but can only be obtained from fully dynamical calculations [50], which are beyond the work presented here. Instead, three limiting cases are investigated. Figure (3.8) shows the absorption spectra calculated with $f_k^{e,h}$ given by i) a Fermi-Dirac distribution, ii) the absolute square of the 1s wave function or iii) according to

$$f^{e/h}(k) = (1 - X_f) f_{\mathrm{FD}}^{e/h}(k) + X_f \sum_q |\Phi_{1\mathrm{s}}(k - \frac{m^{e/h}}{M} q)|^2 f_{1\mathrm{s}}(q) \qquad (3.41)$$

are plotted. The theoretical prediction in Eq. (3.41) describes $f^{e/h}(k)$ as superposition of thermally distributed ionized carriers, weighed with the fraction $(1 - X_f)$ and a contribution due to bound pairs, determined by the 1s wave functions $\Phi_{1\mathrm{s}}(k_{\mathrm{rel}})$. Here $|k_{\mathrm{rel}}| = k - q(m^{e/h}/M)$ is the relative momentum. With the inclusion of the weight $f_{1\mathrm{s}}(q)$ the center-of-mass momentum of the

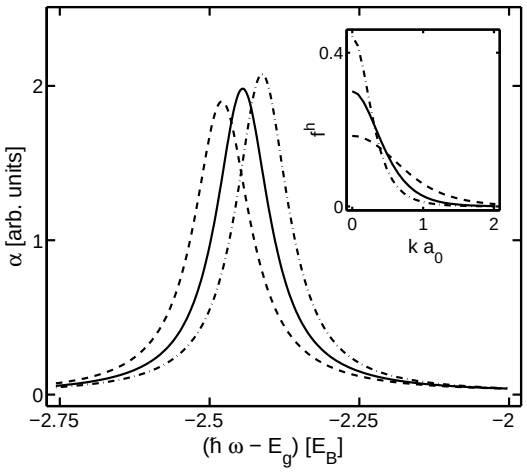

Figure 3.8: Absorption spectra for carrier distribution given by the 1s wave function (dash-dotted line), a $T = 10$ K thermal distribution (dashed line), and an intermediate theoretical prediction (solid line). The corresponding sum of the electron and hole carrier distributions are shown in the inset. In all spectra, diagonal exciton correlations with corresponding to a $X_f = 0.5$ were inserted in a Bose-Einstein distribution.

exciton is thus taken into account. The sums $f_k^e + f_k^h$ of the distributions are plotted in the inset, respectively. Since at $na_0 = 0.125$, 1s-distributed carriers are highly degenerate ($f^e(k=0) + f^h(k=0) \approx 1$), the carrier density was lowered to $na_0 = 0.06$ for these calculations. In all cases diagonal exciton correlations corresponding to $X_f = 0.5$ with $f_{1s}(q) = |\Psi_{1s}(q)|^2$ were included in the calculations. Similar to the carrier densities also the distribution of the center-of-mass momenta $f_{1s}(q)$ of the excitons in the system depends on the experimental conditions, e.g. the excitation process and, since only excitons with $q \sim 0$ may decay radiatively, the coupling to the quantized light field. However, with the interpretation that the main effect of bound pairs on absorption stems from their charge neutrality, the center-of-mass momentum is expected to be of minor importance only. To test this we have performed calculations with f_{1s} either given by a Bose-Einstein distribution or proportional to the square of the 1s wave function. The resulting spectra are plotted in Fig. (3.9), with the center-of-mass momenta being shown in the inset. In line with the expectations the effect of f_{1s} is seen to be limited to a small variation of the oscillator strength.

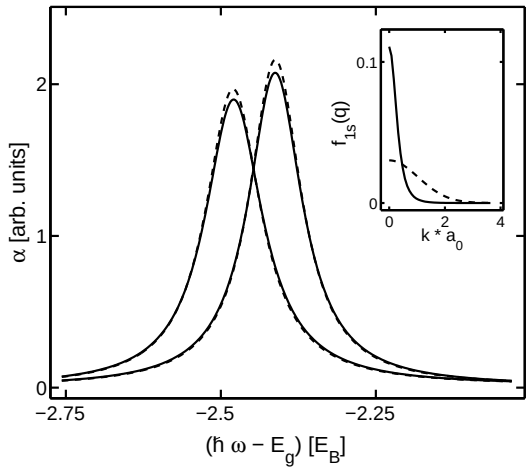

Figure 3.9: Absorption spectra for different combinations of $f_k^{e,h}$ and $f_{1s}(q)$ are shown. In the spectra peaked at $\hbar\omega - E_g = -2.5E_B$ the carriers are thermally distributed, the ones at $-2.4E_B$ were obtained with $f_k^{e,h} \propto |\Phi_{1s}|^2$. The dashed lines indicate Bose-Einstein distributed center-of-mass momenta, the solid lines give the results for $f_{1s}(q) \propto |\Phi_{1s}|^2$ (plotted in the inset). The thermal distributions were calculated with $T = 20$ K. A density of $na_0 = 0.05$ with $X_f = 0.5$ was inserted in all cases.

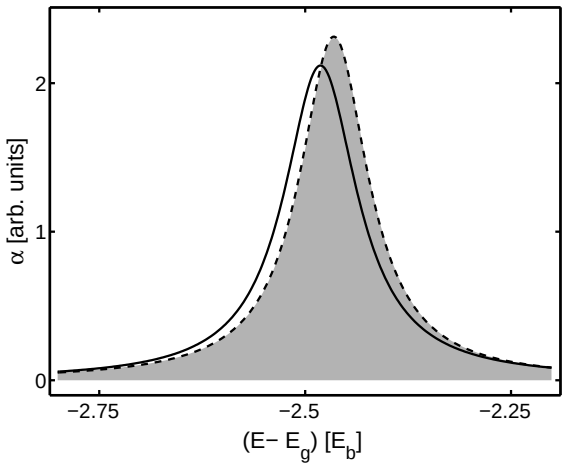

Figure 3.10: Absorption spectra calculated with dynamically equilibrated carrier distributions and doublet correlations are shown. The result obtained by inclusion of $f_k^{e,h}$ but with $c_{e,h,X}(q,k',k) = 0$ is given by the solid line. The dashed line gives the absorption when diagonal excitons are taken into account. The shaded area was calculated with all incoherent doublet correlations included.

3.4.3 General Two-Particle Correlations

So far, of the incoherent two-particle correlations only the diagonal exciton populations were taken into account, with electron-electron, hole-hole and off-diagonal exciton correlations being set to zero. The first step to judge the relative importance of these terms is to assign physically meaningful values to c_{ee}, c_h and c_X. It has already been discussed in the previous chapter, that in general, these correlations cannot be calculated analytically. They have, however, been shown to rapidly build up during the first few picoseconds of the quasi-equilibrium calculations. Thus, after evolving the equations of motion numerically for a short time, a physically consistent full doublet state of the incoherent carrier system is obtained, which can subsequently be imported into the absorption calculations. Figure (3.10) shows the effect of dynamically calculated incoherent two-particle correlations on the linear absorption spectrum. The spectra with and without the off-diagonal exciton correlations and c_e or c_h are next to indistinguishable in the plot.

Due to the restriction of our calculations to a one-dimensional model, a qualitative comparison with experimental findings in two-dimensional quantum wells is not possible. The competing mechanisms, which determine the energetic position of the excitonic resonance via variations in the exciton binding energy and the renormalization of the bandgap, have specific dependencies on the dimensionality of the problem [24, 25]. This has been shown experimentally [24] for the change from bulk like 150 Åwells, where no shift of the exciton line was observed, to narrow 40 Å wells, where the exciton binding energy was seen to be reduced by a factor of $\Delta E/E = 0.67$. The increasing energy shift accompanying the transition from a 3d to a 2d system, however, is again reduced in our 1d quantum-wire calculations, where the ratio is of a few percent's order.

Chapter 4

Conclusion

In this thesis a one-dimensional quantum-wire model is used to study the properties of a correlated electron-hole plasma.

In the first part the dynamics of an incoherent system of correlated electrons and holes, coupled to a thermal bath of LA-phonon, is described. We assume a complete suppression of radiative recombination, so that the carrier densities are conserved in time. Thus, by numerically evolving the equations of motion to sufficently long times t, the system approaches steady state, where the exicton formation and dissociation rates equilibrate. In steady state, less than half of the carriers were found to form bound excitons for the simulated densities and temperatures. As expected, the highest fraction of exciton is obtained at the lowest density $na_0 = 0.025$ and temperature $T_L = 10K$. At higher temperatures the fraction strongly decreases, as thermal ionization of the excitons increases. In contrast to previously reported results, X_f displays an approximately linear dependence on the carrier density. As a complement to earlier calculations of exciton formation rates [15], decay rates for the higher-lying exciton states $\nu = \{2\mathrm{p}, 2\mathrm{s}\}$ were calculated.

The presented theory microscopically describes the correlated electron-hole plasma and, in principle, can be extended to higher order clusters. In practice, the complexity of the model is limited by the available computational power. Due to this, in our calculations an unphysically large grid of k-points has been used, resulting in a numerical error in the phonon-scattering equations. As discussed in detail in Appendix C, this error leads to unphysical negative values in the electron and hole distributions f_k^e and f_k^h, respectively. While a recurring manual correction of $f_k^{e,h}$ allowed X_f to equilibrate, the distributions of the electrons and holes did not reach a clear defined steady state.

With this limitation in mind, we suggest the following improvements of the calculations. By the migrating the calculations to faster CPUs, a finer numerical resolution of the carrier momentum k is possible. This reduces the numerical error in the phonon scattering-rates, enabling the equilibration of

the carrier-distributions at low densities. An analysis of the carrier densities in the presence of a large exciton fraction is then possible.

Furthermore, we propose to expand the calculations to other materials. In particular, the dynamics of correlated charge carriers in a system with enhanced binding energy, such as Zinc-Selenide (ZnSe) may be of interest. Since ZnSe is a polar crystal, where the interaction of electrons with optical phonons is strongly increased in comparison with GaAs, the coupling of electrons with LO-phonons should be included in the system Hamiltonian.

In the second part of this thesis, the effects of correlated carrier densities on the linear absorption spectra have been investigated. In agreement with experimental findings, a shift of the exciton resonance towards higher energies with increasing exciton fraction is observed. The shift is accompanied by a suppression of the EID, while the oscillator strength is not changed. In the physical interpretation of the calculated results we argue that the scattering rates are reduced by binding the free carriers into electron-hole pairs. The shift in the exciton-binding energy is explained by the charge neutrality of the excitons, which, in comparison to free carriers, contributes less to the screening of the Coulomb potential. However, since the Pauli-blocking of the electrons and holes stems from the Fermionic nature of the carriers and thus does not change directly in exciton formation or dissociation processes, the oscillator strength does not display a strong dependence on X_f. Looking forward, in order to allow a quantitative comparison with existing pump-probe experiments, the derived equations of motion should be evaluated for a two-dimensional quantum-well system. In order to reduce the numerical workload, in a first step the electron-electron, hole-hole and off-diagonal electron-hole correlations can presumably be excluded from the two-dimensional model, as they were found to have vanishing effect on the absorption spectrum.

Appendix A

One-Dimensional Coulomb Matrix Elements

In a homogeneous bulk semiconductor the Coulomb interaction between two point charges at $\mathbf{r}_1$ and $\mathbf{r}_2 = \mathbf{r}_1 + \mathbf{r}$ is given by

$$V_{\mathrm{C}}(\mathbf{r}) = \pm \frac{e^2}{4\pi\epsilon_0\epsilon_b} \frac{1}{|\mathbf{r}|} \,, \tag{A.1}$$

where e is the elementary charge of the particles and ϵ_b is the background dielectric constant of the material. In general, the situation is somewhat more complicated in composite structures, where mirror charges at the material interfaces introduce non-trivial contributions to the interaction potential [73]. However, the corrections are relatively small in semiconductor heterostructures, where the dielectric constants are of comparable size for the different materials, and are not taken into account in this work.

We calculate the quasi-one-dimensional interaction by taking the weighted average over the coordinates perpendicular to the wire. Utilizing the confinement functions $\xi_0(\mathbf{r}_\perp)$ derived in Eq. (2.34) the effective one-dimensional potential $V_{\mathrm{eff}}(z)$ is given by

$$\begin{aligned} V_{\mathrm{eff}}(z) &= \iiiint \frac{e^2}{4\pi\epsilon_0\epsilon_b} \frac{1}{\sqrt{(x-x')^2 + (y-y')^2 + z^2}} \\ &\qquad \times |\xi(x,y)|^2 |\xi(x',y')|^2 \mathrm{d}x\,\mathrm{d}y\,\mathrm{d}x'\,\mathrm{d}y' \\ &= \iiiint \frac{e^2}{4\pi\epsilon_0\epsilon_b} \frac{1}{\sqrt{(x-x')^2 + (y-y')^2 + z^2}} \\ &\qquad \times \frac{1}{4\pi^2 R^4} e^{-\frac{1}{2R^2}(x^2+y^2+x'^2+y'^2)} \mathrm{d}x\,\mathrm{d}y\,\mathrm{d}x'\,\mathrm{d}y' \,. \end{aligned} \tag{A.2}$$

With the introduction of relative coordinates $x_R = (x + x')/2$, $x_r = x - x'$,

$y_R = (y + y')/2$ and $y_r = y - y'$ the equation is simplified to

$$\begin{aligned} V_{\text{eff}}(z) &= \frac{e^2}{4\pi\epsilon_0\epsilon_b}\frac{1}{4\pi^2 R^4}\iiiint \frac{1}{\sqrt{x_r^2+y_r^2+z^2}} \\ &\qquad \times e^{-\frac{1}{4R^2}(4x_R^2+x_r^2+4y_R^2+y_r^2)}\mathrm{d}x_R\,\mathrm{d}y_R\,\mathrm{d}x_r\,\mathrm{d}y_r \\ &= \frac{e^2}{4\pi\epsilon_0\epsilon_b}\frac{(\pi R)^2}{4\pi^2 R^4}\iint \frac{1}{\sqrt{x_r^2+y_r^2+z^2}} e^{-\frac{1}{4R^2}(x_r^2+y_r^2)}\mathrm{d}x_r\mathrm{d}y_r\ . \end{aligned} \tag{A.3}$$

Using cylindrical coordinates

$$V_{\text{eff}}(z) = \frac{e^2}{4\pi\epsilon_0\epsilon_b}\frac{1}{4\pi R^2}\int_0^{2\pi}\mathrm{d}\varphi\int_0^{\infty}\frac{e^{\frac{-r^2}{4R^2}}}{2R\sqrt{\frac{r^2}{4R^2}+\frac{z^2}{4R^2}}}r\mathrm{d}r \tag{A.4}$$

and substituting $\tilde{r} = \sqrt{\frac{r^2}{4R^2}+\frac{z^2}{4R^2}}$ yields

$$\begin{aligned} V_{\text{eff}}(z) &= \frac{e^2}{4\pi\epsilon_0\epsilon_b}\frac{1}{4R}e^{\frac{z^2}{4R^2}}\int_{\frac{z^2}{4R^2}}^{\infty} e^{-\tilde{r}^2}\mathrm{d}\tilde{r} \\ &= \frac{e^2}{4\pi\epsilon_0\epsilon_b}\frac{\sqrt{\pi}}{2R}e^{(\frac{z}{2R})^2}(1-\mathrm{erf}(\frac{|z|}{2R}))\ , \end{aligned} \tag{A.5}$$

where $\mathrm{erf}(x)$ is the error function. With the approximation

$$\sqrt{\pi}e^{(\frac{z}{2R})^2}(1-\mathrm{erf}(\frac{|z|}{2R})) \sim \frac{1}{\sqrt{(\frac{z}{2R})^2+(\frac{2}{\pi})^2}} \tag{A.6}$$

the Coulomb interaction in real space is obtained as

$$V_{\text{eff}}(z) = \frac{e^2}{4\pi\epsilon_0\epsilon_b}\frac{1}{2R}\frac{1}{\sqrt{(\frac{z}{2R})^2+(\frac{2}{\pi})^2}} = \frac{e^2}{4\pi\epsilon_0\epsilon_b}\frac{1}{\sqrt{z^2+(\frac{4R}{\pi})^2}}\ . \tag{A.7}$$

Now, a Fourier transformation into momentum space leads to

$$\begin{aligned}
V_{\text{eff}}(q) &= \frac{e^2}{4\pi\epsilon_0\epsilon_b}\frac{1}{L}\int_{-L/2}^{L/2}\frac{1}{\sqrt{z^2+(\frac{4R}{\pi})^2}}e^{-iqz}\mathrm{d}z \\
&= \frac{e^2}{4\pi\epsilon_0\epsilon_b}\frac{1}{L}\int_{0}^{L/2}\frac{e^{-iqz}+e^{iqz}}{\sqrt{z^2+(\frac{4R}{\pi})^2}}\mathrm{d}z \\
&= \frac{e^2}{4\pi\epsilon_0\epsilon_b}\frac{1}{L}\int_{0}^{L/2}\frac{2\cos(qz)}{\frac{4R}{\pi}\sqrt{(\frac{\pi z}{4R})^2+1}}\mathrm{d}z \\
&\approx \frac{e^2}{4\pi\epsilon_0\epsilon_b}\frac{1}{L}\int_{0}^{\inf}\frac{2\cos(qz)}{\frac{4R}{\pi}\sqrt{(\frac{\pi z}{4R})^2+1}}\mathrm{d}z \\
&= \frac{e^2}{4\pi\epsilon_0\epsilon_b}\frac{2}{L}\int_{0}^{\inf}\frac{\cos(4qRz/\pi)}{\sqrt{z^2+1}}\mathrm{d}z \\
&= \frac{e^2}{4\pi\epsilon_0\epsilon_b}\frac{2}{L}K_0(\frac{4|q|R}{\pi})\ , \qquad \text{(A.8)}
\end{aligned}$$

where $K_0(x)$ is the modified Bessel function [74]. With the approximation $K_0(x)=\sqrt{\frac{\pi}{2x}}e^{-x}$ one finally obtains

$$V(q)=\frac{\pi}{L}\frac{e^{-4|q|R/\pi}}{\sqrt{2|q|R}}\ . \qquad \text{(A.9)}$$

The Coulomb potential given in Eq. (A.9) has been used for the numerical calculations throughout this thesis.

Appendix B

Exciton Basis

In Eqs. (2.9) and (2.10) we have defined excitonic operators which create or annihilate an electron-hole pair, respectively, with a wave-vector distribution given by the excitonic wave function $\Phi_{\nu,q}(k)$. In this appendix, the eigenequation of an interaction electron-hole pair in a semiconductor heterostructure is derived, the resulting wave functions $\Phi_{\nu,q}(k)$ were calculated numerically in our calculations.

In a bulk semiconductor, using the effective mass approximation and assuming vanishing carrier densities, the eigenequation of an interacting electron-hole pair is obtained from the Schrödinger equation of an isolated hydrogen atom

$$\left[\frac{\hbar^2\nabla^2_{\mathbf{r}}}{2\mu}+\frac{\hbar^2\nabla^2_{\mathbf{R}}}{2M}-V_C(\mathbf{r})\right]\Phi_{\nu,\mathbf{R}}(\mathbf{r})=E_\nu\Phi_{\nu,\mathbf{R}}(\mathbf{r}) \tag{B.1}$$

by replacing the values of the reduced and total mass with $\mu=(m_e^{-1}+m_h^{-1})^{-1}$ and $M=m_e+m_h$, respectively, and scaling the Coulomb potential $V_C(\mathbf{r})$ with the background dielectric constant ϵ_b of the material [5]. Replacing the vectors $\mathbf{r}$ and $\mathbf{R}$ with the scalars r and R and the interaction potential $V_C(r)$ with the quasi-one-dimensional potential given in Eq. (A.9), respectively, we arrive at the corresponding equation for one-dimensionally confined carriers,

$$\left[\frac{\hbar^2}{2\mu}\frac{d}{dr^2}+\frac{\hbar^2}{2M}\frac{d^2}{dR^2}-V_C(r)\right]\Phi_{\nu,R}(r)=E_\nu\Phi_{\nu,R}(r)\ . \tag{B.2}$$

Fourier transformation of Eq. (B.2) into k-space yields

$$\begin{aligned}\left(\frac{\hbar^2k^2}{2\mu}+\frac{\hbar^2q^2}{2M}\right)\Phi_{\nu,q}(k')-\sum_{k'}V_{k-k'}\Phi_{\nu,q}(k') &= E_\nu\Phi_{\nu,q}(k)\ ,\\ \left(\epsilon^c_{k,q}+\epsilon^h_{k,q}\right)\Phi_{\nu,q}(k)-\sum_{k'}V_{k-k'}\Phi_{\nu,q}(k') &= E_\nu\Phi_{\nu,q}(k)\ ,\end{aligned} \tag{B.3}$$

where $\epsilon^\lambda_{k,q}=\hbar^2k^2_\lambda/(2m_\lambda)$ is the single-particle energy of a charge carrier in band λ with momentum $k_e=(m_e/M)q+k$ or $k_h=(m_h/M)q-k$, respectively.

The generalization of Eq. (B.3) to finite carrier densities is given by [43]

$$\left(\tilde{\epsilon}^e_{k,q} + \tilde{\epsilon}^h_{k,q}\right) \Phi_{\nu,q}(k) - \left(1 - f^e_{k,q} - f^h_{k,q}\right) \sum_{k'} V^s_{k-k'} \Phi_{\nu,q}(k) = E_{\nu,q} \Phi_{\nu,q}(k) \ , \quad \text{(B.4)}$$

where $\tilde{\epsilon}^\lambda_{k,q} = \hbar^2 k^2/(2m_\lambda) + \sum_{k'} V_{k-k'} f^\lambda_{k,q}$ are the renormalized single-particle energies and V^s_k is the screened Coulomb interaction. Since the dependence of the densities $f^\lambda_{k,q}$ on both k and q couples relative and center-of-mass motion, a seperation ansatz is no longer feasible and q-dependent eigenfunctions $\Phi_{\nu,q}(k)$ have to be calculated for each value of q seperately. Furthermore, due to the time dependence of the carrier distributions $f^{e,h}_k(t)$ appearing in Eq. (B.4) the excitonic eigenfunctions are not constant in time. In our simulations, Eq. (B.4) is therefore solved numerically after each $\Delta t \approx 0.2$ ps.

For the following discussion, we define matrices for the kinetic energy

$$\mathbf{E}_{k,k'} = \frac{\hbar^2 k^2}{2\mu} \delta_{k,k'} \ , \quad \text{(B.5)}$$

the Coulomb interaction

$$\mathbf{V}_{k,k'} = V_{k-k'} \ , \quad \text{(B.6)}$$

and the Pauli blocking

$$\mathbf{F}_{k,k'} = \left(1 - f^e_{k_e} - f^h_{k_h}\right) \delta_{k,k'} \ , \quad \text{(B.7)}$$

and rewrite Eq. (B.4) in matrix form as

$$(\mathbf{E} - \mathbf{FV}) \mathbf{\Phi}^r_{\nu,q} = E_{\nu,q} \mathbf{\Phi}^r_{\nu,q} \ , \quad \text{(B.8)}$$

where $\mathbf{\Phi}^r_{\nu,q}$ are the right-hand eigenfunctions. Since the matrix $\mathbf{FV}$ is not Hermitean, the functions $\mathbf{\Phi}^r_{\nu,q}$ are not identical to the left-hand eigenfunctions $\mathbf{\Phi}^l_{\nu,q}$ defined by

$$(\mathbf{\Phi}^l_{\nu,q})^T (\mathbf{E} - \mathbf{FV}) = (\mathbf{\Phi}^l_{\nu,q})^T E_{\nu,q} \ . \quad \text{(B.9)}$$

However, since the calculations presented in this thesis were conducted in a temperature and density regime where $\left(1 - f^e_{k_e} - f^h_{k_h}\right) > 0$ for all k, we may define the matrices $\sqrt{\mathbf{F}}_{k,k'} \equiv \delta_{k,k'} \sqrt{1 - f^e_{k,q} - f^h_{k,q}}$ and its inverse $\sqrt{\mathbf{F}}^{-1}_{k,k'} = \delta_{k,k'} \sqrt{1 - f^e_{k,q} - f^h_{k,q}}^{-1}$ to obtain a symmetrized Hermitean equation:

$$(\mathbf{E} - \sqrt{\mathbf{F}}\mathbf{V}\sqrt{\mathbf{F}}) \mathbf{\Phi}_{\nu,q} = E_{\nu,q} \mathbf{\Phi}_{\nu,q} \ . \quad \text{(B.10)}$$

The eigenfunctions $\mathbf{\Phi}_{\nu,q}$ of Eq. (B.10) are connected to the right-hand and left-hand eigenfunctions of Eq. (B.4) via the equations

$$\mathbf{\Phi}_{\nu,\mathbf{q}} = \sqrt{\mathbf{F}}^{-1} \Phi^r_{\nu,q} \quad \text{and} \quad (\mathbf{\Phi}_{\nu,\mathbf{q}})^T = (\mathbf{\Phi}^l_{\nu,q})^T \sqrt{\mathbf{F}} \quad \text{(B.11)}$$

which is readily verified by inserting Eq. (B.11) into Eq. (B.10). Using Eq. (B.11) properties of the left-hand and right-hand functions can be derived from those of the symmetrized wave functions. In particular, Eq. (B.11) directly yields

$$\Phi^r_{\nu,q} = \mathbf{F}\Phi^l_{\nu,q} \tag{B.12}$$

and generalized orthogonality and completeness relations are obtained as

$$\langle \mathbf{\Phi}^l_{\nu,q} | \mathbf{\Phi}^r_{\nu,q} \rangle = \langle \mathbf{\Phi}_{\nu,q} | \mathbf{\Phi}_{\nu,q} \rangle = \mathbf{1} \ , \tag{B.13}$$

$$\sum |\mathbf{\Phi}^l_{\nu,q}\rangle\langle \mathbf{\Phi}^r_{\nu,q}| = \sum |\mathbf{\Phi}_{\nu,q}\rangle\langle \mathbf{\Phi}_{\nu',q}| = \delta_{\nu,\nu'}\mathbf{1} \ . \tag{B.14}$$

Although not explicitly stated, the calculation of the exciton numbers via Eqs. (2.11) and (2.12) involves the product of one right-hand and one left-hand function. Using Eq. (B.13) this product has been replaced with the product of the symmetrized wave functions in our calculations.

Appendix C

Numerical Stability

This appendix contains a brief comment on the numerical problems encountered in the calculation of the equilibrium fraction of excitons. In order to allow the system to relax toward steady state, the equations of motion are numerically evolved with a fourth-order Runge-Kutta algorithm from the insertion of the carrier densities and excitonic correlations at $t = 0$ to the final time $t_{\max} = 2$ ns. During this, the exciton fraction is artificially kept constant for the first 20 ps, in order to allow the build up of the full two-carrier correlations. Since the electron-phonon interaction is by far the slowest process in the simulated system dynamics, the interaction strength is enhanced by a factor of 10 to increase the exciton formation and dissolving rates, so that the time $t_{\max} = 2$ ns corresponds to a simulated time $\tilde{t}_{\max} = 200$ ps. This enhancement was numerically confirmed not to have a significant effect on the equilibrium exciton fraction X_f. With one step in the Runge-Kutta algorithm spanning $\delta\tilde{t} = 18$ fs approximately 10^4 time steps are required for one calculation.

Additionally, as will be discussed in Appendix E, the effective masses of electrons and holes are rescaled to a ratio $m_h/m_e = 3$, reducing the extension of the holes in k-space. In this way, the simulation can be limited to wave vectors $|k| \leq 4\ a_0^{-1}$. In spite of these optimizations the smallest numerically feasible resolution of k-vectors is $\delta k = 1/12\ a_0^{-1}$, with an overall computing time of one week for a single calculation on a 667 MHz Alpha EV6.7 CPU.

This spacing $\delta k = 1/12\ a_0^{-1}$, while sufficiently narrow at moderate densities and temperatures, introduces numerical errors in the low density and temperature regime. In particular, the carrier-phonon interaction which scatters f_k^e and f_k^h towards comparatively narrow thermal distributions is found to deplete the carriers in the high-energy tails too strongly, resulting in negative values of $f_k^{e,h}$. Due to the smaller effective mass and the resulting narrower distribution in k-space, this effect is most pronounced for the electrons. The ongoing depletion of "carriers" from the already negative parts of the distributions with increasing simulation time $\tilde{t}$ destabilizes the calculations, leading to an acceler-

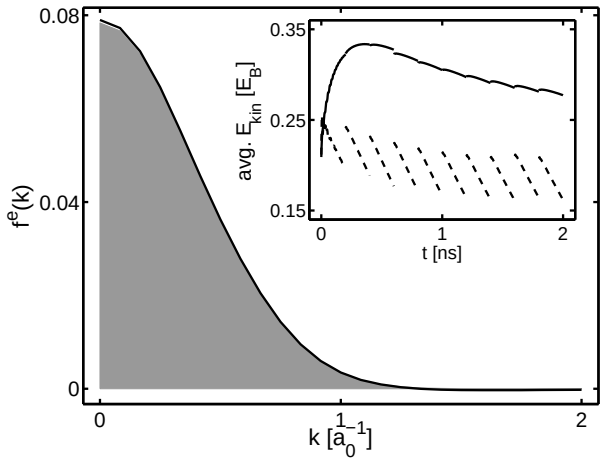

Figure C.1: The electron distribution f_k^e at time $\tilde{t} = 20$ ps after the start of the calculation is plotted as solid line. The shaded area gives the distribution after artificially removing of the negative parts and a subsequent renormalization. A carrier density of $na_0 = 0.025$ was simulated and the lattice temperature was set to $T = 10$K. The inset shows the average kinetic energy of electrons (dashed line) and holes (solid line) during the entire calculation, which includes nine corrections of the distributions.

ating decrease of the population of excitons and preventing the equilibration at a stable X_f. For the low density calculations we therefore artificially reset the carrier distributions to a physical meaningful state. In intervals $\Delta\tilde{t}_{\rm cut} = 20$ ps the negative parts f_k^e and f_k^h are removed and an exponential high-energy tail is fitted to the remaining distribution. In Fig. (C.1) the distributions before (solid line) and after (shaded area) the correction at $\tilde{t} = 20$ ps are plotted. Less than one percent of the electrons are redistributed during the manipulation. However, since the electrons are moved towards the high-energy tail, the correction amounts to a significant heating of the electron-hole plasma. This is seen in the inset of Fig. (C.1), where the average kinetic energies $\overline{E}_{\rm kin}^{e/h}$ of the electrons and holes are plotted. While the steps $\Delta\overline{E}_{\rm kin}^{h}$ caused by the correction are seen to be small compared to the dynamical evolution of $\overline{E}_{\rm kin}^{e/h}$, the situation is much more severe for the electrons. The average kinetic energy of an electron equilibrates only in a time average, fluctuating as much as 25 percent between each correction of the distributions. The time evolution of the exciton fractions is found to be only weakly influenced by the artificial reset of the plasma distributions, provided that the intervals $\tilde{t}$ are sufficiently short, so that the accelerating decay of X_f caused by the negative parts of $f_k^{e,h}$ does not grow strong enough to dominate the dynamics. However, due to the

unphysical decay of X_f and the constant heating introduced with each manipulation, the exciton fraction calculated for the lowest density and temperature in Fig. (2.3) gives only a lower estimate of the correct value.

Appendix D

Phenomenological Dephasing

The polarization induced in a semiconductor by an incident laser beam typically decays on a timescale of a few picoseconds, resulting in a broadening of the infinitely sharp excitonic lines in the absorption spectra. The decay of the polarization is governed by the coupling to the environment, e.g. the carrier system, the crystal lattice or the external light field via spontaneous emission. Additional inhomogeneous line broadening is introduced by variation in the diameter of the confined structure or the fluctuations in the alloy of the barrier.

In the calculations of the absorption spectra presented in this thesis, only the scattering of the interband polarization with the incoherent carrier system is described microscopically by the coupling of P_k^{cv} to the density-assisted polarizations $\langle \mathrm{np} \rangle$. An additional phenomenological constant $\gamma_\mathrm{P} = 0.05\ E_B/\hbar \approx 0.3$ ps is introduced into the equation of motion, Eq. (3.16), to account for the other broadening mechanisms. The effect of γ_P is observed in Fig. (3.2), where the 1s-resonance of the low-density Hartree-Fock absorption spectra is broadened to a width of $0.05\ E_B$.

While the density-induced dephasing of the singlet level polarization P_k^{cv} is consistently described by the coupling to the doublet level expectation values, the scattering of the doublet level correlations is not included microscopically, due to the exclusion of triplet correlations from the calculations. Instead, the density dependence of the decay of c_pe and c_ph is included phenomenologically into the dephasing constant $\gamma_{\langle \mathrm{np} \rangle}(n)$, which enters the equations of motion Eq. (3.21) and (3.33). We argue that $\gamma_{\langle \mathrm{np} \rangle}(n)$ should approximately follow the microscopically calculated density dependence of the dephasing of P_k^{cv}. Therefore, as a first step a set of spectra was calculated with $\gamma_{\langle \mathrm{np} \rangle} = 0.3 E_B/\hbar$ for all densities. The effective singlet-level dephasing constant γ_s extracted from the width of the 1s-exciton resonance was then used to calculate density-dependent values $\gamma_{\langle \mathrm{np} \rangle}(n)$.

Appendix E

Simulation Parameters

In general, the material-specific parameters in the numerical calculations are set to the values measured in GaAs (see e.g. Ref. [75]). Notable exception to this is the ratio between the effective masses of the electrons and holes, which is changed from the GaAs value of $m_h/m_e = 6.87$ to $m_h/m_e = 4$ in order to reduce the width of the hole distribution and hence the size of the numerical grid in k-space. Both m_e and m_h are adjusted, so that the reduced mass of the exciton $\mu = m_e m_h/(m_e + m_h)$ remains unchanged from it's value in GaAs. The mesoscopic confinement by the walls of the wire is not described microscopically in our calculations, but is instead approximated by a harmonic potential.
The following table lists the values material parameters as used in the calculations.

reduced exciton mass	μ	0.058 m_0
electron effective mass	m_e	4/3 μ
hole effective mass	m_h	4 μ
band gap at Brillouin zone center	E_G	1.517 eV
background dielectric constant	ϵ_b	12.4
volume deformation potential	$a(\Gamma_1)$	8.6 eV
velocity of sound	v_{LA}	4.79 10^3 m/s
mass density	ρ_m	5317 kg/m^3
3d exciton binding energy	E_B	4.19 meV
3d exciton Bohr radius	a_0	12.53 nm
effective quantum wire radius	Ra_0	8.25 nm
phenomenogical dephasing constant	γ_P	0.05 meV

Bibliography

[1] M. Faraday. *Experimental Researches in Electricity.* Barnard Quaritch, London, 1839.

[2] F. Jahnke, M. Kira, S. W. Koch, G. Khitrova, E. K. Lindmark, T. R. Nelson, D. V. Wick, J. D. Berger, O. Lyngnes, H. M. Gibbs, and K. Tai. Excitonic Nonlinearities of Semiconductor Microcavities in the Nonperturbative Regime. *Phys. Rev. Lett.*, 77:5257, 1996.

[3] M. Kira, W. Hoyer, T. Stroucken, and S. W. Koch. Exciton Formation in Semiconductors and the Influence of a Photonic Environment. *Phys. Rev. Lett.*, 87:176401, 2001.

[4] J. Frenkel. On the Transformation of light into Heat in Solids. II. *Phys. Rev.*, 37:1276, 1931.

[5] G. H. Wannier. The Structure of Electronic Excitation Levels in Insulating Crystals. *Phys. Rev.*, 52:191, 1937.

[6] S. W. Koch, T. Meier, W. Hoyer, and M. Kira. Theory of the optical properties of semiconductor nanostructures. *Physica E*, 14:45, 2002.

[7] M. Kira and S. W. Koch. Microscopic theory of optical excitations, photoluminescence, and terahertz response in semiconductors. *Europ. Phys. J. D*, 36:143, 2005.

[8] R. Kubo. Statistical mechanical theory of irreversible processes. 1. General theory and simple applications in magnetic and conduction problems. *J. Phys. Soc. Jpn*, 12:570, 1957.

[9] P. C. Martin and J. Schwinger. Theory of Many-Particle Systems. I. *Phys. Rev.*, 115:1342, 1959.

[10] S. Chatterjee, C. Ell, S. Mosor, G. Khitrova, H. M. Gibbs, W. Hoyer, M. Kira, S. W. Koch, J. P. Prineas, and H. Stolz. Excitonic Photoluminescence in Semiconductor Quantum Wells: Plasma versus Excitons. *Phys. Rev. B*, 92:67402, 2004.

[11] T. Timusk, R. Navarro, N. O. Lipari, and M. Altarelli. Far-infrared absorption by excitons in Silicon. *Solid State Commun.*, 25:217, 1978.

[12] M. Kira, W. Hoyer, and S. W. Koch. Terahertz signatures of the exciton formation dynamics in non-resonantly excited semiconductors. *Solid State Commun.*, 129:733, 2004.

[13] I. Galbraith, R. Chari, S. Pellegrini, P. J. Phillips, C. J. Dent, A. F. van der Meer, D. G. Clarke, A. K. Kar, G. S. Buller, C. R. Pidgeon, B. N. Murdin, J. Allam, and G. Strasser. Excitonic signatures in the photoluminescence and terahertz absorption of a GaAs/ Alx Ga1-x As multiple quantum well. *Phys. Rev. B*, 71:73302, 2005.

[14] R. A. Kaindl, M. A. Carnahan, D. Hägele, R. Lövenich, and D. S. Chemla. Ultrafast terahertz probes of transient conducting and insulating phases in an electron-hole gas. *Nature*, 423:734, 2003.

[15] W. Hoyer, M. Kira, and S. W. Koch. Influence of Coulomb and phonon interaction on the exciton formation dynamics in semiconductor heterostructures. *Phys. Rev. B*, 67:155113, 2003.

[16] T. L. Hill. Molecular Clusters in Imperfect Gases. *J. Chem. Phys.*, 23:617, 1953.

[17] G. D. Purvis and R. J. Bartlett. A full coupled-cluster singles and doubles model: The inclusion of disconnected triples. *J. Chem. Phys.*, 76:1910, 1982.

[18] J. Paldus, J. Cízek, and B. Jeziorski. Coupled cluster approach or quadratic configuration interaction? *J. Chem. Phys.*, 90:4356, 1989.

[19] D. A. B. Miller, D. S. Chemla, D. J. Eilenberger, P. W. Smith, A. C. Gossard, and W. T. Tsang. Large room-temperature optical nonlinearity in GaAs/Ga_{1-x} Al_xAs multiple quantum well structures. *Appl. Phys. Lett.*, 41:679, 1982.

[20] C. V. Shank, R. L. Fork, R. Yen, J. Shah, B. I. Green, A. C. Gossard, and C. Weisbuch. Picosecond dynamics of hot carrier relaxation in highly excited multi-quantum well structures. *J. Lumin.*, 47:981, 1983.

[21] D. R. Wake, H. W. Yoon, J. P. Wolfe, and H. Morkoç. Response of excitonic absorption spectra to photoexcited carriers in GaAs quantum wells. *Phys. Rev. B*, 46:13452, 1992.

[22] H. Wang, K. Ferrio, D. G. Steel, Y. Z. Hu, R. Binder, and S. W. Koch. Transient nonlinear optical response from excitation induced dephasing in GaAs. *Phys. Rev. Lett.*, 71:1261, 1993.

[23] N. Peyghambarian, H. M. Gibbs, J. L. Jewell, A. Antonetti, A. Migus, D. Hulin, and A. Mysyrowicz. Blue Shift of the Exciton Resonance due to Exciton-Exciton Interactions in a Multiple-Quantum-Well Structure. *Phys. Rev. Lett.*, 53:2433, 1984.

[24] D. Hulin, A. Mysyrowicz, A. Antonetti, A. Migus, W. T. Masselink, H. Morkoç, H. M. Gibbs, and N. Peyghambarian. Well-size dependence of exciton blue shift in GaAs multiple-quantum-well structures. *Phys. Rev. B*, 33:4389, 1986.

[25] K.-H. Schlaad, C. Weber, J. Cunningham, C. V. Hoof, G. Borghs, G. Weimann, W. Schlapp, H. Nickel, and C. Klingshirn. Many-particle effects and nonlinear optical properties of GaAs/(Al,Ga)As multiple-quantum-well structures under quasistationary excitation conditions. *Phys. Rev. B*, 43:4268, 1991.

[26] Z. I. Alferov. Nobel Lecture: The double heterostructure concept and its applications in physics, electronics, and technology. *Rev. Mod. Phys.*, 73:767, 2001.

[27] A. Haug. Auger recombination in direct-gap semiconductors: band-structure effects . *J. Phys. C*, 16:4159, 1983.

[28] A. Thränhardt, S. Kuckenburg, A. Knorr, T. Meier, and S. W. Koch. Quantum theory of phonon-assisted exciton formation and luminescence in semiconductor quantum wells. *Phys. Rev. B*, 62:2706, 2000.

[29] S. John. Strong localization of photons in certain disordered dielectric superlattices. *Phys. Rev. Lett.*, 58:2486, 1987.

[30] E. Yablonovitch. Inhibited spontaneous emission in solid-state physics and electronics. *Phys. Rev. Lett.*, 58:2059, 1987.

[31] D. Labilloy, H. Benisty, C. Weisbuch, T. F. Krauss, R. M. de La Rue, V. Bardinal, R. Houdré, U. Oesterle, D. Cassagne, and C. Jouanin. Quantitative Measurement of Transmission, Reflection, and Diffraction of Two-Dimensional Photonic Band Gap Structures at Near-Infrared Wavelengths. *Phys. Rev. Lett.*, 79:4147, 1997.

[32] T. Usui. Excitations in a high density electron gas. *Prog. Theor. Phys.*, 23:787, 1960.

[33] M. H. Zhang, Q. Huang, and J. M. Zhou. Calculations of the time taken for excitons to form in GaAs quantum wells. *J. Phys.: Condens. Matter*, 9:10185, 1997.

[34] P. E. Selbmann, M. Gulia, F. Rossi, E. Molinari, and P. Lugli. Coupled free-carrier and exciton relaxation in optically excited semiconductors. *Phys. Rev. B*, 54:4660, 1996.

[35] W. Hoyer. *Quantentheorie zu Exzitonbildung und Photolumineszenz in Halbleitern.* Fachbereich Physik der Philipps-Universität, Marburg, 2002.

[36] W. Hoyer, M. Kira, and S. W. Koch. Pair-Correlation Functions in Incoherent Electron-Hole Plasmas. *Phys. Status Solidi B*, 234:195, 2002.

[37] L. P. Kadanoff and G. Baym. *Quantum Statistical Mechanics.* W. A. Benjamin Inc., New York, 1962.

[38] M. Lindberg and S. W. Koch. Effective Bloch equations for semiconductors. *Phys. Rev. B*, 38:3342, 1988.

[39] P. Meystre and M. Sargent. *Elements of quantum optics.* Springer, Berlin, 2nd edition, 1991.

[40] P. Y. Yu and M. Cardona. *Fundamentals of Semiconductors.* Springer, Berlin, 2nd edition, 1999.

[41] M. Born and R. Oppenheimer. Zur Quantentheorie der Molekeln. *Ann. Phys.*, 84:457, 1927.

[42] J. M. Ziman. *Electrons and Phonons.* University Press, Oxford, 2nd edition, 1967.

[43] H. Haug and S. W. Koch. *Quantum Theory of the Optical and Electronic Properties of Semiconductors.* World Scientific, Singapore, 4th edition, 2004.

[44] W. Nolting. *Grundkurs: Theoretische Physik, Quantenmechanik.* Verlag Zimmermann-Neufang, Ulmen, 1994.

[45] S. Glutsch and D. S. Chemla. Transition to one-dimensional behavior in the optical absorption of quantum-well wires. *Phys. Rev. B*, 53:15902, 1996.

[46] A. N. Forshaw and D. M. Whittaker. Optical absorption of wide quantum wires. *Phys. Rev. B*, 54:8794, 1996.

[47] I.-K. Oh and J. Singh. Excitonic relaxation through phonon interactions in quantum wells. *J. Lumin.*, 85:233, 2000.

[48] J. Bardeen and W. Shockley. Deformation Potentials and Mobilities in Non-Polar Crystals. *Phys. Rev.*, 80:72, 1950.

[49] J. J. Harris, J. A. Pals, and R. Woltjer. Electronic transport in low-dimensional structures. *Rep. Prog. Phys*, 52:1217, 1989.

[50] M. Kira and S. W. Koch. Exciton-Population Inversion and Terahertz Gain in Resonantly Excited Semiconductors. *Phys. Rev. Lett.*, 93:076402, 2004.

[51] S Siggelkow, W. Hoyer, M. Kira, and Koch S. W. Exciton formation and stability in semiconductor heterostructures. *Phys. Rev. B*, 69:73104, 2004.

[52] W. Ebeling, W. D. Kraeft, and D. Kremp. *Theory of Bound States and Ionisation Equilibrium in Plasmas and Solids.* Akademie-Verlag, Berlin, 1st edition, 1976.

[53] R. Zimmermann and H. Stolz. The mass action law in two-component Fermi systems revisited. *Phys. Status Solidi B*, 131:151, 1985.

[54] M. E. Portnoi and I. Galbraith. Ionization degree of the electron-hole plasma in semiconductor quantum wells. *Phys. Rev. B*, 60:5570, 1999.

[55] M. F. Mott. Exciton ionization in semiconductors. *Philos. Mag.*, 6:287, 1961.

[56] W. Schäfer, D. S. Kim, J. Shah, T. C. Damen, J. E. Cunningham, K. W. Goossen, L. N. Pfeiffer, and K. Köhler. Femtosecond coherent fields induced by many-particle correlations in transient four-wave mixing. *Phys. Rev. B*, 53:16429, 1996.

[57] G. Bartels, G. C. Cho, T. Dekorsy, H. Kurz, A. Stahl, and K. Köauthler. Coherent signature of differential transmission signals in semiconductors: Theory and experiment. *Phys. Rev. B*, 55:16404, 1997.

[58] T. Meier and S. W. Koch. Analysis of Excitonic Absorption Changes Induced by Incoherent Exciton and Electron-Hole Pair Populations. *Physica Status Solidi B*, 221:211–214, 2000.

[59] R. J. Elliott. Intensity of Optical Absorption by Excitons. *Phys. Rev.*, 108:1384, 1957.

[60] J. Shah, R. F. Leheny, and W. Wiegmann. Low-temperature absorption spectrum in GaAs in the presence of optical pumping. *Phys. Rev. B*, 16:1577, 1977.

[61] G. W. Fehrenbach, W. Schäfer, J. Treusch, and R. G. Ulbrich. Transient Optical Spectra of a Dense Exciton Gas in a Direct-Gap Semiconductor. *Phys. Rev. Lett.*, 49:1281, 1982.

[62] S. Hunsche, K. Leo, H. Kurz, and K. Köhler. Exciton absorption saturation by phase-space filling: Influence of carrier temperature and density. *Phys. Rev. B*, 49:16565, 1994.

[63] L. Schultheis, J. Kuhl, A. Honold, and C. W. Tu. Ultrafast phase relaxation of excitons via exciton-exciton and exciton-electron collisions. *Phys. Rev. Lett.*, 57:1635, 1986.

[64] G. Manzke, Q. Y. Peng, K. Henneberger, U. Neukirch, K. Hauke, K. Wundke, J. Gutowski, and D. Hommel. Density Dependence of the Exciton Energy in Semiconductors. *Phys. Rev. Lett.*, 80:4943, 1998.

[65] S. Schmitt-Rink, D. S. Chemla, and H. Haug. Nonequilibrium theory of the optical Stark effect and spectral hole burning in semiconductors. *Phys. Rev. B*, 37:941, 1988.

[66] M. U. Wehner, M. H. Ulm, D. S. Chemla, and M. Wegener. Coherent Control of Electron-LO-Phonon Scattering in Bulk GaAs. *Phys. Rev. Lett.*, 80:1992, 1998.

[67] D. S. Chemla and J. Shah. Many-body and correlation effects in semiconductors. *Nature*, 411:549, 2001.

[68] P. Langot, R. Tommasi, and F. Vallée. Nonequilibrium hole relaxation dynamics in an intrinsic semiconductor. *Phys. Rev. B*, 54:1775, 1996.

[69] V. M. Axt and A. Stahl. A dynamics-controlled truncation scheme for the hierarchy of density matrices in semiconductor optics. *Z. Phys. B*, 93:195, 1994.

[70] V. M. Axt and A. Stahl. A dynamics-controlled truncation scheme for the hierarchy of density matrices in semiconductor optics. *Z. Phys. B*, 93:205, 1994.

[71] M. Lindberg, Y. Z. Hu, R. Binder, and S. W. Koch. $\chi(3)$ formalism in optically excited semiconductors and its applications in four-wave-mixing spectroscopy. *Phys. Rev. B*, 50:18060, 1994.

[72] S. T. Cundiff, H. Wang, and D. G. Steel. Polarization-dependent picosecond excitonic nonlinearities and the complexities of disorder. *Phys. Rev. B*, 46:7248, 1992.

[73] R. Eichmann, B. Pasenow, T. Meier, T. Stroucken, P. Thomas, and S. W. Koch. Semiconductor excitons in photonic crystals. *Phys. Status Solidi B*, 238:439, 2003.

[74] M. Abramowitz and A. Stegun. *Handbook of Mathematical Functions.* Dover Publications, New York, 9th edition, 1972.

[75] O. Madelung (Editor). *Semiconductors - Basic Data.* Springer, Berlin, 2nd edition, 1996.

Wissenschaftlicher Werdegang

Seit Sept. 2002	wissenschaftlicher Mitarbeiter in der Arbeitsgruppe Theoretische Halbleiterphysik, Philipps-Universität Marburg Kollegiat des Europäischen Graduiertenkollegs "Electron - Electron Interactions in Solids"
April 2002 - August 2002	Stipendiat des Europäischen Graduiertenkollegs "Electron - Electron Interactions in Solids"
April 2001 - April 2002	Kollegiat des Graduiertenkollegs "Optoelektronik mesoskopischer Halbleiter", Philipps-Universität Marburg
7.2.2001	Beginn der Promotion in der Arbeitsgruppe Theoretische Halbleiterphysik an der Philipps-Universität Marburg
27.1.2001	Verleihung des Abschlusses "Master of Philosophy" durch die University of Cambridge
15.9.2000	Einreichen der Master-Arbeit "Electronic Excitations in Tunnelling Electron Bilayers"
Sept. 1999 - Sept. 2000	Master-Studiengang für Physik an der University of Cambridge, UK
Okt. 1998 - Juli 1999	Hauptstudium Physik an der Philipps-Universität Marburg
6.10. 1998	Vordiplom für Physik
16.7. 1996	Beginn des Studiums der Physik an der Philipps-Universität Marburg

Danksagung

Ich danke allen, die zum Gelingen meiner Promotion beigetragen haben. Mein besonderer Dank gilt dabei meinem Doktorvater, Stephan Koch, für die Betreuung meiner Promotion in ihrer ganzen Länge. Desweiteren stehe ich in der Schuld von Mackillo Kira, der immer Zeit gefunden hat, mit mir Resultate und weiteres Vorgehen zu diskutieren.

Ich danke allen Mitgliedern der Arbeitsgruppe "Theoretische Halbleiter-Physik" für die freundliche und hilfsbereite Atmosphäre, ein besonderer Dank gebührt hier Peter Thomas, der diese Atmosphäre unermüdlich durch Wort und Tat (nicht zuletzt die Organisation von Wanderungen) fördert.

Florian Gebhardt danke ich für die Aufnahme in das European Graduate College "Electron-Electron Interactions in Solids". Die Seminare in Riezlern und Rackeve haben mir dabei geholfen, meinen persönlichen Tellerrand zumindest etwas nach außen zu verschieben. An dieser Stelle möchte ich mich ebenfalls für die finanzielle Unterstützung des Graduate College während meiner Zeit als Stipendiat bedanken.

Und dann waren da noch meine Büro-Mit-Insassen. In der Zeit, die mit Euch zu verbringen mein Schicksal war, habe ich viel gelernt, inklusive einiger erstaunlicher Meinungen zum Thema Zimmertemperatur, bemerkenswert bunt gemischten Wissens, und ab und an wohl auch physikalischer Einsichten. Den als Dank zu verstehenden Teil vorigen Satzes möchte ich ausweiten auf Matthias Reichelt, Angela Thränhardt und Walter Hoyer, die (sofern nicht gerade in Tuscon) für erbauliche Mensa-Besuche gesorgt haben.

Mein ganz besonderer Dank gilt meinen Freunden, die sich auch von von absoluten Kontakt-Unwilligkeit meinerseits in der (ausgedehnten) letzten Phase der Promotion nicht haben abhalten lassen, weiterhin Umgang mit mir zu pflegen: Timm Zwickel für die vielfältigen gemeinsamen Aktivitäten (einschließlich, aber lange nicht beschränkt auf die Einführung ins Mountain-Unicycling), Knuth Posern für vielfältige Kurzweil, Tanja Schwamm für die Zeit hier in Marburg und unsere Telefonate, und sicherlich nicht zuletzt Marc Vor der Brüggen für freundlichen Spott und sehr ausgedehnte Gespräche. Besonders viel leiden mussten, fürchte ich, meine Mitbewohner und Mitbewohnerinnen mitsamt "Anhängen". Warum Ihr immer noch mit mir sprecht, ist mir ein Rätsel (Ihr seid phantastisch).

Ich danke meinen Eltern. Für (so ziemlich) alles.